



UNIVERSIDADE ESTADUAL DE CAMPINAS
Instituto de Matemática, Estatística e Computação Científica

JARDEL VIEIRA

**NUMERICAL MODELING OF THE TWO-PHASE FLOW IN
POROUS MEDIA WITH DYNAMIC CAPILLARY
PRESSURE**

**MODELAGEM NUMÉRICA DO ESCOAMENTO BIFÁSICO
EM MEIOS POROSOS COM PRESSÃO CAPILAR
DINÂMICA**

CAMPINAS
2018

JARDEL VIEIRA

**NUMERICAL MODELING OF THE TWO-PHASE FLOW IN
POROUS MEDIA WITH DYNAMIC CAPILLARY
PRESSURE**

**MODELAGEM NUMÉRICA DO ESCOAMENTO BIFÁSICO
EM MEIOS POROSOS COM PRESSÃO CAPILAR
DINÂMICA**

Thesis presented to the Institute of Mathematics, Statistics and Scientific Computing of the University of Campinas in partial fulfillment of the requirements for the degree of Doctor in Applied Mathematics.

Tese apresentada ao Instituto de Matemática, Estatística e Computação Científica da Universidade Estadual de Campinas como parte dos requisitos exigidos para a obtenção do título de Doutor em Matemática Aplicada.

Advisor/Orientador: Eduardo Cardoso de Abreu

ESTE EXEMPLAR CORRESPONDE À VERSÃO
FINAL DA TESE DEFENDIDA PELO ALUNO
JARDEL VIEIRA, E ORIENTADA PELO PROF.
DR. EDUARDO CARDOSO DE ABREU.

CAMPINAS

2018

Agência(s) de fomento e nº(s) de processo(s): CAPES; CNPq, 140799/2017-6

Ficha catalográfica
Universidade Estadual de Campinas
Biblioteca do Instituto de Matemática, Estatística e Computação Científica
Ana Regina Machado - CRB 8/5467

V673n Vieira, Jardel, 1991-
Numerical modeling of the two-phase flow in porous media with dynamic capillary pressure / Jardel Vieira. – Campinas, SP : [s.n.], 2018.

Orientador: Eduardo Cardoso de Abreu.
Tese (doutorado) – Universidade Estadual de Campinas, Instituto de Matemática, Estatística e Computação Científica.

1. Análise numérica. 2. Equações diferenciais parciais. 3. Método dos elementos finitos. 4. Método dos volumes finitos. 5. Meios porosos. I. Abreu, Eduardo Cardoso de, 1974-. II. Universidade Estadual de Campinas. Instituto de Matemática, Estatística e Computação Científica. III. Título.

Informações para Biblioteca Digital

Título em outro idioma: Modelagem numérica do escoamento bifásico em meios porosos com pressão capilar dinâmica

Palavras-chave em inglês:

Numerical analysis

Partial differential equations

Finite element method

Finite volume method

Porous media

Área de concentração: Matemática Aplicada

Titulação: Doutor em Matemática Aplicada

Banca examinadora:

Eduardo Cardoso de Abreu [Orientador]

Giuseppe Romanazzi

Lucas Catao de Freitas Ferreira

Grigori Chapiro

Wanderson José Lambert

Data de defesa: 18-07-2018

Programa de Pós-Graduação: Matemática Aplicada

**Tese de Doutorado defendida em 18 de julho de 2018 e aprovada
pela banca examinadora composta pelos Profs. Drs.**

Prof. Dr. EDUARDO CARDOSO DE ABREU

Prof. Dr. GIUSEPPE ROMANAZZI

Prof. Dr. LUCAS CATAO DE FREITAS FERREIRA

Prof. Dr. GRIGORI CHAPIRO

Prof. Dr. WANDERSON JOSÉ LAMBERT

As respectivas assinaturas dos membros encontram-se na Ata de defesa

*Aos meus pais Celina e Eterno, a minha
irmã Nathália e ao meu companheiro Valter.*

Agradecimentos

Agradeço o apoio da Coordenadoria de Assistência de Pessoal de Nível Superior (CAPES) e do Conselho Nacional de Desenvolvimento Científico e Tecnológico (CNPq), juntamente com o Programa de Pós-Graduação em Matemática Aplicada e Computacional do IMECC/UNICAMP, pelo apoio via bolsa institucional CAPES, no período de 03/2015 até 02/2015, e via bolsa institucional CNPq, no período de 03/2017 até 07/2018.

Agradeço ao meu orientador, o Professor Eduardo Cardoso de Abreu, pela oportunidade de desenvolvimento deste trabalho, pela a seriedade e o compromisso com a pesquisa, pelos conhecimentos compartilhados e, principalmente, pela dedicação e apoio durante todo o mestrado e doutorado.

Agradeço aos meus colegas de pesquisa pelas importantes e enriquecedoras discussões, em especial a Abel A. Bustos, Arthur M. E. Santo, Ciro J. Diaz, Felipe A. Guedes, Jean R. François, John A. P. Sepulveda, Juan G. Delgado, Luís G. C. Santos e Paola Ferraz. Agradeço também a todos pelo amigoso ambiente de colaboração do nosso grupo, pautado no respeito e na ética científica.

Por fim, agradeço a todos que de alguma maneira contribuíram para a realização desse trabalho, em especial às amigas que dividiram sala comigo Anny, Marina e Stef.

Resumo

É discutida uma modelagem numérica para aproximar o escoamento bifásico em um meio poroso heterogêneo, levando em conta efeitos da pressão capilar dinâmica. O sistema de equações governantes consiste em um sistema pseudo-parabólico para o transporte da saturação e um problema elíptico de pressão-velocidade. O sistema de transporte é reescrito a fim de se obter uma equação elíptica para a pressão capilar. Dessa forma, é possível usar a mesma abordagem numérica para ambos os problemas. São combinadas uma discretização por elementos finitos mistos e técnicas de volumes finitos localmente conservativos. Uma estratégia implícita é aplicada para a solução do problema de transporte de natureza pseudo-parabólica. Foram realizadas simulações bidimensionais em uma variedade de regimes de escoamento com campos de permeabilidade heterogêneos e efeitos de gravidade. Os experimentos numéricos demonstram a viabilidade da formulação proposta e podem ajudar a entender a combinação dos diferentes efeitos físicos.

Palavras-chave: Equação pseudo-parabólica; Pressão capilar dinâmica; Escoamento bifásico; Meios porosos; Volumes finitos; Elementos finitos mistos.

Abstract

We discuss a numerical modeling to approximate a two-phase flow in a heterogeneous porous media taking into account effects of dynamic capillary pressure. The governing system of equations consists of a pseudo-parabolic transport saturation system and an elliptic pressure-velocity problem. We rewrite the transport system in order to obtain a elliptic equation for capillary pressure. Therefore, we are able to use the same numerical approach for both problems. We combine mixed finite element discretization and locally conservative finite volume techniques. An implicit strategy is applied for the numerical solution of the transport problem of pseudo-parabolic nature. We performed two-dimensional simulations in a variety of flow regimes along with heterogeneous permeability fields and gravity effects. Our numerical experiments demonstrate the viability of the proposed formulation and may help understand the combination of the different physical effects.

Keywords: Pseudo-parabolic equation; Dynamic capillary pressure; Two-phase flow; Porous media; Finite volume; Mixed finite element.

List of Figures

3.1	Mesh refinement study to the first operator splitting approach.	38
3.2	Mesh refinement study to the second operator splitting approach.	41
4.1	Element Ω_i and the neighbor elements.	47
4.2	Natural degrees of freedom on the element Ω_i	48
4.3	Staggered mesh (left) and numerical stencil (right) for computing the numerical hyperbolic flux.	53
5.1	Boundary conditions for slab geometry for saturation transport and pressure-velocity problems.	58
5.2	The Gaussian field $\xi(\mathbf{x})$ used to define the heterogeneous rock properties.	60
5.3	Numerical solutions and refinement study for saturation.	62
5.4	Numerical solutions for saturation with different values of viscosity ratio R_μ	63
5.5	Saturation profile during the infiltration in a heterogeneous porous media (3D view).	64
5.6	Saturation profile during the infiltration in a heterogeneous porous media (color map).	65
5.7	Numerical simulations for the flow in the gravity direction and heterogeneous permeability field ($CV_K = 0.5$).	67
5.8	Numerical simulations for the flow against the gravity and heterogeneous permeability field ($CV_K = 0.5$).	68
5.9	Numerical simulations for the flow in the gravity direction and heterogeneous permeability field ($CV_K = 1.0$).	69
5.10	Numerical solution for nonlinear static capillary pressure.	71

B.1	Numerical solutions for saturation and refinement study for the finite difference scheme.	98
C.1	Mesh refinement study for non-increasing initial data and linear high order terms.	101
C.2	Mesh refinement study for non-increasing initial data and nonlinear high order terms.	102
C.3	Numerical solutions for the linear diffusion case with different values of the dynamic effect coefficient τ	103
C.4	Numerical solutions for the nonlinear diffusion case with different values of the dynamic effect coefficient τ	104
C.5	Numerical solutions when the gravity acts in flow direction with different values of dynamic effect number N_{Dy} and gravity number N_{Gr}	105
C.6	Numerical solutions when the gravity acts in the direction opposite to the flow with different values of dynamic effect number N_{Dy} and gravity number N_{Gr}	106

List of Tables

5.1	Refinement study with homogeneous permeability field.	61
5.2	Refinement study with heterogeneous permeability field.	61
B.1	Refinement study with homogeneous permeability field for the finite difference scheme.	97
B.2	Refinement study with heterogeneous permeability field for the finite difference scheme.	97

List of Symbols

Latin symbols

b_{ci}	Right hand side of the capillary pressure discrete equation on element Ω_i .
b_{ni}	Right hand side of the non-wetting phase pressure discrete equation on element Ω_i .
CV	Coefficient of variation.
E	Error of an numerical solution compared to the reference numerical solution.
\mathbf{e}_1	Unit vector in the x direction.
\mathbf{e}_2	Unit vector in the y direction.
\mathbf{F}	Convection flux function.
F_{ij}^n	Numerical hyperbolic flux at interface Γ_{ij} and time t_n .
f_n	Non-wetting phase fractional flow function.
f_w	Wetting phase flow function.
g	Gravity magnitude.
h	Mesh parameter.
H_c	Capillary induced diffusion function.
$[H_c^{\text{eff}}]_{ij}$	Approximated effective value of H_c at the interface Γ_{ij} .
H_{ci}	Approximation of the capillary induced diffusion function at the center of element Ω_i .
$H_{c\text{min}}$	Regularization value to avoid degenerated values for diffusion coefficient.
$[H_G n^{\text{eff}}]_{ij}$	Approximated effective value of H_n at the interface Γ_{ij} .
H_G	Coefficient linked to gravity.
H_{Gi}	Approximation of the gravity coefficient at the center of the element Ω_i .
$[H_n^{\text{eff}}]_{ij}$	Approximated effective value of H_G at the interface Γ_{ij} .
H_n	Coefficient of non-wetting phase pressure gradient.
H_{ni}	Approximation of the coefficient of non-wetting phase pressure gradient at the center of the element Ω_i .
$I_{\tilde{j}}$	Set of all non-staggered elements that intersects $\tilde{\Omega}_{\tilde{j}}$.
K	Absolute permeability.

K_0	Cutoff value for absolute permeability.
K_c	Characteristic absolute permeability.
k_n	Non-wetting phase relative permeability function.
k_w	Wetting phase relative permeability function.
L_c	Characteristic length.
ϱ_{cij}^h	Lagrange multiplier over interface Γ_{ij} associated with the transport problem.
ℓ_{cij}	Local degree of freedom for approximation capillary pressure Lagrange multiplier associated with the interface Γ_{ij} on element Ω_i .
l_{ij}	Local basis function for Lagrange multipliers linked to the interface Γ_{ij} on the element Ω_i .
ϱ_{nij}^h	Lagrange multiplier over interface Γ_{ij} associated with the pressure-velocity problem.
ℓ_{nij}	Local degree of freedom for approximation of non-wetting phase pressure Lagrange multiplier associated with the interface Γ_{ij} on element Ω_i .
$\tilde{\ell}_{ij}$	Test function associated with Lagrange multiplier spaces over interface Γ_{ij} .
M	Number of elements.
\mathbf{n}	Unit outer normal vector.
\mathbf{n}_{ij}	Unit outer vector normal to the interface Γ_{ij} associated with the element Ω_i .
N_{Ca}	Capillary dimensionless number.
N_{Dy}	Dynamic capillary dimensionless number.
N_{Gr}	Gravity dimensionless number.
\tilde{p}	Test function linked to scalar variables.
p_c	Capillary pressure.
p_c^h	Approximation of the capillary pressure.
p_{ci}^h	Local approximation of the capillary pressure on element Ω_i .
p_{cb}	Capillary pressure value imposed on Γ_w^D .
p_{cc}	Characteristic capillary pressure.
p_{ci}	Local degree of freedom for approximation of capillary pressure on element Ω_i .
p_e	Static capillary pressure function.
p_n	Non-wetting phase pressure.
p_n^h	Approximation of the non-wetting phase pressure.
p_{ni}^h	Local approximation of the non-wetting phase pressure on element Ω_i .
p_{nb}	Pressure value imposed on Γ_n^D .
p_{ni}	Local degree of freedom for approximation of non-wetting phase pressure on element Ω_i .

p_n^{ref}	Reference value for non-wetting phase pressure imposed at right boundary.
p_w	Wetting phase pressure.
Q^{in}	Total inflow value impose at left boundary.
R_μ	Viscosity ratio.
R_ρ	Density ration.
S_i^n	Approximation of wetting phase saturation on element Ω_i at time t_n .
S_L	Wetting phase saturation value imposed at left boundary.
$S^{n,k}$	Approximation of wetting phase saturation at time t_n and iteration k .
S_n	Non-wetting phase saturation.
S^{ref}	Reference numerical approximation for wetting phase saturation calculated over the most refined mesh.
S_w	Wetting phase saturation.
S_{wb}	Saturation value imposed on Γ_w^D .
t	Time.
u_c	Characteristic velocity.
\mathbf{v}	Total velocity.
$\tilde{\mathbf{v}}$	Test function linked to gradient flux variables.
\mathbf{v}^h	Approximation of the total velocity.
\mathbf{v}_i^h	Local approximation of the total velocity on element Ω_i .
V_c	Functional space of the diffusive flux.
V_{c0}	Subspace of V_c of functions that have null normal component at Γ_w^N .
V_c^h	Discrete space to approximate the diffusive flux.
\hat{V}_c^h	Relaxed discrete space to approximate the diffusive flux.
$V_{c,i}^h$	Local discrete space to approximate the diffusive flux on element Ω_i .
\mathbf{v}_c	Correction velocity linked to capillary pressure.
$\mathbf{v}_{c,i}^h$	Local approximation of correction velocity linked to capillary pressure on element Ω_i .
v_{cij}	Coefficient thats represents the approximated value of correction velocity linked to capillary pressure at interface Γ_{ij} .
\mathbf{v}_G	Correction velocity linked to gravity.
$\mathbf{v}_{G,i}^h$	Local approximation of correction velocity linked to gravity on element Ω_i .
v_{Gij}	Coefficient thats represents the approximated value of correction velocity linked to gravity at interface Γ_{ij} .
v_{ij}	Local degree of freedom for approximation of total velocity associated with the interface Γ_{ij} on element Ω_i .
v_{max}	Maximum value of the total velocity norm.
V_n	Functional space of the total velocity.
V_{n0}	Subspace of V_n of functions that have null normal component at Γ_n^N .
V_n^h	Discrete space to approximate the total velocity.

\hat{V}_n^h	Relaxed discrete space to approximate the total velocity.
$V_{n i}^h$	Local discrete space to approximate the total velocity on element Ω_i .
\mathbf{v}_n	Non-wetting phase velocity.
v_b	Normal component value of the total velocity imposed on Γ_n^N .
\mathbf{v}_w	Wetting phase velocity.
v_{wb}	Normal component value of \mathbf{v}_w imposed on Γ_w^R .
\mathbf{w}	Diffusive flux.
\mathbf{w}^h	Approximation of the diffusive flux.
\mathbf{w}_i^h	Local approximation of the diffusive flux on element Ω_i .
w_b	Value of the normal component of the diffusive flux imposed on Γ_w^N .
W_c	Functional space of the capillary pressure.
W_c^h	Discrete space for approximate the capillary pressure.
$W_{c i}^h$	Local discrete space for approximate the capillary pressure on element Ω_i .
w_{ij}	Local degree of freedom for approximation of diffusive flux associated with the interface Γ_{ij} on element Ω_i .
W_n	Functional space of the non-wetting phase pressure.
W_n^h	Discrete space to approximate the non-wetting phase pressure.
$W_{n i}^h$	Local discrete space to approximate the non-wetting phase pressure on element Ω_i .
\mathbf{x}	Position vector.
x	First space coordinate.
y	Second space coordinate.
Z	Depth function.

Greek symbols

β	Scaling exponent of Gaussian field covariance function.
Γ	Domain boundary.
Γ_i	Part of the boundary subdomain (element) Ω_i that intersects the domain boundary.
Γ_{ij}	Interface between subdomains Ω_i and Ω_j .
Γ_n^D	Subset of the domain boundary where Dirichlet conditions are imposed to the pressure-velocity problem.
Γ_n^N	Subset of the domain boundary where Neumann conditions are imposed to the pressure-velocity problem.
Γ_w^D	Subset of the domain boundary where Dirichlet conditions are imposed to the transport problem.

Γ_w^N	Subset of the domain boundary where Neumann conditions are imposed to the transport problem.
Γ_w^R	Subset of the domain boundary where Robin conditions are imposed to the transport problem.
Δx	Element length in x direction.
Δy	Element length in y direction.
ε	Tolerance for convergence criterion of the iterative procedure.
η	Initial value of wetting phase saturation.
Λ_c^h	Global Lagrange multiplier space for the transport problem.
$\Lambda_{c_{ij}}^h$	Local Lagrange multiplier space over Γ_{ij} for the transport problem.
Λ_n^h	Global Lagrange multiplier space for the pressure-velocity problem.
$\Lambda_{n_{ij}}^h$	Local Lagrange multiplier space over Γ_{ij} for the pressure-velocity problem.
λ	Total mobility.
λ_n	Non-wetting phase mobility.
λ_w	Wetting phase mobility.
μ_n	Non-wetting phase viscosity.
μ_w	Wetting phase viscosity.
ξ	Gaussian stochastic field.
ϖ_K	Scaling factor for absolute permeability.
ϖ_ϕ	Normalizing factor for porosity.
ρ_n	Non-wetting phase density.
ρ_w	Wetting phase density.
σ_{CFL}	Stability parameter.
τ	Dimensionless dynamic effect coefficient.
τ_H	Dynamic effect coefficient.
ϕ	Porosity.
$\bar{\phi}$	Porosity mean.
ϕ_i	Porosity value at the center of the element Ω_i .
ϕ_{\min}	Minimum value of porosity.
φ_{ij}	Local basis function for gradient flux variables linked to the interface Γ_{ij} on the element Ω_i .
ψ_i	Local basis function for scalar variables on element Ω_i .
Ω	Domain.
Ω_i	i -th subdomain (element) of the domain partition.
$\tilde{\Omega}_{\tilde{j}}$	\tilde{j} -th element of the staggered mesh.
$\partial\Omega$	Domain boundary.
$\partial\Omega$	Boundary of subdomain (element) Ω_i .

Superscripts and subscripts

$*$	Dimensionless variables (superscript).
c	Linked to capillary pressure (subscript); characteristic values (subscript).
d	Lower element index (subscript).
i, j	Element indexes (subscript).
\tilde{i}, \tilde{j}	Element indexes of staggered mesh (subscript).
k	Iteration level.
l	Left element index (subscript).
max	Maximum value.
min	Minimum value.
n	Time index (superscript); non-wetting phase (subscript).
r	Right element index (subscript).
u	Upper element index (subscript).
w	Wetting phase (subscript).
α, β	Phase index (subscript); interface index (subscript).

Contents

1	Introduction	20
1.1	Literature review	20
1.2	Motivation and significance of the work	26
1.3	Aims and objectives of the thesis	27
1.4	Main results and scientific contributions	27
1.5	Overview of the thesis	28
2	Mathematical model of two-phase flow in porous media with dynamic capillary pressure	29
2.1	Governing equations	29
2.2	Phase formulation	31
2.3	Dimensional analysis	31
2.4	Computational modeling of the flow equations	33
3	Numerical study of operator splitting techniques applied to the pseudo-parabolic problem	34
3.1	Operator splitting based on advective and diffusive processes	35
3.2	Operator splitting based on dispersive-like character	39
4	Mixed finite element approximation for the pseudo-parabolic two-phase flow problem	42
4.1	Approximation by mixed finite elements	42
4.2	Reduction to the lowest index Raviart-Thomas spaces over rectangles	46
4.3	Discretization in time	51

4.4	Numerical hyperbolic flux	53
4.5	Boundary conditions	54
4.6	Iterative procedure	55
5	Numerical experiments	57
5.1	Refinement study	60
5.2	Numerical study of viscosity ratio effects	61
5.3	Numerical study of gravity effects	66
5.4	Nonlinear model for capillary pressure	70
6	Concluding remarks	72
6.1	Final Considerations	72
6.2	Perspectives for future work	73
	References	74
A	Stability analysis for a simplified pseudo-parabolic model	83
A.1	One-dimensional simplified model	83
A.2	One-dimensional numerical scheme	84
A.3	Linear stability analysis	85
A.4	Convergence of iterative procedure	89
B	Finite difference method for two-phase flow with dynamic capillary pressure	92
B.1	Finite difference scheme for the pseudo-parabolic transport equation	92
B.2	Finite difference scheme for the elliptic pressure-velocity problem	95
B.3	Numerical experiments	97
C	Further one-dimensional simulations	99
C.1	Numerical experiments for nondecreasing initial data	100
C.2	Numerical study of gravity effects on solution profile	102

Chapter 1

Introduction

The main interest of this work is the design and implementation of a numerical scheme for approximation of a two-phase immiscible flow in porous media with dynamic capillary pressure model to account non-equilibrium effects in difference of pressure between the two fluids. The governing equations can be described by a pseudo-parabolic transport equation coupled with a pressure-velocity problem of elliptic nature. Here we are interested in solution of the two-dimensional two-phase flow problem with gravity effects and heterogeneous fields of permeability and porosity.

1.1 Literature review

To design our novel computational approach, we must consider some recent developments related to pseudo-parabolic differential models, in particular linked to regularity issues. Thus, in this section we provide a brief review of the analytical and numerical studies, as well as a brief description of experimental and thermodynamics studies that have led to the dynamic model of capillary pressure, with no pretense of exhausting the subject.

Significance of the non equilibrium effects on capillary pressure

Capillary pressure, the difference between pressures of fluid phases, plays a central role in the description of two-phase flow in porous media. In the past decades, many capillary pressure-saturation models were correlated from laboratory experiments under equilibrium conditions. These static capillary pressure models have been used in most of the mathematical studies on modeling of a multiphase flow in a porous medium. In most traditional treatments of capillary pressure, it is assumed to be a function of saturation [8, 11, 15, 83]. This standard relationship between capillary pressure and saturation is empirical in nature, therefore it lacks a firm theoretical foundation [49].

Several experimental evidences in the past decades demonstrated that the description of capillary pressure must include non-equilibrium effects. For example, it was found that, in the case of large velocity regimes, the laboratory measured capillary pressure

does not correspond to the standard model assumed under equilibrium conditions. The works [49] and [73] present a review of these experimental studies. As a consequence, new empirical and theoretical studies were developed to generalize the functional dependence of capillary pressure to include dynamic effects [10, 54, 55, 60, 98].

In the recent years, the dynamic capillary pressure relationship proposed by Hassanizadeh and Gray [51] has received considerably attention. This macroscopic model of capillary pressure is a result of a solid thermodynamic theory of two-phase flow in a porous medium developed by Hassanizadeh and Gray in a series of works [46, 47, 50, 51, 52]. Since then, this dynamic capillary pressure has been applied successfully to model the two-phase flow in porous media in various contexts such as laboratory experiments [1, 14, 26, 72, 79, 82], numerical simulation [41, 42, 53, 84] and mathematics [18, 31, 32].

It is worth mentioning that some authors believe that the dynamic capillary pressure could help to explain instabilities in gravity-driven flows and viscous fingering phenomena [80, 103]. In this respect, gravity-driven fingers in porous medium are known to have a nonmonotonic saturation profile (saturation overshoot) [27]. The observed saturation overshoot is inconsistent with classical continuum descriptions of porous media but qualitatively matches observations and predictions from discrete pore-filling mechanisms. In [27], the authors suggest that pore-scale physics controls saturation overshoot and in turn gravity-driven fingering. The dynamic capillary pressure may help to explain the saturation overshoot phenomenon. In [32] and [31], the authors discuss extensions of the Buckley–Leverett equation describing two-phase flow in porous media with dynamic effects in the capillary pressure. They obtained nonmonotone weak solutions for these extended Buckley–Leverett equation. In this connection, in the works [90, 105], the authors study saturation and pressure overshoots with a related model that incorporates dynamic capillary pressure and capillary pressure hysteresis.

Under certain physical assumptions, the governing equations of the two-phase flow can be described by a transport equation for saturation coupled with a pressure-velocity problem of elliptic nature. From a mathematical point of view, the transport equation with the standard capillary pressure model is a degenerate nonlinear parabolic equation on the saturation. On the other hand, when we consider the dynamic capillary pressure model, the equation becomes pseudo-parabolic.

Definition of pseudo-parabolic equation

Pseudo-parabolic equations appear in many areas of physics, for instance, to model imprisoned radiation through a gas [57, 58, 78], fluid flow in fissured rock [9], heat conduction in heterogeneous media [21, 88], out-of-equilibrium viscoelastic relaxation effects [81] and porous media applications [41, 51, 59].

Pseudo-parabolic differential equations are characterized by having mixed time and space derivatives appearing in the highest-order terms [62, 101]. While there is not a single definition in the literature [68, 95, 101], we can define a pseudo-parabolic equation as an arbitrary higher-order partial differential equation with the first-order derivative with respect to time as follows,

$$\frac{\partial}{\partial t} \mathcal{A}(u) + \mathcal{B}(u) = 0. \quad (1.1)$$

where \mathcal{A} and \mathcal{B} are elliptic nonlinear operators. This equation is an example of a general class of equations of Sobolev type, sometimes referred to as Sobolev-Galpern type [62]. It differs from the parabolic equations by the additional higher order terms [101]. According to [68], pseudo-parabolic equations are equations in which the operator $\mathcal{A}(u)$ has a continuous inverse operator in appropriate Banach spaces. In the opposite case, the equation is said to be a Sobolev-type equation.

Showalter and Ting [95] called this class of equation as pseudo-parabolic for two main reasons: first, well posed initial-boundary value problems for parabolic equations are well posed for related pseudo-parabolic equations; second, in certain cases, the solution of an initial-boundary value problem for a parabolic equation can be obtained as the limit of solutions to the corresponding problem for a related class of pseudo-parabolic equations. Therefore, a solution of the parabolic equation can be approximated by a solution of pseudo-parabolic equations [95].

Mathematical analysis

The choice of numerical approximations must be guided by the mathematical nature of the differential model, in order to recover the same physical and mathematical properties of the original continuous problem at the discrete level. Therefore, in connection with the computational modeling, we must consider the recent progresses on mathematical analysis of pseudo-parabolic differential equations, in particular, linked to the two-phase flow in porous media.

The early existence, uniqueness, and regularity theory for pseudo-parabolic equations [93, 94, 95, 101] predicts that the additional pseudo-parabolic term decreases the smoothing property characteristic to parabolic problems. This character has consequences on the behavior of the solution and it was also observed in subsequent works. For instance, if the initial data has jump discontinuity at some point, then so does the solution for every time [24, 25]. In general, there is no maximum principle for pseudo-parabolic equations such as one expected of solutions to parabolic equations [99].

There are some recent results in the literature on existence and uniqueness

of weak solutions for pseudo-parabolic equations that models distinct physical processes. Assuming linearity of the pseudo-parabolic term, existence and uniqueness results can be found in [35, 85] for simplified nonlinear pseudo-parabolic models related to two-phase flow problems in porous media. On the other hand, the existence of weak solutions was studied for degenerate nonlinear pseudo-parabolic problems associated to sorption processes in coal [77] and unsaturated flow in porous media, respectively [76]. In addition, we refer in particular to [17, 18], where the global existence and uniqueness results were obtained for a more comprehensive pseudo-parabolic problem modeling two-phase flow in a porous medium with dynamic capillary pressure.

An important issue about the pseudo-parabolic equations modeling multiphase flow in porous media is the existence and behavior of solutions in the context of traveling waves. Traveling waves solutions for pseudo-parabolic problems linked to unsaturated flow in porous media is analyzed in [23, 24, 80]. On the other hand, in the context of two-phase flow in porous media, the existence and uniqueness of traveling waves solutions were investigated in [31, 32, 97] for pseudo-parabolic Buckley-Leverett models. It is worth mentioning that in [32] the pseudo-parabolic equation is interpreted as a regularization of the hyperbolic Buckley-Leverett equation.

The heterogeneous case of two-phase porous media flow model, in which dynamic effects are taken into account in phase pressure difference is investigated in [33, 67]. In [67], the authors investigate the singular limit as the diffusion and dispersion parameters tend to zero, showing strong convergence towards a weak solution of the limit conservation law. In [33], the authors consider a one-dimensional heterogeneous case, with two adjacent homogeneous blocks separated by an interface. Therefore, the interface conditions coupling the models in each homogeneous block are derived.

The Richards equation with a dynamic capillary pressure including hysteresis is studied in [91], which the authors provided existence and approximation results for degenerate capillary pressure curves.

Numerical approximation

From the point of view of numerical analysis for pseudo-parabolic differential problems, we review the approaches available in the literature in order to better understand the computational aspects related to the approximation of these models. In general, the most used numerical methodologies are finite differences methods, finite volumes methods and finite element methods. These three classes of methods were already exploited for pseudo-parabolic problems.

The finite difference method is regarded as the simplest approach to numerical

solution of differential problems. In [38, 39], finite difference approximations to the solution of a pseudo-parabolic problem are constructed and shown to converge. In [84], the authors consider numerical modeling of unsaturated flow models incorporating dynamic capillary pressure terms. They systematically study the difficulties associated with numerical approximation of such equations using two classes of methods, a cell-centered finite difference method and a locally conservative Eulerian-Lagrangian method based on the finite difference method. A study of finite difference schemes for one-dimensional problems with discontinuous initial data are presented in [25].

Pseudo-parabolic equations modeling fluid flow in porous media arises from conservation laws of some physical quantity, e.g., the mass of fluid. Therefore, finite volume techniques are quite suitable to discretize such equations. In [53], the authors use a semi-implicit upwind finite volume scheme to study the two-phase flow in one-dimensional heterogeneous porous media with dynamic capillary pressure. On the other hand, a fully implicit discretization based on finite volume method is proposed in [41, 42]. In [104], the authors study a finite volume element approximation of pseudo-parabolic equations in three spatial dimensions. Pseudo-parabolic problems may be written in different formulations that are equivalent in a formal point of view, however, they may lead to different numerical schemes. In [36], the authors investigate the equivalence of three different formulations for a class of pseudo-parabolic equations and the corresponding numerical discretizations.

Numerical methods are often used as a auxiliary tool to mathematical analysis of PDEs. In the works [31, 32, 97], finite difference and finite volume numerical schemes are exploited in order to illustrate the solution profile described in the traveling wave analysis for pseudo-parabolic problems in homogeneous porous media. The heterogeneous porous media case is studied in [33], where the authors present some numerical results supporting the theoretical findings for an interface condition between two homogeneous blocks.

Finite element methods constitute a huge and flexible class of numerical techniques suitable to different differential problems. In [34, 37], time-stepping Galerkin methods were proposed for pseudo-parabolic Sobolev models. The nodal superconvergence for a Galerkin method for a quasilinear equation of Sobolev is presented and analyzed in [7]. Interior penalty discontinuous Galerkin scheme are discussed in [65, 66] for a two-phase porous media flow model with dynamic capillary pressure. Fourier spectral methods for pseudo-parabolic equations were analyzed in [86].

Operator splitting techniques for the approximation of solutions of partial differential equations have a long history and have been developed with various objectives in mind (see, e.g., [56]). In porous media application, operator splitting has been used successfully in the numerical approximation of parabolic models of two-phase flow [28]

and, more recently, three-phase flow in porous media [2, 4]. In [84], an operator splitting scheme is used to approximate the Richards' equation with dynamic capillary pressure. In [102], splitting schemes for a pseudo-parabolic equation were analyzed. In [61], the authors propose a fast explicit operator splitting method to solve the modified Buckley-Leverett equations of pseudo-parabolic nature.

Other related models

There is a very interesting connection between pseudo-parabolic and dispersive models, specially with respect to Benjamin-Bona-Mahony (BBM) equation [13], that is an alternative to the Korteweg-de Vries equation for describing unidirectional, long, dispersive waves. This connection arise from the dispersive character associated to the third-order mixed derivative operator found in both differential equations. However, in the best of our knowledge, the relation between pseudo-parabolic and dispersive equations is not clear in the literature and just few works connect this two class of differential models. For instance, Benjamin-Bona-Mahony-Burgers (BBMB) equation is sometimes referred to as pseudo-parabolic or Sobolev-type [7, 34, 45, 92]. This relation is also referenced in [97], where the authors mention the dispersive character of third order derivative introduced in the Buckley-Leverett equation by the rate-dependence of dynamic capillary pressure.

Regarding the new advances on non-equilibrium models for flow in porous media, it must be mentioned that some authors has considered extensions of dynamic capillary pressure model that include further non-equilibrium effects, such as hysteresis. In [12], the authors propose a theoretical capillary pressure model for two-phase flow in porous media including dynamic and hysteretic effects. Concerning this model, analytical existence, instability results and numerical calculations are presented in [89] for flow problems in unsaturated porous media, whereas the uniqueness of weak solutions for a two-phase flow model is demonstrated in [16]. In [90], one and two-dimensional numerical solutions are presented for an alternative non-equilibrium model for a modified Richards equation which incorporates a dynamic hysteretic capillary pressure model. On the other hand, in [96] the authors perform traveling wave analysis for a generalized model of dynamic capillary pressure that incorporates thermodynamically constrained averaging theory (TCAT) capillary pressure.

In [22] the authors point out that a pseudo-parabolic equation can be obtained by Brinkman regularization of the classical Darcy's law in two-phase flow in porous media. Formally applying the Helmholtz operator to the saturation transport equation and using the Brinkman velocity model, they obtain a third-order problem that is very similar to a model of dynamic capillary pressure. They emphasize that two independent mechanisms do lead to very similar regularization terms for the transport equation.

1.2 Motivation and significance of the work

As presented in our brief review, several recent studies about pseudo-parabolic equations in porous media flow problems can be found in the literature in fields of theory, numerics and applications. We emphasize that most works in the literature for the computational modeling of two-phase flow problems considering models for dynamic capillary pressure are restricted to one spatial dimension. Only some few and interesting two-dimensional simulations can be found in the literature, e.g., [66, 84, 89] and thus the need of efforts from the community to enlarge insights on this subject is justified.

Many reliable discretizations have been proposed for the pseudo-parabolic Richards equation modeling unsaturated flow with dynamic capillary pressure – see, for instance, [25, 84]. Despite some similarity with pseudo-parabolic Richards equation, the model considered in this work consists of a pseudo-parabolic Buckley-Leverett equation for the saturation transport coupled with an elliptic pressure-velocity problem. This model arises from governing equations written in phase formulation (see, e.g., [2] and references cited there in), which is appropriated due to its generality with respect to the fundamental constitutive relations as such phase relative permeabilities and capillarity pressure relations. The pseudo-parabolic nature, induced by dynamic capillary pressure, combined with the effects of gravity and discontinuous geologic properties leads to distinct flow regimes, but retains typical flow path situations as such with saturation overshoot and nonmonotone saturation profile.

As previously stated, operator splitting has been used successfully in the numerical approximation of parabolic models of flow in porous media application [2, 4, 28]. In [5], we discussed two numerical schemes based on the operator splitting technique. We found that the standard operator splitting may fail to capture the correct behavior of the solutions. In this sense, the operator splitting must take into account the dispersive-like character in both splitting steps. Thus, here we focus on a non-splitting numerical method which is based on a fully coupled space-time mixed-hybrid finite element and finite volume discretizations.

In the present work, we present a two-dimensional numerical study of two-phase flow in porous media with dynamic capillary pressure taking into account different flow regimes, heterogeneous permeability fields and gravity effects. This is a distinctive point of this work.

1.3 Aims and objectives of the thesis

In general, the aim of this work is the numerical modeling of the two-phase flow in heterogeneous porous media with dynamic effects in capillary pressure. The specific objectives of this work are:

- To formulate a numerical approach for pseudo-parabolic problems based on mixed finite element method;
- To simulate the flow in a two-dimensional domain;
- To study numerically the structure of solution taking into account heterogeneous fields of porosity and permeability;
- To study numerically the combined effects of gravity and dynamic capillary pressure.

1.4 Main results and scientific contributions

In this work, we developed new computational methods to approximate the solution of pseudo-parabolic equations linked to transport phenomena in porous media. We used a space discretization by hybridized mixed finite element method in both elliptic and pseudo-parabolic problems. For the time direction, we applied an implicit strategy. This approach is a two-dimensional extension of the method proposed in [5]. Hybridized mixed finite elements is locally conservative by construction and it is quite adequate for accurate computation of fluxes and velocity fields in the case of heterogeneous porous media transport problems [2, 4, 28].

The hyperbolic operator for the transport problem is approximated by a conservative finite volume numerical flux. Due to the dispersive nature of the pseudo-parabolic equation, and motivated by the numerical hyperbolic flux used in [32] and the good one-dimensional results of [5], we chose a dispersive numeric flux. Thus, we constructed a two-dimensional extension of the Richtmyer scheme for hyperbolic conservation laws. We designed this extension to take advantage of the velocity field approximated by mixed finite elements.

Our strategy of time discretization allowed us to decouple the calculations of the saturation transport problem from the pressure-velocity system. Therefore, the subproblems are solved sequentially. We used an implicit approach to the transport problem leading to a system of nonlinear algebraic equations. The resulting nonlinear algebraic problem is solved by a simple fixed-point iterative procedure. Thus, we avoided more sophisticated techniques, such as the Newton method. Our numerical experiments showed

that the fixed-point iteration is robust and effective alternative to solve the nonlinear systems.

We performed a dimensional analysis of the governing system of equations and identified the main dimensionless groups, which allowed us guide the numerical experiments in order to study the different physical effects and flow regimes. As a result, we investigated the interaction between gravity and dynamic capillary effects combined with heterogeneous permeability fields. Our numerical results suggest the viability and accuracy of the proposed approach. The mesh refinement study suggested a first-order numerical convergence.

The scientific learning of this work embraces the Computational and Applied Mathematics in the fields of Numerical Analysis and Computational Simulation of physical processes. The main scientific works generated by the current thesis are listed as follows:

- The article “Computing numerical solutions of the pseudo-parabolic Buckley-Leverett equation with dynamic capillary pressure”, published in the journal *Mathematics and Computers in Simulation* [5];
- The submitted manuscript “Numerical resolution of a pseudo-parabolic Buckley-Leverett model with gravity and dynamic capillary pressure in heterogeneous porous media”.

1.5 Overview of the thesis

The rest of this manuscript is organized as follows: Chapter 2 presents the mathematical model of two-phase flow problem in porous media; Chapter 3 presents the numerical study of two operator splitting approaches applied to a one-dimensional pseudo-parabolic problem; in Chapter 4, we describe the numerical approach based on mixed finite element discretization; in Chapter 5, we report our numerical results on the performance of the proposed method for homogeneous and heterogeneous media; We present some concluding remarks and perspectives for future works in Chapter 6. In addition, in the Appendix A, we present a preliminary stability analysis for the one-dimensional linear pseudo-parabolic problem. Appendix B discusses a finite difference scheme for the pseudo-parabolic problem. Finally, we present further one-dimensional numerical experiments in Appendix C.

Chapter 2

Mathematical model of two-phase flow in porous media with dynamic capillary pressure

In this chapter, we present the governing equations of the two-phase flow in porous media with dynamic capillary pressure. The equations governing the fluid flow with dynamic capillary pressure in two dimensions can be described using phase formulation by a pseudo-parabolic transport equation coupled with a pressure-velocity problem of elliptic nature. The pseudo-parabolic equation comes with the inclusion of the dynamic capillary pressure model.

The two-phase flow model considered herein takes into account capillary forces, general expressions for the relative permeability functions, variable porosity and permeability fields and gravity effects.

2.1 Governing equations

In the discussion of the governing equations we consider two-dimensional flow of two immiscible and incompressible fluid phases in heterogeneous porous media. We also assume that there are no internal sources or sinks, mass transfer between phases and thermal effects are neglected.

We indicate the wetting phase and the non-wetting phase by the subscripts w and n , respectively. Thus, we denote by S_w and S_n the saturations of the fluid phases. We assume that they occupy the whole pore space, i.e.,

$$S_w + S_n = 1. \tag{2.1}$$

To describe the two-dimensional flow, we consider a domain $\Omega \subset \mathbb{R}^2$ with

Lipschitz boundary. Then, the conservation of mass for each phase is given by,

$$\frac{\partial}{\partial t}(\phi \rho_\alpha S_\alpha) + \nabla \cdot (\rho_\alpha \mathbf{v}_\alpha) = 0, \quad \mathbf{x} \in \Omega, \quad t \geq 0, \quad \alpha = w, n, \quad (2.2)$$

where, for phase α , S_α is the saturation, ρ_α is the mass density, \mathbf{v}_α is the seepage velocity and ϕ is the rock porosity.

According to an extension of Darcy's law for two-phase flow in a porous medium, the seepage velocity of phase α is given by,

$$\mathbf{v}_\alpha = -K \frac{k_\alpha}{\mu_\alpha} \rho_\alpha (\nabla p_\alpha - \rho_\alpha \mathbf{g} \nabla Z), \quad \mathbf{x} \in \Omega, \quad t \geq 0, \quad \alpha = w, n, \quad (2.3)$$

where K is the absolute permeability of the rock, which measures its capability of allowing the flow of a pure fluid. The magnitude of gravity is \mathbf{g} and Z is the depth. For each phase α , k_α is a dimensionless function of saturation, measured in the laboratory, and μ_α is the viscosity and p_α denotes the pressure of phase α .

For two-phase flow model it is natural that each phase exhibits a distinct pressure. The pressure difference between the non-wetting phase and wetting phase is called the capillary pressure which is given by an equation of state:

$$p_c = p_n - p_w, \quad (2.4)$$

In standard multiphase flow models on porous media, a capillary pressure relationship developed under static conditions is assumed. In the classical models, capillary pressure is a function of wetting phase saturation, i.e.,

$$p_c = p_e(S_w), \quad (2.5)$$

The function $p_e(S_w)$ is called static capillary pressure model. On the basis of experimental measurements, a monotonically decreasing relationship between p_e and S_w can be determined. Hassanizadeh and Gray [51] proposed a model that takes the dynamics into account by letting the capillary pressure p_c depend on the time derivative of the water saturation S_w . Thus, we consider the model for dynamic capillary pressure given by,

$$p_c = p_e(S_w) - \tau_H \frac{\partial}{\partial t}(\phi S_w) \quad (2.6)$$

with τ being a positive parameter, which is called dynamic effect coefficient. In general models, τ may depend on S_w . The function $p_e(S_w)$ is the same static capillary pressure model (2.5).

2.2 Phase formulation

In order to solve the fundamental governing equations numerically, we rewrite equations such that its mathematical nature is better understood. Thus, let us first introduce the following auxiliary variables, i.e., the relative mobilities, the total mobility, the fractional flow functions of the phase α , respectively:

$$\lambda_\alpha = \frac{k_\alpha}{\mu_\alpha}, \quad \lambda = \lambda_w + \lambda_n, \quad f_\alpha = \frac{\lambda_\alpha}{\lambda}. \quad (2.7)$$

We define the total velocity as the sum of the velocities of the two phases:

$$\mathbf{v} = \mathbf{v}_w + \mathbf{v}_n. \quad (2.8)$$

After algebraic manipulations, the governing systems of equations can be rewritten in volumetric form in a so-called phase formulation [19],

$$\frac{\partial}{\partial t}(\phi S_w) + \nabla \cdot \left[\mathbf{v} f_w + K \lambda_w f_n (\rho_w - \rho_n) \mathbf{g} \nabla Z \right] = -\nabla \cdot \left[K \lambda_w f_n \nabla p_c \right]. \quad (2.9)$$

The pressure-velocity system is obtained by adding, respectively, the conservation equations (2.2) and the Darcy's law (2.3) for the two phases. Thus, the pressure-velocity system reads:

$$\nabla \cdot \mathbf{v} = 0, \quad \mathbf{v} = -K \lambda \nabla p_n + K \lambda_w \nabla p_c + K (\lambda_w \rho_w + \lambda_n \rho_n) \mathbf{g} \nabla Z. \quad (2.10)$$

To complete the mathematical model we need to specify boundary and initial conditions. The boundary conditions and initial conditions will be introduced in the description of the numerical simulations in Chapter 5. We are setting up to calculate fluid flows on a rectangular domain, but more general domains and other boundary conditions can be treated by our techniques.

2.3 Dimensional analysis

Equations (2.9)-(2.10) can be nondimensionalized by identifying characteristic values for each variable [74]. So consider the characteristic values for length L_c , velocity

u_c , porosity ϕ_c , absolute permeability K_c and capillary pressure p_{cc} . We set:

$$\begin{aligned} t^* &= \frac{t u_c}{L_c}, & \mathbf{x}^* &= \frac{\mathbf{x}}{L_c}, & Z^* &= \frac{Z}{L_c}, & \nabla^* &= L_c \nabla, & \phi^* &= \frac{\phi}{\phi_c} \\ K^* &= \frac{K}{K_c}, & \mathbf{v}^* &= \frac{\mathbf{v}}{u_c}, & p_n^* &= \frac{p_n}{p_{cc}}, & p_c^* &= \frac{p_c}{p_{cc}}, & p_e^* &= \frac{p_e}{p_{cc}}. \end{aligned} \quad (2.11)$$

Following [74], we identify three important dimensionless groups, i.e., the capillary number N_{Ca} , the gravity number N_{Gr} and the dynamic effect number N_{Dy} . They are given by,

$$N_{Ca} = \frac{K_c p_{cc}}{\mu_w u_c L_c}, \quad N_{Gr} = \frac{K_c \rho_w g}{\mu_w u_c}, \quad N_{Dy} = \frac{\tau_H u_c}{p_{cc} L_c \phi_c}, \quad (2.12)$$

where the capillary number N_{Ca} is interpreted as the ratio of equilibrium capillary to viscous force; the gravity number N_{Gr} represents the ratio of gravitational to viscous force; finally, the ‘‘dynamic effect number’’ N_{Dy} is interpreted as the ratio of dynamic capillary to equilibrium capillary force. We also identify the viscosity and density ratios,

$$R_\mu = \frac{\mu_w}{\mu_n}, \quad R_\rho = \frac{\rho_w}{\rho_n}. \quad (2.13)$$

Remark 2.3.1. In [74], besides N_{Dy} , the authors define another dimensionless group related to dynamic capillary force. The other number is called ‘‘dynamic number’’ and represents the ratio between dynamic capillary to viscous force. We can obtain this other number by the product $N_{Ca} N_{Dy}$. We choose to write the dimensionless equations in terms of N_{Dy} .

Thus, after nondimensionalizing, the two-phase system reads:

$$\begin{aligned} \frac{\partial}{\partial t^*}(\phi^* S_w) + \nabla^* \cdot \left[\mathbf{v}^* f_w + N_{Gr} K^* k_w f_n (1 - R_\rho^{-1}) \nabla^* Z^* \right] = \\ -N_{Ca} \nabla^* \cdot \left[K^* k_w f_n \nabla^* p_c^* \right], \end{aligned} \quad (2.14a)$$

$$\nabla^* \cdot \mathbf{v}^* = 0, \quad (2.14b)$$

$$\begin{aligned} \mathbf{v}^* = -N_{Ca} K^* (k_w + R_\mu k_n) \nabla^* p_n^* + N_{Ca} K^* k_w \nabla^* p_c^* \\ + N_{Gr} K^* (k_w + R_\mu R_\rho^{-1} k_n) \nabla^* Z^*, \end{aligned} \quad (2.14c)$$

$$p_c^* = p_e^*(S_w) - N_{Dy} \frac{\partial}{\partial t^*}(\phi^* S_w). \quad (2.14d)$$

Note that K^* and ϕ^* stand for the heterogeneous parts of the permeability and porosity fields, respectively.

2.4 Computational modeling of the flow equations

From now on, we drop the superscript $*$ to indicate the nondimensionalized quantities. For simplicity of notation, we rewrite the governing equations. The saturation transport problems is written as follows,

$$\frac{\partial}{\partial t}(\phi S_w) + \nabla \cdot \mathbf{F}(\mathbf{v}, S_w) = -\nabla \cdot [H_c(S_w) \nabla p_c], \quad (2.15a)$$

$$p_c = p_e(S_w) - \tau \frac{\partial}{\partial t}(\phi S_w), \quad (2.15b)$$

where $\tau = N_{Dy}$, the term H_c is the capillary induced diffusion function and $\mathbf{F}(\mathbf{u}, S_w)$ is the convection flux and they are defined by,

$$H_c(S_w) = N_{Ca} K(\mathbf{x}) k_w(S_w) f_n(S_w), \quad (2.16a)$$

$$\mathbf{F}(\mathbf{v}, S_w) = \mathbf{v} f_w(S_w) + N_{Gr} K(\mathbf{x}) k_w(S_w) f_n(S_w) [1 - R_\rho^{-1}] \nabla Z. \quad (2.16b)$$

We write the pressure-velocity system as,

$$\nabla \cdot \mathbf{v} = 0, \quad \mathbf{v} = -H_n(S_w) \nabla p_n + \mathbf{v}_c + \mathbf{v}_G, \quad (2.17)$$

where the coefficient $H_n(S_w)$ is given by,

$$H_n(S_w) = N_{Ca} K(\mathbf{x}) [k_w(S_w) + R_\mu k_n(S_w)]. \quad (2.18)$$

The terms \mathbf{v}_c and \mathbf{v}_G are correction velocities linked to the capillary pressure and gravity effects, respectively. They are given by,

$$\mathbf{v}_c = N_{Ca} K(\mathbf{x}) k_w(S_w) \nabla p_c, \quad (2.19a)$$

$$\mathbf{v}_G = N_{Gr} K(\mathbf{x}) [k_w(S_w) + R_\mu R_\rho^{-1} k_n(S_w)] \nabla Z. \quad (2.19b)$$

Note that, when we consider the static capillary model (2.5), the transport equation (2.15a) has a parabolic nature. On the other hand, if we assume the dynamic model (2.6), the equation (2.15a) becomes pseudo-parabolic and a third order mixed derivative appears in the diffusive flux.

Chapter 3

Numerical study of operator splitting techniques applied to the pseudo-parabolic problem

In this chapter, we discuss two operator splitting strategies to approach the one-dimensional pseudo-parabolic equation. Operator splitting techniques for the approximation of solutions of systems of partial differential equations arising in many fields of application have a long history and have been developed with various objectives in mind; see, e.g., [56] for an excellent survey of the use of operator splitting techniques along with rigorous analysis. After splitting the differential operators, it is not a simple task to define the local approximations and correction strategies in order to account and control the nonlinear error. For a comprehensive list of works where distinct successful procedures were developed on separating the underlying physical processes, see [2, 4, 28, 30, 43, 64], and the references cited therein.

We consider the following pseudo-parabolic equation defined on an one-dimensional domain $\Omega = (a, b)$,

$$\frac{\partial}{\partial t}(\phi S) + \frac{\partial F(S)}{\partial x} = -\frac{\partial}{\partial x} \left(H(S) \frac{\partial}{\partial x} \left(p_\epsilon(S) - \tau \frac{\partial}{\partial t}(\phi S) \right) \right), \quad x \in \Omega, \quad t > 0, \quad (3.1)$$

along with the initial and boundary conditions,

$$S(x, 0) = \eta(x), \quad x \in \Omega, \quad (3.2)$$

$$S(a, t) = S_L, \quad S(b, t) = S_R, \quad t > 0. \quad (3.3)$$

Eq. (3.1) represents a one-dimensional version of the transport problem (2.15) linked to the two-phase flow in porous media with dynamic capillary pressure.

3.1 Operator splitting based on advective and diffusive processes

In our first splitting scheme, we take into account convection and diffusion effects separately. This approach has been used successfully in the numerical approximation of parabolic models of two-phase flow [28] and, more recently, three-phase flow in porous media [2, 4] with static capillary pressure (2.5). In [84], an operator splitting scheme is used to approximate the Richards' equation with dynamic capillary pressure. Those studies are a motivation to apply this approach to the pseudo-parabolic two-phase flow model as well. Thus, consider a splitting of the pseudo-parabolic model (3.1) as follows:

$$\frac{\partial}{\partial t}(\phi\tilde{S}) + \frac{\partial F(\tilde{S})}{\partial x} = 0, \quad (3.4a)$$

$$\frac{\partial}{\partial t}(\phi\hat{S}) = -\frac{\partial}{\partial x} \left(H(\hat{S}) \frac{\partial}{\partial x} \left(p_e(\hat{S}) - \tau \frac{\partial}{\partial t}(\phi\hat{S}) \right) \right). \quad (3.4b)$$

So we solve the advection problem and the diffusion problem sequentially. Note that the first equation in (3.4) is a first order hyperbolic equation, so we can use explicit strategies to solve this subproblem. On the other hand, the second equation in (3.4) is a third order differential equation of pseudo-parabolic type. Thus, for this subproblem it is better to use an implicit approach.

Let us introduce the time step Δt . We take $t_n = n\Delta t$, and the integer N defines the total simulation time T . Then, the algorithm is defined as follows:

1. Let $t_n = n\Delta t$ and assume that S is known for $t < t_n$.
2. For $t \in [t_n, t_{n+1}]$, solve the convection problem given by:

$$\frac{\partial}{\partial t}(\phi\tilde{S}) + \frac{\partial F(\tilde{S})}{\partial x} = 0, \quad (3.5)$$

with initial condition given by $\tilde{S}(x, t_n) = S(x, t_n)$.

3. Compute the diffusive effects on $[t_n, t_{n+1}]$ by solving the equation

$$\frac{\partial}{\partial t}(\phi\hat{S}) = -\frac{\partial}{\partial x} \left(H(\hat{S}) \frac{\partial}{\partial x} \left(p_e(\hat{S}) - \tau \frac{\partial}{\partial t}(\phi\hat{S}) \right) \right), \quad (3.6)$$

with initial condition $\hat{S}(x, t_n) = \tilde{S}(x, t_{n+1})$.

4. Set $S(x, t_{n+1}) = \hat{S}(x, t_{n+1})$.

Numerical scheme

For the purpose of numerical simulation, we solve each subproblem using finite difference schemes. These schemes are based on the numerical method presented in [32] to solve the complete model (3.1) with linear high order terms. Similar schemes are also used in [36, 84].

For brevity, let us limit ourselves to a very short description of the numerical method. The first and second order spatial differential operators are approximated by standard centered finite differences, and the time differential operators are discretized by backward Euler formula. The first order term is explicit, i.e., evaluated at t_n , and the high order derivatives are the implicit terms, i.e., evaluated at t_{n+1} . To avoid the solution of nonlinear algebraic systems, the nonlinear coefficients of high order terms are linearized by taking the values in time t_n .

Here, for simplicity, we present a discretization for the complete model (3.1). We use the same ideas for each step of the operator splitting approach. Consider a uniform partition of Ω into cells Ω_i , for $i = 1, \dots, M$, with length Δx and center denoted by x_i . Let S_i^n be a finite difference approximation for $S(x_i, t_n)$. A discretization of (3.1) by the finite difference method is given by,

$$\phi_i \frac{S_i^{n+1} - S_i^n}{\Delta t} + \frac{F_{i+1/2}^n - F_{i-1/2}^n}{\Delta x} = \frac{W_{i+1/2}^{n+1} - W_{i-1/2}^{n+1}}{\Delta x} \quad (3.7)$$

where the approximations of the convective and diffusive fluxes are given by,

$$F_{i+1/2}^n = F(S_i^n), \quad (3.8a)$$

$$W_{i+1/2}^{n+1} = D_{i+1/2}^n \left(\frac{S_{i+1}^{n+1} - S_i^{n+1}}{\Delta x} \right) + \frac{C_{i+1/2}^n}{\Delta t} \left(\frac{S_{i+1}^{n+1} - S_i^{n+1}}{\Delta x} - \frac{S_{i+1}^n - S_i^n}{\Delta x} \right), \quad (3.8b)$$

where $D(S) = -H(S) p'_e(S)$ and $C(S) = \tau H(S)$. The coefficients are chosen as the arithmetic mean at interfaces [36]. Because of the advective term, the time step is determined by a necessary Courant-Friedrichs-Levy (CFL) condition for stability,

$$\frac{\Delta t}{\Delta x} \max_{S \in [0,1]} \{|F'(S)|\} < \sigma_{\text{CFL}}, \quad (3.9)$$

where σ_{CFL} is a positive constant.

In Appendix B we present a two-dimensional finite difference scheme for approximation of the two-phase flow in porous media with dynamic capillary pressure. For more details of the constructions of such one-dimensional finite difference schemes, we refer [32, 36].

Numerical experiments

To discuss the viability of this approach, we present some numerical experiments based on numerical results presented in [36]. Here, we consider the case with linear high order terms, where we take the diffusion function $H(S)$ to be identically 1. Following [36], we take $p_e(S) = -S$. The hyperbolic flux function is the Buckley-Leverett flux,

$$F(S) = \begin{cases} 0, & S < 0 \\ \frac{S^2}{S^2 + 2(1 - S)^2}, & 0 \leq S \leq 1, \\ 1, & S > 1. \end{cases} \quad (3.10)$$

The initial value for all examples is a Riemann data defined by,

$$\eta(x) = \begin{cases} S_L, & x \leq 0, \\ S_R, & x \geq 0, \end{cases} \quad (3.11)$$

with consistent boundary values S_L and S_R . We simulate the cases for $\tau = 5$ and $S_R = 0$ with two different inflow values: $S_L = 0.9$ and $S_L = 0.55$. The computation time is $T = 150$ and the computational domain is $(-60, 210)$.

Figure 3.1 shows the mesh refinement study for the operator splitting scheme. The first solution ($S_L = 0.9$) presents a nonmonotone profile with a plateau value [32, 36]. For the second case ($S_R = 0.55$), the profile presents damped oscillations. The reference solution is obtained from the numerical scheme presented in [32] with relatively large number of 1024 cells. This reference solution is in agreement with the theoretical analysis [32]. We can see that this operator splitting approach seems to not converge to the correct solution by means of mesh refinement. Moreover, the qualitative structure of the solution is not recovered. Figure 3.1 shows numerical solutions with up to 512 cells, but more refined meshes were used in our experiments and the solutions present the same incorrect profile.

In the Figure 3.1, we take the time step Δt using (3.9) with $\sigma_{\text{CFL}} = 0.5$ for all simulations. However, it is well-known that the error in operator splitting techniques always depends on Δt . Thus, we performed tests with smaller Δt for a fixed mesh with 512 cells. First we decrease the parameter σ_{CFL} from 0.5 to 0.001. After, we set $\Delta t = \sigma \Delta x^2$ and we repeated the tests with decreasing σ from 1 to 0.01. The computed numerical solutions are not in good agreement with the exact solutions from the literature and exhibit the same incorrect profiles.

In [84], the authors compared several numerical methods for pseudo-parabolic models linked to porous media flow with dynamic capillary pressure. They used operator splitting schemes as well as unsplit approaches. One of those methods based on operator splitting consists on a variant of LCELM (Locally Conservative Eulerian-Lagrangian

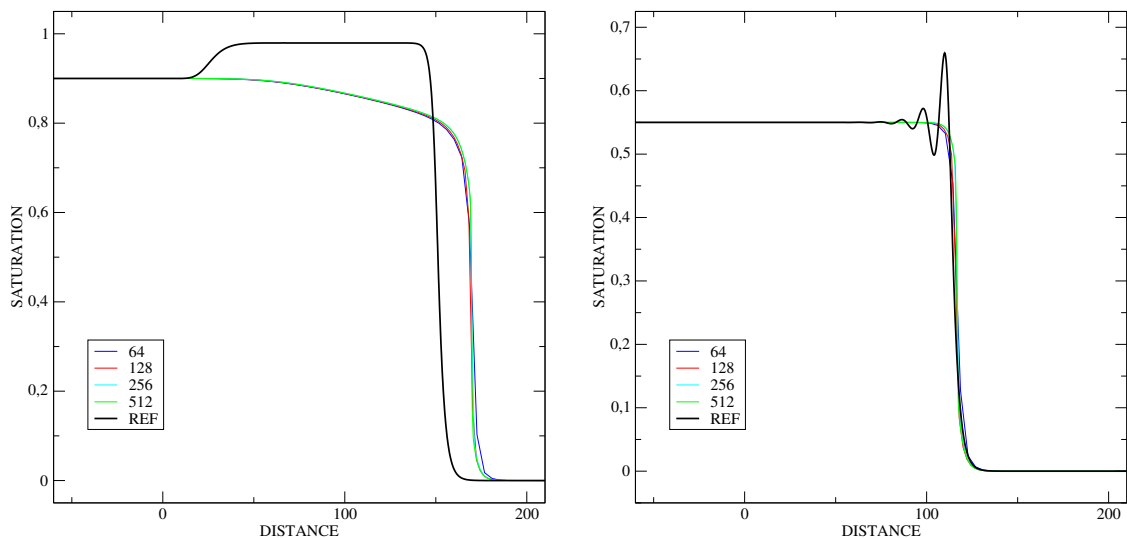


Figure 3.1: Mesh refinement study to the first operator splitting approach, with $\tau = 5$, $S_R = 0$ and two different left values: (left) $S_L = 0.9$ and (right) $S_L = 0.55$. Number of cells used in the meshes: 64, 128, 256 and 512. The reference solution (REF) is obtained with numerical scheme from [32] with 1024 cells.

Method). Such variant decomposes the pseudo-parabolic equation similarly to (3.4). The numerical approximations obtained from this splitting approach in [84], similarly we found in Fig. 3.1, does not agree with unsplit schemes. On the other hand, Pesynska [84] presented a correction of the operator splitting LCELM scheme as well. The numerical results of this corrected LCELM scheme agrees with the unsplit schemes. In the next section, we will also present a corrected operator splitting scheme, but in a different approach from that used in [84]. We also point out that the nonmonotone profiles of the solutions were not well understood in [84].

In our current understanding, the operator splitting decomposition technique affects the interaction between the various differential operators and the dispersive-like character is lost. Moreover, when applied to the pseudo-parabolic equation (3.1), this operator splitting approach decompose the time derivative term, unlike what occurs for parabolic model. In other words, when we deal with a parabolic equation and we apply the operator splitting technique in order to decompose the physical effects of convection and diffusion, only the space differential term is split into two. However, in the case of two-phase flow pseudo-parabolic equation with convection first order term, there are two terms with time derivatives: the accumulation term and the dynamic term in the capillary pressure. When we try to use the same idea and decompose those two physical effects, the purely hyperbolic step of operator splitting technique lacks the time derivative from the dynamic term.

To highlight the effects of the operator splitting technique, we consider a

particular case of pseudo-parabolic equation (3.1) with linear high order terms:

$$\frac{\partial S}{\partial t} + \frac{\partial F(S)}{\partial x} = \varepsilon \frac{\partial^2}{\partial x^2} \left(S + \tau \frac{\partial S}{\partial t} \right), \quad \varepsilon > 0, \tau > 0, \quad (3.12)$$

which can be written as

$$\frac{\partial}{\partial t} \left(S - \varepsilon \tau \frac{\partial^2 S}{\partial x^2} \right) + \frac{\partial F(S)}{\partial x} - \varepsilon \frac{\partial^2 S}{\partial x^2} = 0. \quad (3.13)$$

We can see the time derivative term is $(S - \varepsilon \tau S_{xx})_t$. Now, if we use the first operator splitting approach, we will obtain the two steps:

$$\frac{\partial \tilde{S}}{\partial t} + \frac{\partial F(\tilde{S})}{\partial x} = 0, \quad \frac{\partial \hat{S}}{\partial t} = \varepsilon \frac{\partial^2}{\partial x^2} \left(\hat{S} + \tau \frac{\partial \hat{S}}{\partial t} \right), \quad (3.14)$$

which can be written as

$$\frac{\partial \tilde{S}}{\partial t} + \frac{\partial F(\tilde{S})}{\partial x} = 0, \quad \frac{\partial}{\partial t} \left(\hat{S} - \varepsilon \tau \frac{\partial^2 \hat{S}}{\partial x^2} \hat{S}_{xx} \right) - \varepsilon \frac{\partial^2 \hat{S}}{\partial x^2} = 0. \quad (3.15)$$

Thus, we can see that the first step has a ‘‘incomplete’’ term in the time derivative that affects the dispersion relation. In first order hyperbolic equation, waves of different wavelengths have the same propagation velocities, thus the solution did not present dispersion behavior. On the other hand, pseudo-parabolic equations without convection term represents a controlled diffusion process. Although this argument is not rigorous, we believe that it is closely related to the failure of this approach. In [63] and [64] the authors present strategies to correct the operator splitting technique for nonlinear parabolic equations.

Figure 3.1 shows the distinct numerical example in which the standard splitting may fail if a nonlinear balance dispersive term linked to the full pseudo-parabolic Buckley-Leverett model with dynamic capillary pressure model (3.1)-(3.3) is not properly handled. Therefore, this motivates us to study another operator splitting approach.

3.2 Operator splitting based on dispersive-like character

The second proposed splitting scheme for the pseudo-parabolic (3.1)-(3.3) takes into account the dispersive-like character in both subproblems. Thus, we consider the

following splitting of the pseudo-parabolic equation (3.1),

$$\frac{\partial}{\partial t}(\phi\tilde{S}) + \frac{\partial F(\tilde{S})}{\partial x} = \frac{\partial}{\partial x} \left(H(\tilde{S}) \frac{\partial}{\partial x} \left(\tau \frac{\partial}{\partial t}(\phi\tilde{S}) \right) \right), \quad (3.16a)$$

$$\frac{\partial}{\partial t}(\phi\hat{S}) = -\frac{\partial}{\partial x} \left(H(\hat{S}) \frac{\partial}{\partial x} \left(p_e(\hat{S}) - \tau \frac{\partial}{\partial t}(\phi\hat{S}) \right) \right). \quad (3.16b)$$

Note the presence of the third order mixed derivative in both equations. The first equation (3.16) looks like a nonlinear BBM equation and the second equation in (3.16) is a pseudo-parabolic equation without convection term. A similar procedure is investigated in [106] for a BBM-type equation and in [61] for a modified Buckley–Leverett equations, both with constant coefficients in high order terms.

Similarly to the previous approach, the numerical algorithm is defined as follows:

1. Let $t_n = n\Delta t$ and assume that S is known for $t < t_n$.
2. For $t \in [t_n, t_{n+1}]$, solve the problem given by:

$$\frac{\partial}{\partial t}(\phi\tilde{S}) + \frac{\partial F(\tilde{S})}{\partial x} = \frac{\partial}{\partial x} \left(H(\tilde{S}) \frac{\partial}{\partial x} \left(\tau \frac{\partial}{\partial t}(\phi\tilde{S}) \right) \right), \quad (3.17)$$

with initial condition given by $\tilde{S}(x, t_n) = S(x, t_n)$.

3. Compute the diffusive effects on $[t_n, t_{n+1}]$ by solving the equation

$$\frac{\partial}{\partial t}(\phi\hat{S}) = -\frac{\partial}{\partial x} \left(H(\hat{S}) \frac{\partial}{\partial x} \left(p_e(\hat{S}) - \tau \frac{\partial}{\partial t}(\phi\hat{S}) \right) \right), \quad (3.18)$$

with initial condition $\hat{S}(x, t_n) = \tilde{S}(x, t_{n+1})$.

4. Set $S(x, t_{n+1}) = \hat{S}(x, t_{n+1})$.

Numerical experiments

Here we present the numerical experiments for the second operator splitting approach. To approximate the solution of each subproblem, we use finite difference schemes based on the same ideas presented in the previous section. As in the previous simulations presented in the Figure 3.1, we take here the time step Δt using (3.9) with $\sigma_{\text{CFL}} = 0.5$. We study the same test cases and Figure 3.2 shows the mesh refinement. Overall, the numerical method was able to capture the correct behavior of the solutions reported in the literature.

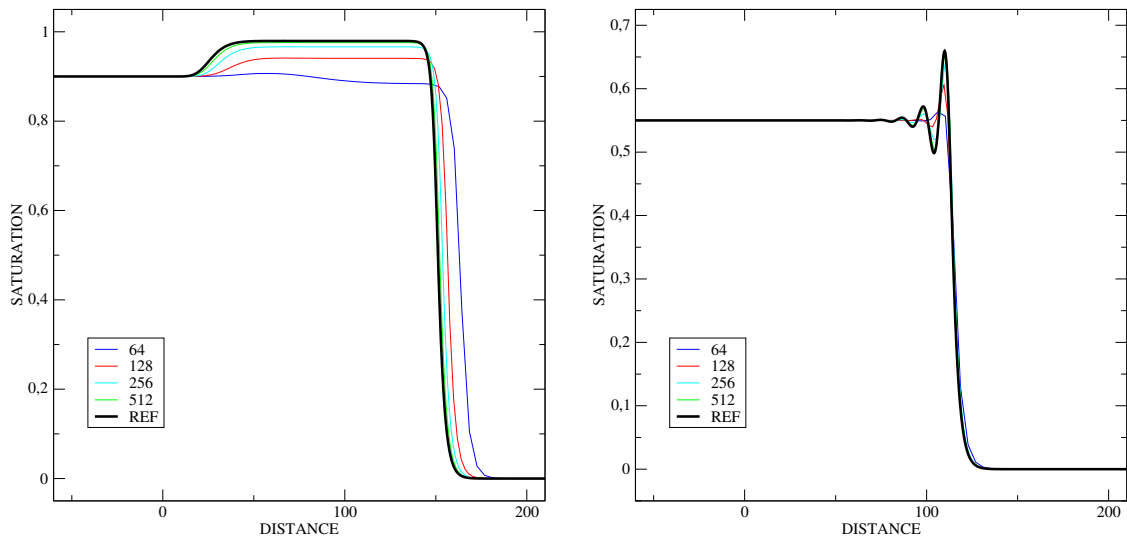


Figure 3.2: Mesh refinement study to the second operator splitting approach, with $\tau = 5$, $S_R = 0$ and two different left values: (left) $S_L = 0.9$ and (right) $S_L = 0.55$. Number of cells used in the meshes: 64, 128, 256 and 512. The reference solution (REF) is obtained with numerical scheme from [32] with 1024 cells.

Although this approach seems more successful, the goal of computational efficiency has not been reached yet. In our implementation, we use implicit strategies for both subproblems. Thus, the solution of each subproblem (3.17) and (3.18) is as expensive as the solution of the complete problem (3.1). However, this is still a point to be better explored in a future work.

Since, in our simulations, operator splitting techniques did not show good features for this class of pseudo-parabolic equations, from now on we propose an efficient approach not based on operator splitting.

Chapter 4

Mixed finite element approximation for the pseudo-parabolic two-phase flow problem

In this chapter, we present the numerical approach to approximate the governing equations (2.15)-(2.19). The numerical scheme is based on the mixed-hybrid finite element and finite volumes schemes along with a implicit time discretization. We use the ideas of one-dimensional approach presented in [5] and we extend this framework to two spatial dimensions.

We remark that the pressure-velocity (2.17) and saturation transport (2.15) systems compose a strongly coupled nonlinear problem. Though, by taking an explicit approximation for hyperbolic flux (2.16b), we separate the calculation of pressure-velocity problem from the pseudo-parabolic transport equation. Thus we solve these problems sequentially. Similar ideas are present in some operator splitting techniques [2, 3, 75] and IMPES (Implicit Pressure Explicit Saturation) strategies.

4.1 Approximation by mixed finite elements

We now turn our attention to the continuous-time mixed finite element approximations to the elliptic and to the pseudo-parabolic problems. For the convenience of readers, let us write the transport system (2.15a)-(2.15b) again,

$$\frac{\partial}{\partial t}(\phi S_w) + \nabla \cdot \mathbf{F}(\mathbf{v}, S_w) = -\nabla \cdot [H_c(S_w) \nabla p_c], \quad (4.1a)$$

$$p_c = p_e(S_w) - \tau \frac{\partial}{\partial t}(\phi S_w) \quad (4.1b)$$

Now, from the particular form of the dynamic capillary pressure (4.1b) and the transport equation (4.1a), we can obtain a nonlinear reaction-diffusion elliptic equation

for p_c [5, 25, 36],

$$-\nabla \cdot [H_c(S_w) \nabla p_c] + \frac{1}{\tau} p_c = \nabla \cdot \mathbf{F}(\mathbf{v}, S_w) + \frac{1}{\tau} p_e(S_w), \quad (4.2)$$

Thus, we can write an equivalent differential system given by,

$$\frac{\partial}{\partial t}(\phi S_w) + \nabla \cdot \mathbf{F}(\mathbf{v}, S_w) = -\nabla \cdot [H_c(S_w) \nabla p_c], \quad (4.3a)$$

$$-\nabla \cdot [H_c(S_w) \nabla p_c] + \frac{1}{\tau} p_c = \nabla \cdot \mathbf{F}(\mathbf{v}, S_w) + \frac{1}{\tau} p_e(S_w), \quad (4.3b)$$

This formulation is equivalent to (4.1a)-(4.1b) from a formal point of view. For the equivalence proof for similar formulations we mention [36].

To solve the elliptic equation (4.3b) using mixed element method, first we identify a diffusive-gradient flux \mathbf{w} linked to capillary pressure. Thus, we can rewrite Eq. (4.2) in its mixed form given by,

$$\mathbf{w} = -H_c(S_w) \nabla p_c, \quad (4.4a)$$

$$\nabla \cdot \mathbf{w} + \frac{1}{\tau} p_c = \nabla \cdot \mathbf{F} + \frac{1}{\tau} p_e(S_w). \quad (4.4b)$$

Note that (4.4) is still linked to an evolution equation for saturation. First, we use mixed finite elements to approximate the pair (\mathbf{w}, p_c) . The value of the capillary pressure is then used to calculate the water saturation by solving the time evolution equation (4.3a) by the implicit method.

Without loss of generality, consider a rectangular domain $\Omega = (x_a, x_b) \times (y_a, y_b) \in \mathbb{R}^2$. We consider the following boundary conditions,

$$\mathbf{w} \cdot \mathbf{n} = w_b \text{ on } \Gamma_w^N, \quad S_w = S_{wb} \text{ on } \Gamma_w^D, \quad (\mathbf{F} - \mathbf{w}) \cdot \mathbf{n} = v_{wb} \text{ on } \Gamma_w^R, \quad (4.5a)$$

$$\mathbf{v} \cdot \mathbf{n} = v_b \text{ on } \Gamma_n^N, \quad p_n = p_{nb} \text{ on } \Gamma_n^D, \quad (4.5b)$$

where we have

$$\partial\Omega = \overline{\Gamma_n^N} \cup \overline{\Gamma_n^D} = \overline{\Gamma_w^N} \cup \overline{\Gamma_w^R} \cup \overline{\Gamma_w^D} \quad (4.6)$$

$$\Gamma_n^N \cap \Gamma_n^D = \Gamma_w^N \cap \Gamma_w^R = \Gamma_w^N \cap \Gamma_w^D = \Gamma_w^R \cap \Gamma_w^D = \emptyset.$$

We denote by \mathbf{n} the unit outer vector normal to domain boundary. For the system (4.4), we have to impose a value of capillary pressure p_c on Γ_w^D consistent with the Dirichlet

condition for saturation,

$$p_c = p_{cb} = p_e(S_{wb}) \quad \text{on } \Gamma_w^D. \quad (4.7)$$

Also, consider the spaces

$$\begin{aligned} V_c &= \left\{ \tilde{\mathbf{v}} \in H(\text{div}; \Omega) : \tilde{\mathbf{v}} \cdot \mathbf{n} = w_b \text{ on } \Gamma_w^N \right\} & W_c &= L^2(\Omega) \\ V_{c0} &= \left\{ \tilde{\mathbf{v}} \in H(\text{div}; \Omega) : \tilde{\mathbf{v}} \cdot \mathbf{n} = 0 \text{ on } \Gamma_w^N \right\} \end{aligned} \quad (4.8a)$$

$$\begin{aligned} V_n &= \left\{ \tilde{\mathbf{v}} \in H(\text{div}; \Omega) : \tilde{\mathbf{v}} \cdot \mathbf{n} = v_b \text{ on } \Gamma_n^N \right\} & W_n &= L^2(\Omega) \\ V_{n0} &= \left\{ \tilde{\mathbf{v}} \in H(\text{div}; \Omega) : \tilde{\mathbf{v}} \cdot \mathbf{n} = 0 \text{ on } \Gamma_n^N \right\} \end{aligned} \quad (4.8b)$$

The weak mixed formulation for (4.4) is given by seeking $(\mathbf{w}, p_c) \in V_c \times W_c$ such that:

$$\left(H_c^{-1} \mathbf{w}, \tilde{\mathbf{v}} \right)_\Omega - (p_c, \nabla \cdot \tilde{\mathbf{v}})_\Omega + \langle p_{cb}, \tilde{\mathbf{v}} \cdot \mathbf{n} \rangle_{\partial\Omega} = 0 \quad (4.9a)$$

$$(\nabla \cdot \mathbf{w}, \tilde{p})_\Omega + \left(\frac{1}{\tau} p_c, \tilde{p} \right)_\Omega = (\nabla \cdot \mathbf{F}, \tilde{p})_\Omega + \left(\frac{p_e}{\tau}, \tilde{p} \right)_\Omega, \quad (4.9b)$$

for all $(\tilde{\mathbf{v}}, \tilde{p}) \in V_{c0} \times W_{c0}$.

Similarly, the weak mixed formulation for the pressure-velocity system (2.17) is given by seeking $(\mathbf{u}, p_n) \in V_n \times W_n$ such that:

$$\left(H_n^{-1} \mathbf{v}, \tilde{\mathbf{v}} \right)_\Omega - (p_n, \nabla \cdot \tilde{\mathbf{v}})_\Omega + \langle p_{nb}, \tilde{\mathbf{v}} \cdot \mathbf{n} \rangle_{\Gamma_n^D} = \left(H_n^{-1} \mathbf{v}_{cj}, \tilde{\mathbf{v}} \right)_\Omega + \left(H_n^{-1} \mathbf{v}_{Gj}, \tilde{\mathbf{v}} \right)_\Omega, \quad (4.10a)$$

$$(\nabla \cdot \mathbf{v}, \tilde{p})_\Omega = 0, \quad (4.10b)$$

for all $(\tilde{\mathbf{v}}, \tilde{p}) \in V_{n0} \times W_{n0}$.

To define the numerical mesh, let $\{\Omega_i, i = 1, \dots, M\}$ be a uniform partition of Ω into disjoint elements Ω_i , i.e.,

$$\bar{\Omega} = \bigcup_{i=1}^M \bar{\Omega}_i, \quad \Omega_i \cap \Omega_j = \emptyset, \quad i \neq j. \quad (4.11)$$

The elements Ω_i have dimensions $\Delta x \times \Delta y$. Let $\Gamma = \partial\Omega$, $\Gamma_i = \partial\Omega_i \cap \partial\Omega$, $\Gamma_{ij} = \partial\Omega_i \cap \partial\Omega_j$.

Let $V_c^h \times W_c^h$ and $V_n^h \times W_n^h$ be mixed finite element spaces over $\{\Omega_i\}$. These spaces are defined through local spaces $V_{c_i}^h \subset H(\text{div}; \Omega_i)$, $V_{n_i}^h \subset H(\text{div}; \Omega_i)$, $W_{c_i}^h \subset L^2(\Omega_i)$

and $W_{ni}^h \subset L^2(\Omega_i)$ [28, 29]. Then, the global mixed finite element spaces are defined as,

$$V_c^h = \{ \tilde{\mathbf{v}} \in V_c : \tilde{\mathbf{v}}|_{\Omega_i} \in V_{ci}^h \}, \quad W_c^h = \{ \tilde{p} \in W_c : \tilde{p}|_{\Omega_i} \in W_{ci}^h \}, \quad (4.12a)$$

$$V_n^h = \{ \tilde{\mathbf{v}} \in V_n : \tilde{\mathbf{v}}|_{\Omega_i} \in V_{ni}^h \}, \quad W_n^h = \{ \tilde{p} \in W_n : \tilde{p}|_{\Omega_i} \in W_{ni}^h \}. \quad (4.12b)$$

Note that the functions $\tilde{p} \in W_\alpha^h$ are allowed to be discontinuous across each interface Γ_{ij} , for $\alpha = w, n$, while normal component of the functions $\tilde{\mathbf{v}} \in V_\alpha^h$ must be continuous across Γ_{ij} . In the hybridized mixed finite element method, we relax this constraint by defining,

$$\hat{V}_c^h = \{ \tilde{\mathbf{v}} \in [L^2(\Omega)]^2 : \tilde{\mathbf{v}}|_{\Omega_i} \in V_{ci}^h \}, \quad \hat{V}_n^h = \{ \tilde{\mathbf{v}} \in [L^2(\Omega)]^2 : \tilde{\mathbf{v}}|_{\Omega_i} \in V_{ni}^h \}. \quad (4.13a)$$

We then need to introduce Lagrange multipliers to enforce the required continuity on \hat{V}_c^h and \hat{V}_n^h . We define the local spaces of Lagrange multipliers as the space of the normal component of the functions in V_c^h and V_n^h , respectively, restricted to Γ_{ij} , i.e.,

$$\Lambda_{cij}^h = \{ \tilde{\ell} \in L^2(\Gamma_{ij}) : \tilde{\ell} \in V_c^h \cdot \mathbf{n}|_{\Gamma_{ij}} \}, \quad (4.14a)$$

$$\Lambda_{nij}^h = \{ \tilde{\ell} \in L^2(\Gamma_{ij}) : \tilde{\ell} \in V_n^h \cdot \mathbf{n}|_{\Gamma_{ij}} \}, \quad (4.14b)$$

We set the global Lagrange multipliers spaces as,

$$\Lambda_c^h = \left\{ \tilde{\ell} \in L^2 \left(\bigcup_{i \neq j} \Gamma_{ij} \right) : \tilde{\ell}|_{\Gamma_{ij}} \in \Lambda_{cij}^h, \Gamma_{ij} \neq \emptyset \right\}, \quad (4.15a)$$

$$\Lambda_n^h = \left\{ \tilde{\ell} \in L^2 \left(\bigcup_{i \neq j} \Gamma_{ij} \right) : \tilde{\ell}|_{\Gamma_{ij}} \in \Lambda_{nij}^h, \Gamma_{ij} \neq \emptyset \right\}, \quad (4.15b)$$

For simplicity, we will describe the hybridized mixed element method for the two problems in a local framework. Let $\mathbf{w}^h \in \hat{V}_c^h$, $p_c^h \in W_c^h$, $\mathbf{v}^h \in \hat{V}_n^h$, and $p_n^h \in W_n^h$ the hybridized mixed finite element approximations for \mathbf{w} , p_c , \mathbf{v} , and p_n , respectively. We define the local approximations as,

$$\mathbf{w}_i^h = \mathbf{w}^h|_{\Omega_i} \quad p_{ci}^h = p_c^h|_{\Omega_i} \quad \mathbf{v}_i^h = \mathbf{v}^h|_{\Omega_i} \quad p_{ni}^h = p_n^h|_{\Omega_i}. \quad (4.16)$$

We denote the Lagrange multipliers at Γ_{ij} by ℓ_{cij}^h and ℓ_{nij}^h related to (\mathbf{w}, p_c) and (\mathbf{v}, p_n) problems, respectively. By definition, we must have just one Lagrange multiplier per interface. Since $\Gamma_{ij} = \Gamma_{ji}$, we have,

$$\ell_{cij}^h = \ell_{cji}^h \quad \ell_{nij}^h = \ell_{nji}^h. \quad (4.17)$$

The hybridized mixed finite element method for the diffusive system (4.4) is

given by seeking $(\mathbf{w}_i^h, p_{ci}^h, \ell_{cij}^h) \in V_{ci}^h \times W_{ci}^h \times \Lambda_{cij}^h$, $i = 1, \dots, M$, such that:

$$\left(H_c^{-1} \mathbf{w}_i^h, \tilde{\mathbf{v}} \right)_{\Omega_i} - \left(p_{ci}^h, \nabla \cdot \tilde{\mathbf{v}} \right)_{\Omega_i} + \sum_{j \neq i} \langle \ell_{cij}^h, \tilde{\mathbf{v}} \cdot \mathbf{n} \rangle_{\Gamma_{ij}} = 0, \quad (4.18a)$$

$$\left(\nabla \cdot \mathbf{w}_i^h, \tilde{p} \right)_{\Omega_i} + \left(\frac{1}{\tau} p_{ci}^h, \tilde{p} \right)_{\Omega_i} = \left(\nabla \cdot \mathbf{F}, \tilde{p} \right)_{\Omega_i} + \left(\frac{p_e}{\tau}, \tilde{p} \right)_{\Omega_i}, \quad (4.18b)$$

$$\langle \mathbf{w}_i^h \cdot \mathbf{n}_{ij} + \mathbf{w}_j^h \cdot \mathbf{n}_{ji}, \tilde{\ell}_{ij} \rangle_{\Gamma_{ij}} = 0, \quad j \neq i, \quad \Gamma_{ij} \neq \emptyset, \quad (4.18c)$$

for all $\tilde{\mathbf{v}} \in V_{ci}^h$, $\tilde{p} \in W_{ci}^h$ and $\tilde{\ell}_{ij} \in \Lambda_{cij}^h$. Here, \mathbf{n}_{ij} is the unit vector normal to Γ_{ij} in the outward direction of element Ω_i .

Similarly, the hybridized mixed finite element method for the pressure-velocity (2.17) system is given by seeking $(\mathbf{v}_i^h, p_{ni}^h, \ell_{nij}^h) \in W_{nj}^h \times V_{ni}^h \times \Lambda_{nij}^h$, $i = 1, \dots, M$, such that:

$$\left(H_n^{-1} \mathbf{v}_i^h, \tilde{\mathbf{v}} \right)_{\Omega_i} - \left(p_{ni}^h, \nabla \cdot \tilde{\mathbf{v}} \right)_{\Omega_i} + \sum_{j \neq i} \langle \ell_{nij}^h, \tilde{\mathbf{v}} \cdot \mathbf{n} \rangle_{\Gamma_{ij}} = \left(H_n^{-1} \mathbf{v}_{ci}, \tilde{\mathbf{v}} \right)_{\Omega_i} + \left(H_n^{-1} \mathbf{v}_{Gi}, \tilde{\mathbf{v}} \right)_{\Omega_i}, \quad (4.19a)$$

$$\left(\nabla \cdot \mathbf{v}_i^h, \tilde{p} \right)_{\Omega_i} = 0, \quad (4.19b)$$

$$\langle \mathbf{v}_i^h \cdot \mathbf{n}_{ij} + \mathbf{v}_j^h \cdot \mathbf{n}_{ji}, \tilde{\ell}_{ij} \rangle_{\Gamma_{ij}} = 0, \quad j \neq i, \quad \Gamma_{ij} \neq \emptyset, \quad (4.19c)$$

for all test functions $\tilde{\mathbf{v}} \in V_{ni}^h$, $\tilde{p} \in W_{ni}^h$ and $\tilde{\ell}_{ij} \in \Lambda_{nij}^h$.

4.2 Reduction to the lowest index Raviart-Thomas spaces over rectangles

We choose the fundamental lowest index Raviart-Thomas space over rectangles [87]. The natural local degrees of freedom on the element Ω_i , are the constant value of the scalar variables p_{ci}^h and p_{ni}^h , which we associate to the center of Ω_i , and the four constant values of the outward normal component of the gradient fluxes \mathbf{w}_i^h and \mathbf{v}_i^h across the edges of the element [2, 28]. Thus, the Lagrange multipliers are also constants on the interfaces of elements. We also assume the absolute permeability and porosity fields to be constant on each element.

Now, consider a element $\Omega_i = (x_{il}, x_{ir}) \times (y_{id}, y_{iu})$, where the neighbor elements are denoted by l, r, d and u (see Figure 4.1). The center of the element Ω_i is denoted by (x_i, y_i) . We choose the same basis functions for local the spaces V_{ci}^h and V_{ni}^h on Ω_i as follows,

$$\varphi_{il} = \frac{(x - x_{ir})}{\Delta x} \mathbf{e}_1, \quad \varphi_{ir} = \frac{(x - x_{il})}{\Delta x} \mathbf{e}_1, \quad \varphi_{id} = \frac{(y - y_{iu})}{\Delta y} \mathbf{e}_2, \quad \varphi_{iu} = \frac{(y - y_{id})}{\Delta y} \mathbf{e}_2, \quad (4.20)$$

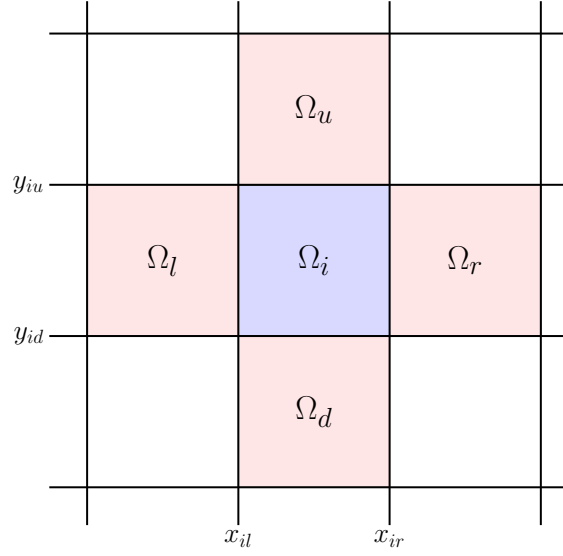


Figure 4.1: Element Ω_i and the neighbor elements.

where \mathbf{e}_1 and \mathbf{e}_2 are unit vectors of \mathbb{R}^2 in x and y direction, respectively. The basis for $W_{\alpha i}^h$ and $\Lambda_{\alpha ij}^h$, $\alpha = c, n$, is given by,

$$\psi_i = 1, \text{ on } \Omega_i, \quad l_{ij} = 1, \text{ on } \Gamma_{ij}. \quad (4.21)$$

We can write the local solutions as a linear combination of the basis functions as follows,

$$\mathbf{w}_i^h = \sum_{j \in \{l, r, d, u\}} w_{ij} \boldsymbol{\varphi}_{ij}, \quad p_{ci}^h = p_{ci} \psi_i, \quad \ell_{cij}^h = \ell_{cij} l_{ij}, \quad j = l, r, d, u, \quad (4.22a)$$

$$\mathbf{v}_i^h = \sum_{j \in \{l, r, d, u\}} v_{ij} \boldsymbol{\varphi}_{ij}, \quad p_{ni}^h = p_{ni} \psi_i, \quad \ell_{nij}^h = \ell_{nij} l_{ij}, \quad j = l, r, d, u. \quad (4.22b)$$

We also define a discretization of the corrector velocities \mathbf{v}_{ci}^h and \mathbf{v}_{Gi}^h as a linear combination of the basis functions,

$$\mathbf{v}_{ci}^h = \sum_{j \in \{l, r, d, u\}} v_{cij} \boldsymbol{\varphi}_{ij}, \quad \mathbf{v}_{Gi}^h = \sum_{j \in \{l, r, d, u\}} v_{Gij} \boldsymbol{\varphi}_{ij}, \quad (4.23)$$

Figure 4.2 presents the position of the nine natural degrees of freedom for each problem. Note that for the transport problem, in addition to capillary pressure value, we associate a saturation value to the element center.

If we choose the test functions in (4.18) and (4.19) as the basis functions (4.20)-(4.21), and apply a trapezoidal rule to integrations, we can write the resulting algebraic problem in a particularly simple form [2, 20, 28]. For elliptic problems, this quadrature rule preserves the order of convergence [20].

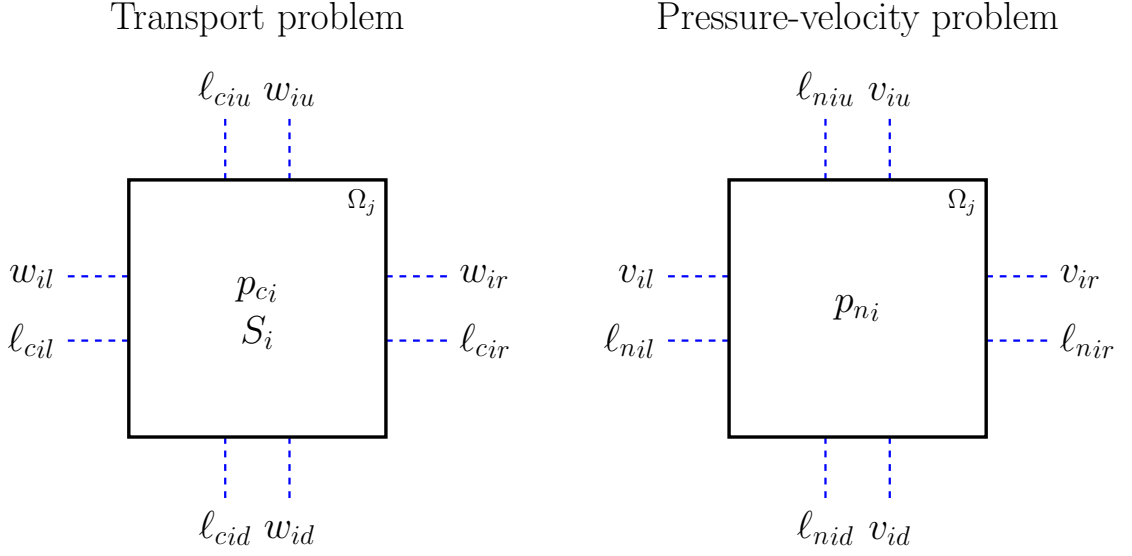


Figure 4.2: Natural degrees of freedom on the element Ω_i . For each problem, there are nine degrees of freedom: one constant value of the scalar variables, associated to the center of Ω_i ; four constant values of the outward normal component of the gradient fluxes across the edges of the element; four constant values of the the Lagrange multipliers at the interfaces of elements. For the transport problem (left), in addition to capillary pressure, we associate a saturation value to the element center

The local algebraic problem on Ω_i for the diffusive system (4.18) is given by,

$$w_{il} - \frac{2 H_{ci}}{\Delta x} (p_{ci} - \ell_{cil}) = 0, \quad (4.24a)$$

$$w_{ir} - \frac{2 H_{ci}}{\Delta x} (p_{ci} - \ell_{cir}) = 0, \quad (4.24b)$$

$$w_{id} - \frac{2 H_{ci}}{\Delta y} (p_{ci} - \ell_{cid}) = 0, \quad (4.24c)$$

$$w_{iu} - \frac{2 H_{ci}}{\Delta y} (p_{ci} - \ell_{ciu}) = 0, \quad (4.24d)$$

$$\frac{w_{il} + w_{ir}}{\Delta x} + \frac{w_{id} + w_{iu}}{\Delta y} + \frac{p_{ci}}{\tau} = \frac{p_{ei}}{\tau} + \frac{(F_{ri} - F_{li})}{\Delta x} + \frac{(F_{iu} - F_{di})}{\Delta y}, \quad (4.24e)$$

with the consistency conditions at interfaces Γ_{ij} ,

$$w_{ij} + w_{ji} = 0. \quad (4.25)$$

The terms F_{ij} denote an approximation of hyperbolic flux. We will discuss the a finite volume approach for this term in Section 4.4.

Remark 4.2.1. Although we use piecewise constant in this work, the mixed finite element approach allows us to use higher order spaces [87]. In this context, the first-order hyperbolic flux approximation is an issue to be explored further. Conceptually, by writing the test function as $\tilde{p} = \tilde{p}_0 + \tilde{p}'$, where \tilde{p}_0 and \tilde{p}' the constant and nonconstant part of \tilde{p} , it is

possible to decompose inner product $(\nabla \cdot \mathbf{F}, \tilde{p}) = (\nabla \cdot \mathbf{F}, \tilde{p}_0) + (\nabla \cdot \mathbf{F}, \tilde{p}')$. The first term on the right hand side can be handled by the same framework as presented here. The second term is more intricate, but can be interpreted as a higher order term approximation (e.g., an anti-diffusion term as a Q -form [100]).

For the system (4.19), the resulting algebraic problem on Ω_i reads,

$$v_{il} - \frac{2 H_{ni}}{\Delta x} (p_{ni} - \ell_{nil}) = v_{cil} + v_{Gil}, \quad (4.26a)$$

$$v_{ir} - \frac{2 H_{ni}}{\Delta x} (p_{ni} - \ell_{nir}) = v_{cil} + v_{Gir}, \quad (4.26b)$$

$$v_{id} - \frac{2 H_{ni}}{\Delta y} (p_{ni} - \ell_{nid}) = v_{cil} + v_{Gid}, \quad (4.26c)$$

$$v_{iu} - \frac{2 H_{ni}}{\Delta y} (p_{ni} - \ell_{niu}) = v_{cil} + v_{Giu}, \quad (4.26d)$$

$$\frac{v_{il} + v_{ir}}{\Delta x} + \frac{v_{id} + v_{iu}}{\Delta y} = 0, \quad (4.26e)$$

along with the consistency conditions at interfaces Γ_{ij} ,

$$v_{ij} + v_{ji} = 0. \quad (4.27)$$

Note that, for both local systems (4.24) and (4.26), we have five equations and nine variables linked to the element Ω_i . For each problem, the four consistency conditions, respectively (4.25) and (4.27), link the local variables of element Ω_i to the variables of neighbor elements.

We choose to eliminate the Lagrange multipliers and the gradient fluxes since the resulting linear system is symmetric positive definite [2, 20], then we can apply a suitable solver for linear systems. Combining the consistency conditions (4.25) and (4.27) with the system (4.24) and (4.26), respectively, we obtain the following discrete equations for the capillary pressure p_c and non-wetting phase pressure p_n :

$$\frac{[H_c^{\text{eff}}]_{il}(p_{ci} - p_{cl}) + [H_c^{\text{eff}}]_{ir}(p_{ci} - p_{cr})}{\Delta x^2} + \frac{[H_c^{\text{eff}}]_{id}(p_{ci} - p_{cd}) + [H_c^{\text{eff}}]_{iu}(p_{ci} - p_{cu})}{\Delta y^2} + \frac{p_{ci}}{\tau} = b_{ci}, \quad (4.28a)$$

$$\frac{[H_n^{\text{eff}}]_{il}(p_{ni} - p_{nl}) + [H_n^{\text{eff}}]_{ir}(p_{ni} - p_{nr})}{\Delta x^2} + \frac{[H_n^{\text{eff}}]_{id}(p_{ni} - p_{nd}) + [H_n^{\text{eff}}]_{iu}(p_{ni} - p_{nu})}{\Delta y^2} = b_{ni}, \quad (4.28b)$$

where, the effective coefficients $[H_c]_{ij}^{\text{eff}}$ and $[H_n]_{ij}^{\text{eff}}$ across the interface Γ_{ij} naturally appear

as a harmonic mean,

$$[H_c^{\text{eff}}]_{ij} = \frac{2 H_{ci} H_{cj}}{H_{ci} + H_{cj}}, \quad [H_n^{\text{eff}}]_{ij} = \frac{2 H_{ni} H_{nj}}{H_{ni} + H_{nj}}. \quad (4.29)$$

The right hand side terms b_{ci} and b_{ni} are given by,

$$b_{ci} = \frac{p_{ei}}{\tau} + \frac{(F_{ri} - F_{li})}{\Delta x} + \frac{(F_{iu} - F_{di})}{\Delta y}, \quad (4.30a)$$

$$b_{ni} = - \left(\frac{v_{cil} + v_{cir}}{\Delta x} + \frac{v_{cid} + v_{ciu}}{\Delta y} \right) - \left(\frac{v_{Gil} + v_{Gir}}{\Delta x} + \frac{v_{Gid} + v_{Giu}}{\Delta y} \right). \quad (4.30b)$$

The diffusive flux and velocity in each interface Γ_{ij} can be calculated from the capillary pressure and non-wetting phase pressure, respectively, of the elements Ω_i and Ω_j as follows,

$$\begin{aligned} w_{il} &= [H_c^{\text{eff}}]_{il} \frac{(p_{ci} - p_{cl})}{\Delta x}, & w_{ir} &= [H_c^{\text{eff}}]_{ir} \frac{(p_{ci} - p_{cr})}{\Delta x}, \\ w_{id} &= [H_c^{\text{eff}}]_{id} \frac{(p_{ci} - p_{cd})}{\Delta y}, & w_{iu} &= [H_c^{\text{eff}}]_{iu} \frac{(p_{ci} - p_{cu})}{\Delta y}, \end{aligned} \quad (4.31)$$

$$\begin{aligned} v_{il} &= [H_n^{\text{eff}}]_{il} \frac{(p_{ni} - p_{nl})}{\Delta x} + v_{cil} + v_{Gil}, & v_{ir} &= [H_n^{\text{eff}}]_{ir} \frac{(p_{ni} - p_{nr})}{\Delta x} + v_{cir} + v_{Gir}, \\ v_{id} &= [H_n^{\text{eff}}]_{id} \frac{(p_{ni} - p_{nd})}{\Delta y} + v_{cid} + v_{Gid}, & v_{iu} &= [H_n^{\text{eff}}]_{iu} \frac{(p_{ni} - p_{nu})}{\Delta y} + v_{ciu} + v_{Giu}. \end{aligned} \quad (4.32)$$

We have to define consistent approximations for the correction velocities. If $f_w(S_w) \neq 0$, we can write the correction velocity linked to the capillary pressure as

$$\mathbf{v}_c = - \frac{1}{f_n(S_w)} \mathbf{w}. \quad (4.33)$$

Thus, we can determine suitable approximation for \mathbf{v}_c from the numerical approximation of the diffusive flux \mathbf{w} . For \mathbf{v}_G , first we define the coefficient,

$$H_G(S_w) = N_{Gr} K(\mathbf{x}) \left[k_w(S_w) + R_\mu R_\rho^{-1} k_n(S_w) \right], \quad (4.34)$$

and using a continuity argument, we obtain

$$v_{Gij} = [H_G^{\text{eff}}]_{ij} \nabla Z \cdot \mathbf{n}_{ij}, \quad [H_G^{\text{eff}}]_{ij} = \frac{2 H_{Gi} H_{Gj}}{H_{Gi} + H_{Gj}}. \quad (4.35)$$

The equations (4.28a) and (4.28b) define systems of algebraic equations for

p_{c_i} and p_{n_i} , respectively. However, at this point these systems are nonlinear since they are coupled through their coefficients, right hand terms and the evolution equation for saturation. We emphasize that the right hand term b_{c_i} depends on Darcy flux \mathbf{v} through the numerical hyperbolic fluxes F_{ij} and b_{n_i} depends on the ∇p_c through the corrector velocity approximations $v_{c_{ij}}$. In the next sections, we will discuss a time discretization and an iterative approach along with a linearization strategy. In this context, the systems (4.28a) and (4.28b) becomes linear and symmetric positive defined, and we solve them sequentially. In this work, the arising systems of linear equations are solved efficiently with an algebraic multigrid method, along with the conjugate gradient method.

4.3 Discretization in time

To define the time discretization, consider that we want to approximate the solution over time interval $(0, T]$. Let $N \in \mathbb{N}$ be the number of time steps, we take $\Delta t = T/N$ and $t_n = n\Delta t$, for $n = 0, 1, \dots, N$. Now, we denote S_i^n and $p_{c_i}^n$ the numerical approximations for $S_w(\mathbf{x}, t_n)$ and $p_c(\mathbf{x}, t_n)$ at the center of element Ω_i , respectively.

We consider an implicit discretization of (4.3a) by means of finite volume framework. First, from the definition of diffusive flux (4.4a), rewrite the transport equation (4.3a) as follows,

$$\frac{\partial}{\partial t}(\phi S_w) + \nabla \cdot \mathbf{F}(\mathbf{v}, S_w) = \nabla \cdot \mathbf{w}. \quad (4.36)$$

Thus, by taking advantage of the Raviart-Thomas mixed finite element formulation, we propose the following implicit finite volume scheme for (4.36),

$$S_i^{n+1} = S_i^n - \frac{\Delta t}{\phi_i} \left[\frac{(F_{ri}^n - F_{li}^n)}{\Delta x} + \frac{(F_{iu}^n - F_{di}^n)}{\Delta y} \right] + \frac{\Delta t}{\phi_i} \left[\frac{(w_{ri}^{n+1} + w_{il}^{n+1})}{\Delta x} + \frac{(w_{iu}^{n+1} + w_{id}^{n+1})}{\Delta y} \right]. \quad (4.37)$$

Note that this finite volume approach uses constant values of saturation and four values of hyperbolic fluxes and diffusive fluxes.

The first-order hyperbolic term is evaluated at time t_n , hence, to evolve saturation, we need the velocity field evaluated only at t_n (see Eq. (2.16b)). On the other hand, the diffusive flux is evaluated at time t_{n+1} , therefore the capillary pressure have to be calculated implicitly, leading to a nonlinear problem. Accordingly, we have to rewrite

(4.28)-(4.30) to take into account the time discretization,

$$\begin{aligned}
& \frac{[H_c^{\text{eff}}]_{il}^{n+1}}{\Delta x^2} (p_{c_i}^{n+1} - p_{c_l}^{n+1}) + \frac{[H_c^{\text{eff}}]_{ir}^{n+1}}{\Delta x^2} (p_{c_i}^{n+1} - p_{c_r}^{n+1}) \\
& + \frac{[H_c^{\text{eff}}]_{id}^{n+1}}{\Delta y^2} (p_{c_i}^{n+1} - p_{c_d}^{n+1}) + \frac{[H_c^{\text{eff}}]_{iu}^{n+1}}{\Delta y^2} (p_{c_i}^{n+1} - p_{c_u}^{n+1}) \\
& + \frac{p_{c_i}^{n+1}}{\tau} = \frac{p_e(S_i^{n+1})}{\tau} + \frac{(F_{ri}^n - F_{li}^n)}{\Delta x} + \frac{(F_{iu}^n - F_{di}^n)}{\Delta y},
\end{aligned} \tag{4.38a}$$

$$\begin{aligned}
& \frac{[H_n^{\text{eff}}]_{il}^n}{\Delta x^2} (p_{n_i}^n - p_{n_l}^n) + \frac{[H_n^{\text{eff}}]_{ir}^n}{\Delta x^2} (p_{n_i}^n - p_{n_r}^n) \\
& + \frac{[H_n^{\text{eff}}]_{id}^n}{\Delta y^2} (p_{n_i}^n - p_{n_d}^n) + \frac{[H_n^{\text{eff}}]_{iu}^n}{\Delta y^2} (p_{n_i}^n - p_{n_u}^n) = \\
& - \left(\frac{v_{cil}^n + v_{cir}^n}{\Delta x} + \frac{v_{cid}^n + v_{ciu}^n}{\Delta y} \right) - \left(\frac{v_{G_{il}}^n + v_{G_{ir}}^n}{\Delta x} + \frac{v_{G_{id}}^n + v_{G_{iu}}^n}{\Delta y} \right).
\end{aligned} \tag{4.38b}$$

Due to the advective nature of the first-order term of (4.36) we adopted the following stability criterion:

$$\frac{\Delta t v_{\max}}{\min\{\Delta x, \Delta y\} \phi_{\min}} \left[\max_{S_w \in [0,1]} \{|f'_w(S_w)|\} \right] < \sigma_{\text{CFL}}, \tag{4.39}$$

where $v_{\max} = \max v_{ij}$ and $\phi_{\min} = \min \phi_i$. The parameter σ_{CFL} is chosen to ensure stability. We emphasize that this choice was also made based on previous one-dimensional results [5]; see also the Appendix A for convergence proof for a one-dimensional linear pseudo-parabolic equation.

Remark 4.3.1. Alternatively to (4.37), we can simply write an implicit strategy by means of the backward Euler procedure to the evolution equation (2.6), which reads:

$$S_i^{n+1} = S_i^n + \frac{\Delta t}{\tau \phi_i} [p_e(S_i^{n+1}) - p_{c_i}^{n+1}]. \tag{4.40}$$

This approach was used in [5, 25, 35] for one-dimensional pseudo-parabolic problems. We also performed numerical tests with (4.40) in two-dimensional problems, but we choose those numerical results since we obtained similar performance.

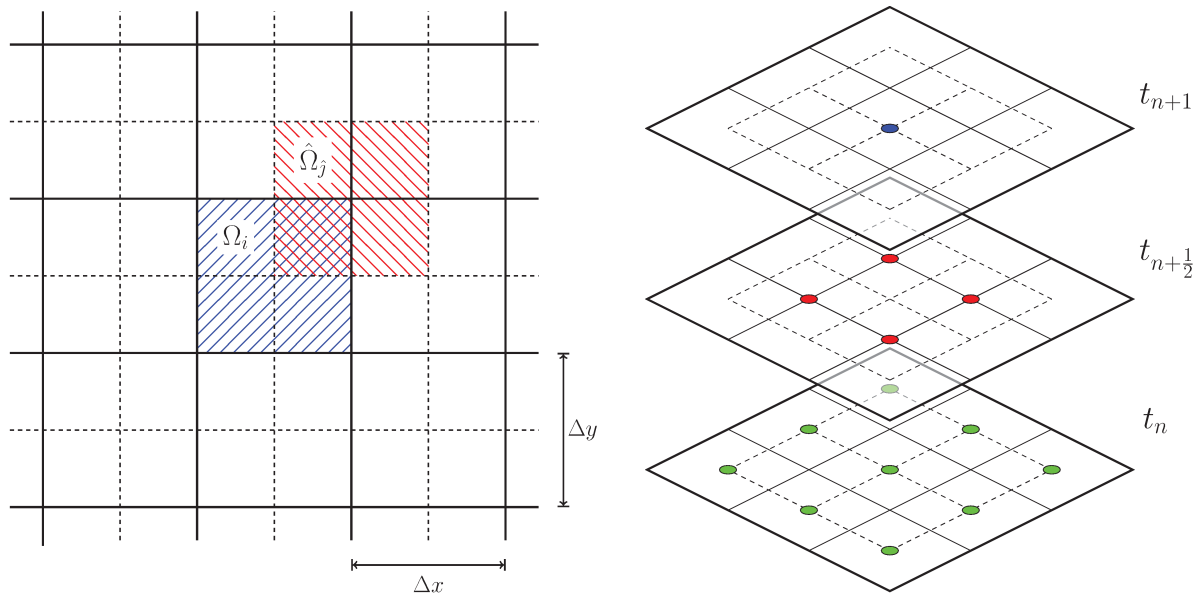


Figure 4.3: Staggered mesh (left) and numerical stencil (right) for computing the numerical hyperbolic flux. In the left figure, the blue (Ω_i) and red ($\hat{\Omega}_j$) areas correspond to the elements of original and staggered mesh, respectively. In the right figure, the colored points represents the local where the variables are evaluated at each time step. At the time t_n , all needed information is evaluated at the center of the non-staggered cells, while at the time $t_{n+1/2}$ the information is obtained from the center of the staggered cells.

4.4 Numerical hyperbolic flux

In this section, we describe the approximation of the hyperbolic term. We use an approach based on finite volume methods for hyperbolic conservations laws. The pseudo-parabolic equation has a dispersive nature [5], so we choose a numerical flux that presents numerical dispersive nature. We use a two-dimensional extension of Richtmyer's scheme. Our choice is simple at first glance, but it is worth noting that it is not obvious [5]; see also [32]. The dispersive nature of the pseudo-parabolic transport equation lead to solutions with saturation overshoot that exhibits both nonmonotone saturation profile and phase mode dispersion similar to that in the Benjamin-Bona-Mahony equation [13]. In addition, here we are dealing with nontrivial heterogeneous geologic media with high-contrast.

The Richtmyer's method for one-dimensional hyperbolic conservation laws is a two-step Lax-Wendroff type scheme. The first step consists on approximating the solution defined on the points of a staggered mesh by means of Lax-Friedrichs scheme at an intermediary time $t_{n+1/2}$. The second step uses a Leapfrog scheme to evolve the solution to the time t_{n+1} . We use the same ideas to define a two-dimensional version of Richtmyer's numerical flux.

First we define a staggered mesh $\{\hat{\Omega}_j\}$ by shifting at $\Delta x/2$ and $\Delta y/2$ (see Figure 4.3). The centers of the staggered elements correspond to the corner of the non-staggered

elements. For each staggered element $\hat{\Omega}_j$, we define a set of all non-staggered element indexes that intersect $\hat{\Omega}_j$ as $I_j = \{i : \hat{\Omega}_j \cap \Omega_i \neq \emptyset\}$. To approximate the saturation $\hat{S}_j^{n+1/2}$ on the staggered mesh, we use a two-dimensional Lax-Friedrichs type scheme given by,

$$\hat{\phi}_j \hat{S}_j^{n+1/2} = \frac{1}{4} \sum_{i \in I_j} (\phi_i S_i^n) - \frac{\Delta t}{\Delta x} (\hat{F}_{j\hat{r}} - \hat{F}_{\hat{l}j}) - \frac{\Delta t}{\Delta y} (\hat{F}_{j\hat{u}} - \hat{F}_{\hat{d}j}), \quad (4.41)$$

where the numerical flux $\hat{F}_{j\hat{k}}$ at the boundaries of staggered element $\hat{\Omega}_j$ are defined as a arithmetic mean of the fluxes of intersected non-staggered elements. Similarly, by following the ideas of [2], we define $\hat{\phi}$ at the staggered element $\hat{\Omega}_j$ as,

$$\hat{\phi}_j \equiv \frac{1}{4} \sum_{i \in I_j} \phi_i. \quad (4.42)$$

To evolve from time t_n to time t_{n+1} , the numerical flux is given by at interface Γ_{ij} of the non-staggered mesh,

$$F_{ij}^n = \mathbf{F}(\mathbf{u}_i^n(x_{ij}, y_i), S_{ij}^{n+1/2}) \cdot \mathbf{n}_{ij}, \quad (4.43)$$

where $S_{ij}^{n+1/2}$ is defined as a arithmetic mean of saturation given by (4.41) on staggered elements that intersect Γ_{ij} . Figure 4.3 (right) shows the numerical stencil for the numerical approximation of the hyperbolic term.

4.5 Boundary conditions

To complete the method description, we have to impose the boundary conditions (4.5). Our local framework allows us to write easily the discrete equations for the elements the intersects the boundary of the domain. We just have to define appropriately the values of the some degree of freedom defined on the boundary of the domain (gradient fluxes and Lagrange multipliers) in (4.26).

Remark 4.5.1. We assume that if a (rectangular) element Ω_i intersects the boundary of Ω at the edge $\Gamma_{i\beta}$, then just one type of boundary condition for each problem is imposed over $\Gamma_{i\beta}$. So the mesh matches the boundary partition.

Let $\ell_{wi\alpha}$ and $\ell_{nj\beta}$ denote the Lagrange multipliers associated to $\Gamma_{i\alpha}$ and $\Gamma_{j\beta}$, respectively, where we define Dirichlet boundary conditions, i.e., $\Gamma_{i\alpha} \subset \partial\Omega_i \cap \Gamma_w^D$ and $\Gamma_{j\beta} \subset \partial\Omega_j \cap \Gamma_n^D$, then we impose,

$$\ell_{wi\alpha} = S_{wb}, \text{ on } \Gamma_{i\alpha}, \quad \ell_{nj\beta} = p_{nb}, \text{ on } \Gamma_{i\beta}. \quad (4.44)$$

Similarly, let $w_{i\alpha}$ and $v_{nj\beta}$ denote the diffusive flux and total velocity associated to $\Gamma_{i\alpha}$ and $\Gamma_{j\beta}$, respectively, where we define Neumann boundary conditions, i.e., $\Gamma_{i\alpha} \subset \partial\Omega_i \cap \Gamma_w^N$ and $\Gamma_{j\beta} \subset \partial\Omega_j \cap \Gamma_n^N$, then we impose,

$$v_{i\alpha} = v_b, \text{ on } \Gamma_{i\alpha}, \quad w_{j\beta} = w_b, \text{ on } \Gamma_{j\beta}. \quad (4.45)$$

Finally, we impose the total flux (Robin) conditions for the transport problem at $\Gamma_{i\alpha} \subset \partial\Omega_i \cap \Gamma_w^R$ by setting,

$$F_{i\alpha}^n - v_{i\alpha} = v_{wb}, \text{ on } \Gamma_{i\alpha}. \quad (4.46)$$

4.6 Iterative procedure

As previously stated, the discrete equations becomes a nonlinear semi-implicit scheme. At each time step, we solve the transport problem through an iterative procedure, but we have to solve the pressure-velocity problem only once. To handle the nonlinear problem, we exploit a successive approximation framework already used in one-dimensional problem [5]. In [25], the author employs a similar strategy for approximate a pseudo-parabolic Burgers equation.

Let k be the iteration index, we denote $S_j^{n,k}$ as a approximation for at the iteration level k and S_j^n the approximation after convergence. As an initial approximation, we take the response of the last time step, i.e., $S^{n+1,0} = S^n$ and $p_c^{n+1,0} = p_c^n$, then we solve sequentially (4.38a) and (4.37) until the convergence. The criterion of convergence for the iterative procedure is given by,

$$\|S^{n,k} - S^{n,k-1}\|_2 < \varepsilon, \quad (4.47)$$

where $\varepsilon > 0$ is the tolerance for the difference between the responses of the iteration levels $k-1$ and k .

The sequential time-marching approach to evolve the solution from t_n and t_{n+1} is defined as follows,

1. Calculate the coefficients $[H_n^{\text{eff}}]_{ij}^n$ and the right-hand-side term $b_{n_i}^{n,k-1}$ of (4.38b) from S_i^n and $p_{c_i}^n$;
2. Solve the linear system (4.38b) for $p_{n_i}^n$;
3. Recover the velocity field \mathbf{v}_i^n from $p_{n_i}^n$;

4. By (4.43), calculate the numerical fluxes F_{ij}^n from S_i^n and \mathbf{v}_i^n ;
5. Calculate the saturation S_i^{n+1} of next time step t_{n+1} by means of the following iterative procedure:
 - a. Set the initial approximations $S_i^{n+1,0} = S_i^n$ and $p_{c_i}^{n+1,0} = p_{c_i}^n$;
 - b. Calculate the coefficients $[H_c^{\text{eff}}]_{ij}^{n+1,k-1}$ and the right-hand-side term $b_{c_i}^{n+1,k-1}$ from $S_i^{n+1,k-1}$;
 - c. Solve the linear system (4.38a) for $p_{c_i}^{n+1,k}$;
 - d. By means of (4.37), update $S_i^{n+1,k}$ from $p_{c_i}^{n+1,k}$;
 - e. Check for convergence for S :
 If not attained, go back to the step **b**.;
 If attained, set $S_i^{n+1} = S_i^{n+1,k}$.

The saturation calculation depicted in the step 5 is based in a simple and robust fixed-point iteration to solve the nonlinear algebraic equations. This iterative procedure concludes the presentation of our numerical approach. Appendix A shows a convergence proof of the iterative procedure for a one-dimensional linear problem. In the next chapter, we present numerical experiments that evinces the convergence of the iterative procedure.

Chapter 5

Numerical experiments

This chapter presents numerical experiments of two-phase flow in porous media with dynamic capillary pressure. All parameters and details on the flow equations, boundary and initial conditions and numerical experiments are described in details to allow the proper reproduction of them. The simulations aims:

- to demonstrate the viability of the proposed numerical method;
- to study the effects of heterogeneities of porosity and permeability fields in presence of dynamic capillary pressure and gravity.

We used the one-dimensional numerical experiments presented in [31, 32, 36] and reproduced in [5] as reference guide to our two-dimensional experiments. It is important to mention that gravity and viscosity ratio effects are not explored in those one-dimensional studies. Hence, we use an one-dimensional version of our approach to study numerically this effects and provide reference solutions for the two-dimensional simulations (see [5] for details of the one-dimensional scheme). We implemented the method in C language in a serial framework and we performed all the experiments on a Linux Debian 7.2.0-8 computer with processor Intel® Xeon® CPU E5-2643 v2 3.50GHz.

Since our approach does not handle degenerated values, i.e., saturation values such that $H_c(S_w) = 0$, we perform only experiments that the saturation profile does not attain degenerated values. Nevertheless, to prevent degeneracy problems on coarser meshes, we modify the diffusion coefficient $H_c(S_w)$ near to degeneracy points by taking $H_c(S_w) = H_{c\min}$, if $H_c(S_w) < H_{c\min}$, with $H_{c\min} > 0$. We set $H_{c\min} = 1 \times 10^{-8}$ for all simulations.

We chose the slab geometry to compose the boundary conditions of our simulations (see Figure 5.1). We set Neumann zero flux conditions in the horizontal boundaries (Γ_D and Γ_U) for both problems (transport of saturation an pressure-velocity system). For the transport problem, we defined the saturation S_w at left boundary (Γ_L) (Dirichlet condition) according to the initial data, and zero diffusive flux (Neumann condition) at

right boundary (Γ_R),

$$S_w = S_L, \quad \mathbf{x} \in \Gamma_L, \quad (5.1a)$$

$$\mathbf{w} \cdot \mathbf{n} = 0, \quad \mathbf{x} \in \Gamma_R, \quad (5.1b)$$

$$(\mathbf{F} - \mathbf{w}) \cdot \mathbf{n} = 0, \quad \mathbf{x} \in \Gamma_D, \quad (5.1c)$$

$$(\mathbf{F} - \mathbf{w}) \cdot \mathbf{n} = 0, \quad \mathbf{x} \in \Gamma_U. \quad (5.1d)$$

For the pressure-velocity problem, we set the flux at left boundary (Neumann condition) and a reference pressure at right boundary (Dirichlet condition)

$$\mathbf{v} \cdot \mathbf{n} = -Q^{\text{in}}, \quad \mathbf{x} \in \Gamma_L, \quad (5.2a)$$

$$p_n = p_n^{\text{ref}}, \quad \mathbf{x} \in \Gamma_R, \quad (5.2b)$$

$$\mathbf{v} \cdot \mathbf{n} = 0, \quad \mathbf{x} \in \Gamma_D, \quad (5.2c)$$

$$\mathbf{v} \cdot \mathbf{n} = 0, \quad \mathbf{x} \in \Gamma_U. \quad (5.2d)$$

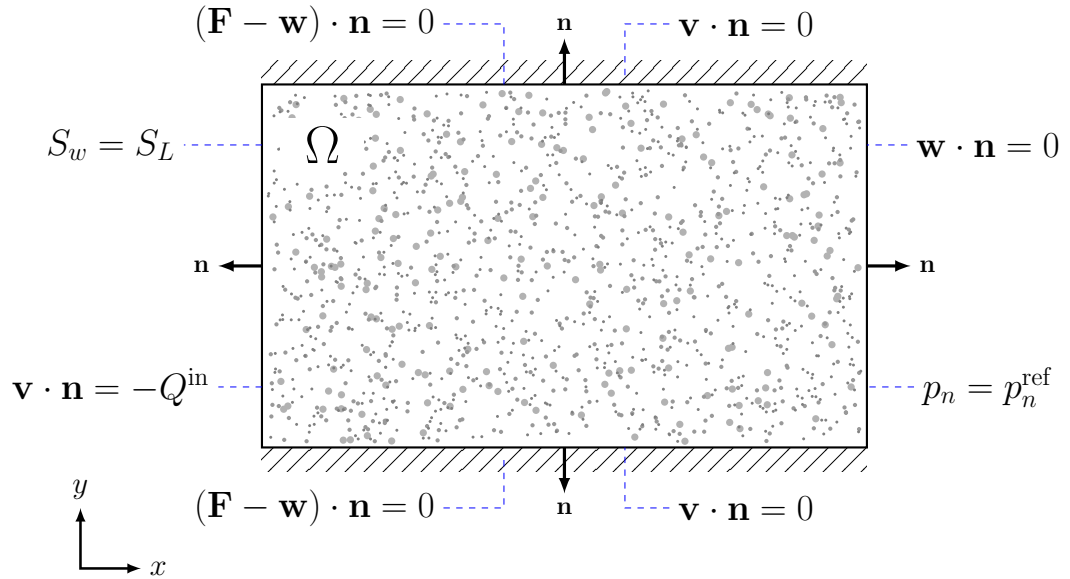


Figure 5.1: Boundary conditions for slab geometry for saturation transport and pressure-velocity problems. Zero flux conditions are imposed on top and bottom boundaries for both problems. A total inflow flux Q^{in} and a reference saturation are defined on left boundary. A reference pressure p_n^{ref} and a zero diffusive flux condition are imposed on right boundary.

The initial value for all examples is a Riemann data defined by,

$$\eta(\mathbf{x}) = \begin{cases} S_L, & x \leq 0, \\ S_R, & x \geq 0, \end{cases} \quad (5.3)$$

with consistent boundary values S_L and S_R . We focus on the case $S_L > S_R$ and $Q^{\text{in}} > 0$, which the wetting phase displaces the non-wetting phase (imbibition).

Following [31, 36], we use the models of relative permeabilities and static capillary pressure given by:

$$k_w(S_w) = S_w^{1.5}, \quad k_n(S_w) = (1 - S_w)^{1.5}, \quad p_e(S_w) = -S_w, \quad 0 \leq S_w \leq 1. \quad (5.4)$$

We performed numerical simulations using homogeneous and heterogeneous fields of porosity and permeability. For experiments with heterogeneous fields, we use a log-normal model for multiscale rock heterogeneity proposed in the seminal work by Glimm and Sharp [44]. In this model, we consider a Gaussian field $\xi(\mathbf{x})$ with its distribution determined by its mean and covariance function,

$$\text{cov}(\xi(\mathbf{x}_1), \xi(\mathbf{x}_2)) = \|\mathbf{x}_1 - \mathbf{x}_2\|^{-\beta}, \quad (5.5)$$

β is a scaling exponent that controls the nature of multiscale heterogeneity [44]. Its realization on a finite lattice (e.g. a mesh grid) provides a short distance regularization [2]. Then the absolute permeability is given by,

$$K(\mathbf{x}) = K_0 \exp(\varpi_K \xi(\mathbf{x})), \quad (5.6)$$

where K_0 is a cutoff value for absolute permeability, and $\varpi_K \geq 0$ is a scaling factor [44]. We assume the same multiscale field $\xi(\mathbf{x})$ to construct a variable porosity field,

$$\phi(\mathbf{x}) = \phi_0 + \varpi_\phi \xi(\mathbf{x}), \quad (5.7)$$

where ϕ_0 is a cutoff value for porosity and normalizing factor $\varpi_\phi \geq 0$ is chosen to bound the porosity. Note that, if we take $\varpi_K = 0$ and $\varpi_\phi = 0$ we have the homogeneous case. We use the coefficient of variation CV (the ratio of the standard deviation to the mean) as a dimensionless measure of the heterogeneity of the field. Figure 5.2 shows the high-contrast multiscale field $\xi(\mathbf{x})$ used for the simulations reported in this work.

To solve the linear system of algebraic equation, we used a implementation of the conjugate gradient method with an algebraic multigrid (AMG) preconditioner of Manfred Liebmann's Parallel Toolbox [71]. It is a academic C++ package for the numerical solution of linear systems. For the nonlinear iterative procedure, we set the tolerance parameter as $\varepsilon = 1 \times 10^{-9}$ for all simulations.

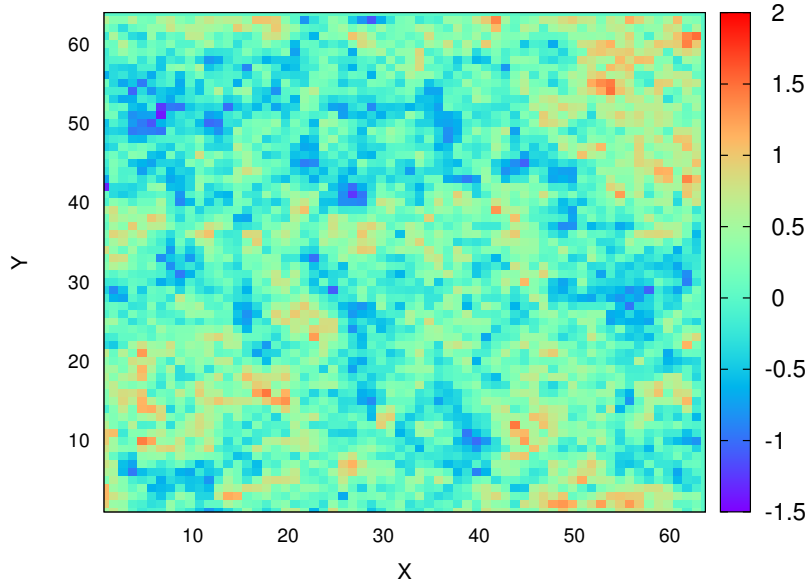


Figure 5.2: The Gaussian field $\xi(\mathbf{x})$ used to define the heterogeneous rock properties. This field is defined in a 64×64 geologic reference element mesh and scaling factor $\beta = 0.5$.

5.1 Refinement study

The numerical accuracy and convergence study for the proposed computational procedure is based on a simple mesh refinement study. Thus, we compute errors in different norms using an approximate solution on a fine mesh grid (1024×1024 elements) labeled as the reference solution S^{ref} . In order to measure the difference between the reference solution S^{ref} and an approximate solution S^h , at a fixed time t^n of simulation, we will use residual-errors $E(h) = S^h - S^{\text{ref}}$ along with L_q^n -errors defined by $E_q^n \equiv \|E(h)\|_q$, $q = 1, 2, \infty$, where,

$$\begin{aligned} \|E(h)\|_\infty &= \max |S_i^h - S_i^{\text{ref}}|, \\ \|E(h)\|_q &= \left(\Delta x \Delta y \sum_{i=1}^M |S_i^h - S_i^{\text{ref}}|^q \right)^{1/q}. \end{aligned} \quad (5.8)$$

Notice, here quantity S_i^h stands for the projection of the numerical solution S^h onto the refined mesh in the computational domain. The superscript h denotes the mesh parameter taken as $h = \max(\Delta x, \Delta y)$. In our simulation, we discretized the domain in square elements, thus, $h = \Delta x = \Delta y$.

We performed numerical experiments with different values for the flow parameter. In this section, we choose to present the refinement study of a representative simulation with the following parameters,

Computational domain:	$\Omega_{2D} = (-5, 20) \times (0, 25)$	Final time of simulation:	$T = 5.0$
Left saturation value:	$S_L = 0.85$	Inflow flux:	$Q^{\text{in}} = 1.0$
Right saturation value:	$S_R = 0.10$	Right pressure value:	$p_n^{\text{ref}} = 0.0$
Viscosity ratio:	$R_\mu = 1.0$	Capillary number:	$N_{Ca} = 1.0$
Density ratio:	$R_\rho = 1.0$	Gravity number:	$N_{Gr} = 0.0$
Dynamic effect number:	$N_{Dy} = 0.5$	Stability parameter:	$\sigma_{\text{CFL}} = 0.5$

We observe the formal convergence from numerical experiments reported in Fig 5.3 (homogeneous on the top and heterogeneous on the bottom), and Table 5.1 and Table 5.2, which shows a good resolution first-order convergence rate behavior (see right column in Figure 5.3). Indeed, Fig 5.3 shows the refinement study, where we used meshes from 64×64 to 512×512 elements and the reference solution was obtained on 1024×1024 element mesh. We notice that the pseudo-parabolic model lead to nonmonotone solutions. No spurious numerical artifacts are observed. Indeed, our numerical simulations indicates that, the nonclassical pseudo-parabolic structure persists under the presence of heterogeneities imposed for long-range correlations and stronger heterogeneity over permeability (5.6) and porosity (5.7) fields. The proposed scheme seems to be robust and efficient and accurate to show features on the flow path.

Table 5.1: Refinement study with homogeneous permeability field.

Mesh	h	$\ E\ _1$	$\ E\ _2$	$\ E\ _\infty$	Run time (s)
64×64	3.13×10^{-1}	1.78×10^0	2.03×10^{-1}	7.12×10^{-2}	8.87×10^0
128×128	1.56×10^{-1}	7.21×10^{-1}	9.10×10^{-2}	3.01×10^{-2}	5.71×10^1
256×256	7.81×10^{-2}	3.27×10^{-1}	4.31×10^{-2}	1.26×10^{-2}	3.64×10^2
512×512	3.91×10^{-2}	1.57×10^{-1}	1.91×10^{-2}	4.13×10^{-3}	2.99×10^3

Table 5.2: Refinement study with heterogeneous permeability field.

Mesh	h	$\ E\ _1$	$\ E\ _2$	$\ E\ _\infty$	Run time (s)
64×64	3.13×10^{-1}	2.04×10^0	2.25×10^{-1}	1.35×10^{-1}	1.63×10^1
128×128	1.56×10^{-1}	8.08×10^{-1}	9.79×10^{-2}	5.97×10^{-2}	1.12×10^2
256×256	7.81×10^{-2}	3.64×10^{-1}	4.74×10^{-2}	2.58×10^{-2}	8.59×10^2
512×512	3.91×10^{-2}	1.60×10^{-1}	2.05×10^{-2}	9.66×10^{-3}	5.86×10^3

5.2 Numerical study of viscosity ratio effects

In this section, we study the effect of viscosity ratio R_μ in the solution profile. The objective is to numerically study the solution behavior in different flow regimes. We simulate cases for $R_\mu < 1$ (i.e. the wetting phase is less viscous than the non-wetting phase) and $R_\mu > 1$ (the wetting phase is more viscous than the non-wetting phase). It is worth mentioning that both cases have physical applications in two-phase flow in porous

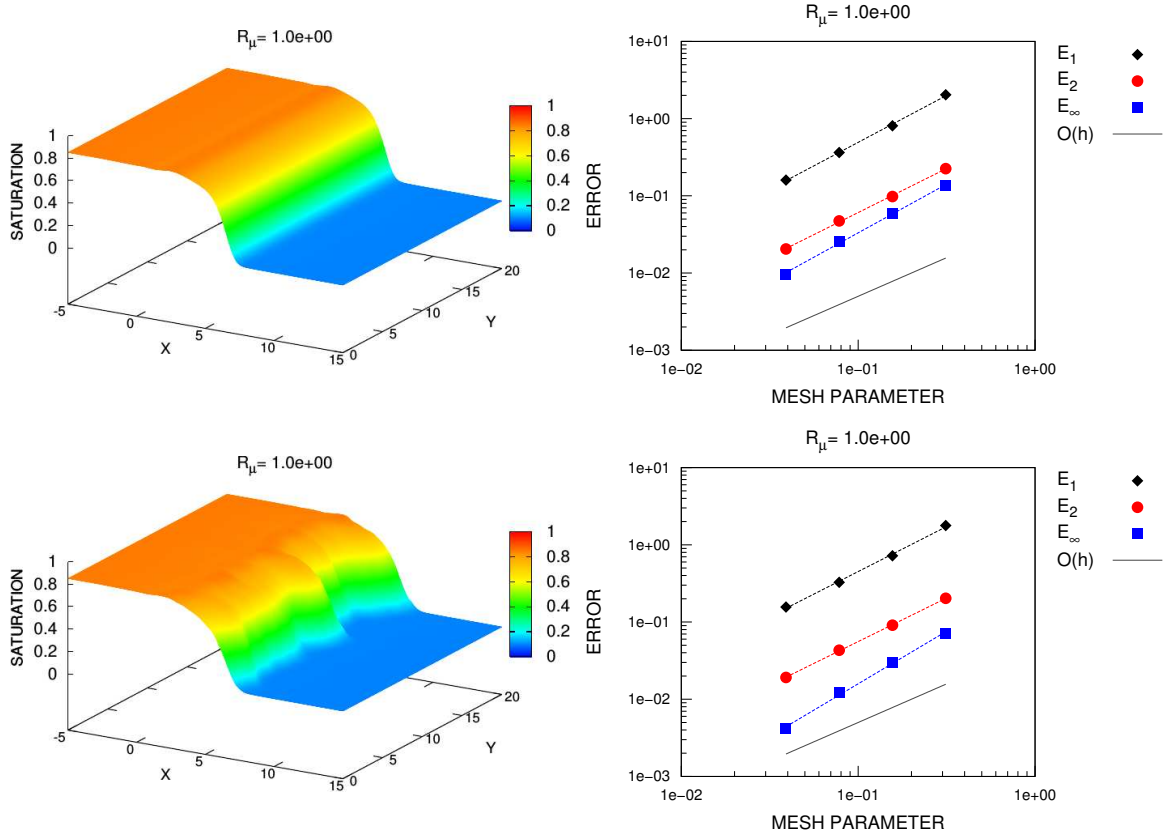


Figure 5.3: Numerical solutions and refinement study for saturation. Simulations are presented for homogeneous (top) and heterogeneous permeability fields (bottom). The left columns present the saturation profile for 1024×1024 element mesh. The right column presents the numerical error with respect the reference numerical solution (1024×1024 elements). Dots denote the numerical error on different norms, while dashed lines are the linear adjusted curve.

media. For $R_\mu > 1$, we may cite the problem of water infiltration in the soil. On the other hand, regimes where $R_\mu < 1$ occur in petroleum reservoir applications.

In this section, we performed numerical experiments for $R_\mu = 0.5, 1.0, 2.0$. For each of value of the viscosity ratio, we used homogeneous and heterogeneous permeability fields. We used the following simulation parameters:

Computational domain:	$\Omega_{2D} = (-5, 20) \times (0, 25)$	Final time of simulation:	$T = 5.0$
Left saturation value:	$S_L = 0.85$	Inflow flux:	$Q_n^{\text{in}} = 1.0$
Right saturation value:	$S_R = 0.10$	Reference pressure value:	$p_n^{\text{ref}} = 0.0$
Viscosity ratio:	$R_\mu = 0.5, 2.0$	Capillary number:	$N_{Ca} = 1.0$
Density ratio:	$R_\rho = R_\mu$	Gravity number:	$N_{Gr} = 0.0$
Dynamic effect number:	$N_{Dy} = 0.5$	Stability parameter:	$\sigma_{\text{CFL}} = 0.5$

Figure 5.4 shows the solution profile for saturation for the different values of R_μ with homogeneous (left) and heterogeneous (right) permeability field. We can see that for the smaller value of viscosity ratio, the solution profile presents viscous finger-like

patterns, whereas for the bigger viscosity ratio these patterns are less developed. This result is consistent with the immiscible and incompressible two-phase (water-oil) flow problems in petroleum reservoir applications and with typical water infiltration problems in soils. Figures 5.6 and 5.5 show the evolution of the solution profiles on the heterogeneous permeability field for $R_\mu = 0.5$ (left column) and $R_\mu = 2.0$ (right column). The numerical solutions are presented for $T = 5, 7.5, 10$, from top to bottom, and for $R_\mu = 0.5$ (top) and $R_\mu = 2.0$. The non-classical one-dimensional pseudo-parabolic structure is observed in the presence of heterogeneities (this structure is also similar for homogeneous media, with and without gravity effect) where there is a nontrivial coupling between the transport equations and flow velocities field, which is dynamically governed by the pressure equation. This interaction has not been reported on rigorous mathematical grounds in the literature.

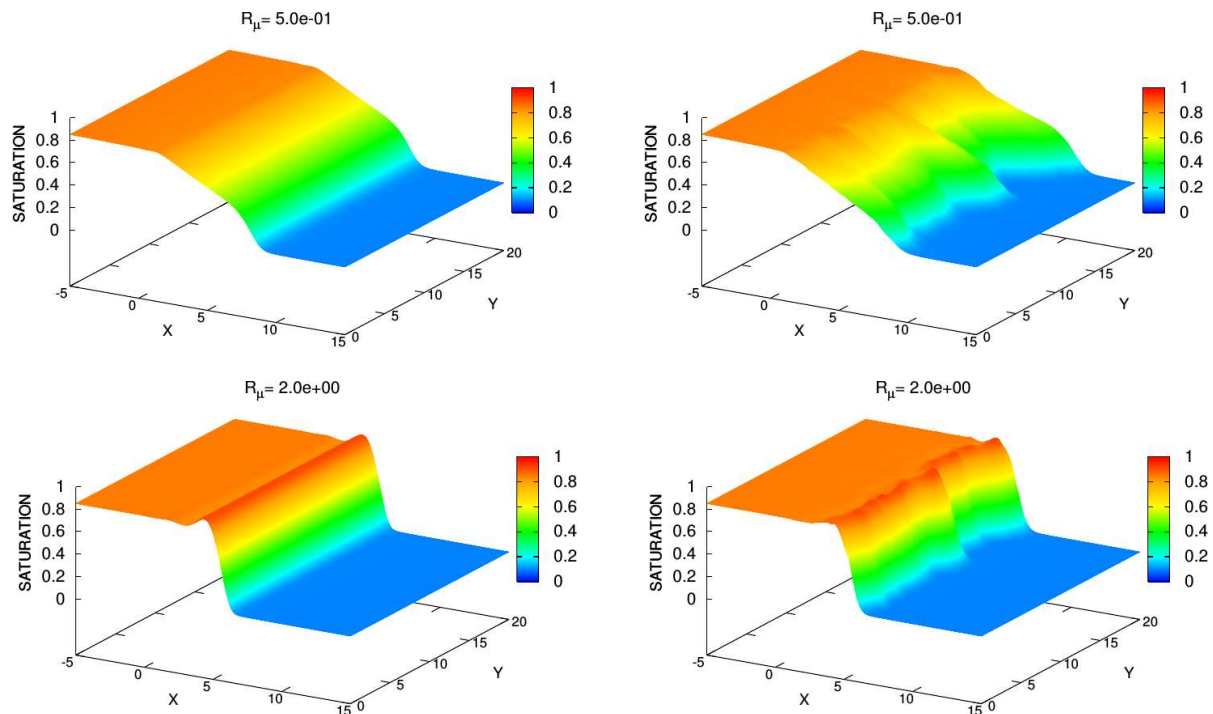


Figure 5.4: Numerical solutions for saturation with different values of viscosity ratio R_μ . On the left (resp. right) column we present simulations with homogeneous (resp. heterogeneous) geologic permeability fields. From top to bottom, we have $R_\mu = 0.5, 2.0$. The solutions were obtained with 1024×1024 elements.

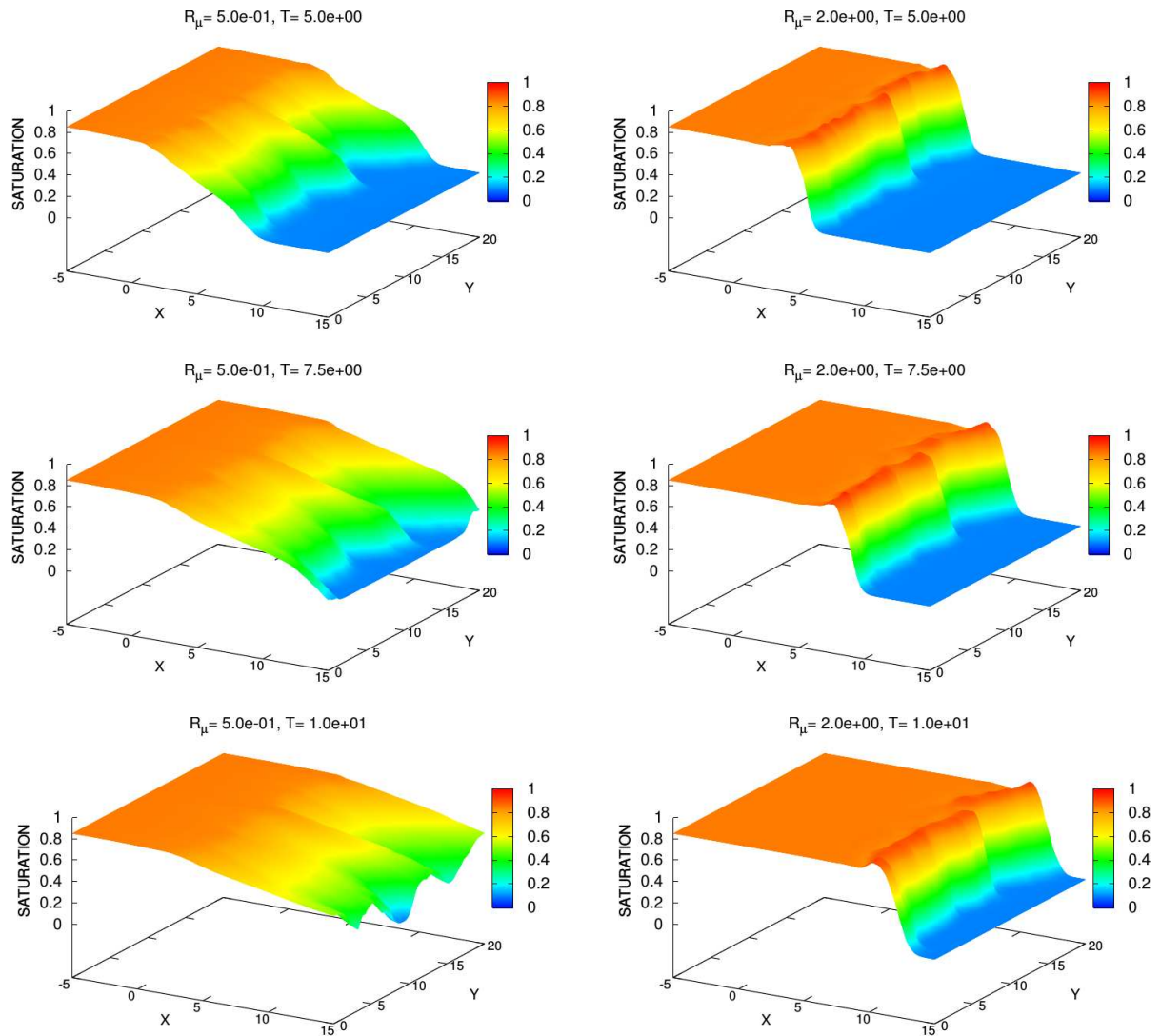


Figure 5.5: Saturation profile during the infiltration in a heterogeneous porous media (3D view). The numerical solutions are presented for $T = 5, 7.5, 10$, from top to bottom, and for $R_\mu = 0.5$ (left) and $R_\mu = 2.0$ (right). The solutions were obtained with 512×512 elements.

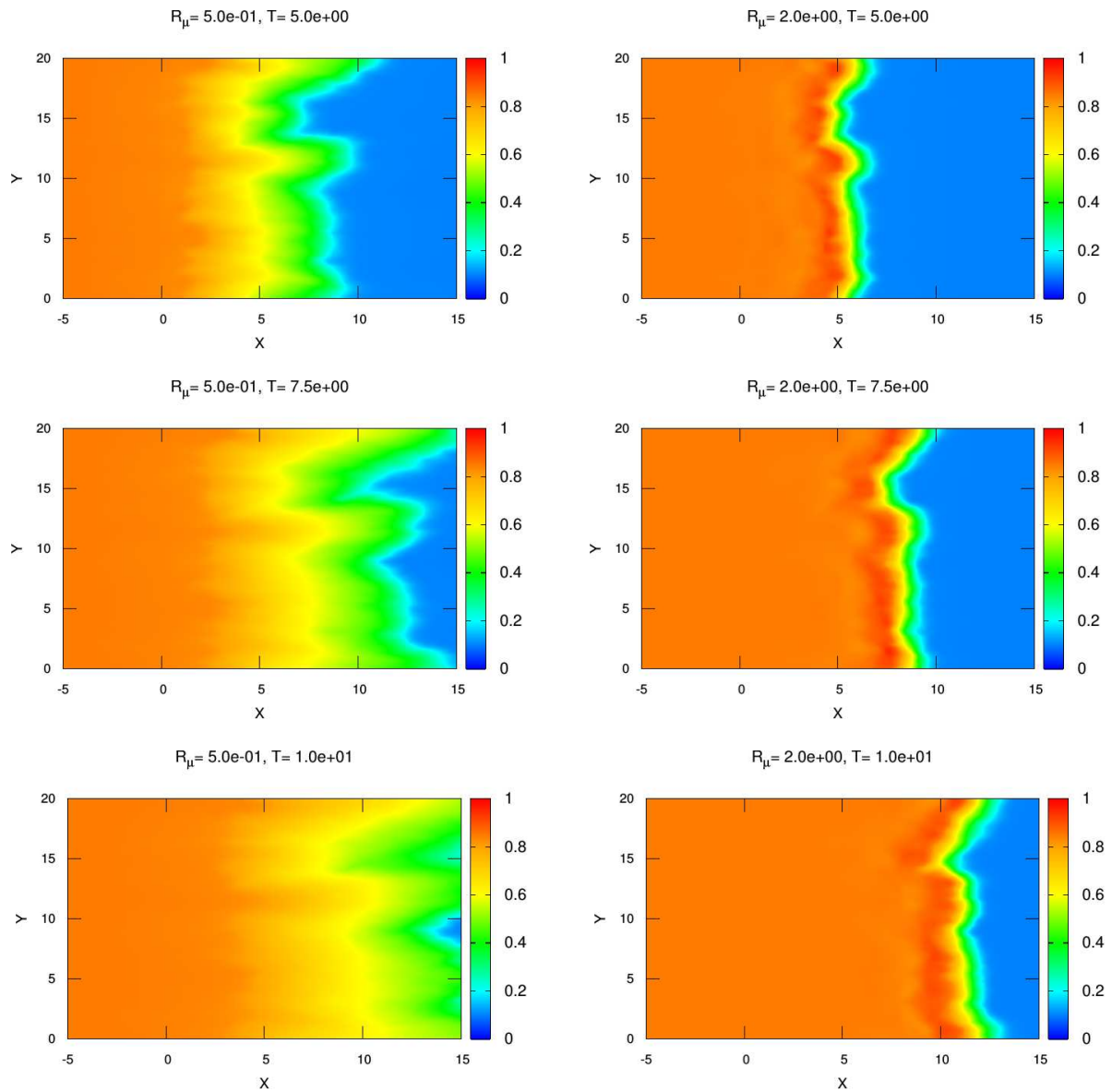


Figure 5.6: Saturation profile during the infiltration in a heterogeneous porous media (color map). The numerical solutions are presented for $T = 5, 7.5, 10$, from top to bottom, and for $R_\mu = 0.5$ (left) and $R_\mu = 2.0$ (right). The solutions were obtained with 512×512 elements.

5.3 Numerical study of gravity effects

In this section we study the gravitational effects on two-phase flow with capillary pressure. We performed numerical simulations with several values of gravity number N_{Gr} . We focused on two cases of direction of gravity: the predominant direction of the flow, i.e., $\nabla Z = \mathbf{e}_1$, and the opposite direction, i.e., $\nabla Z = -\mathbf{e}_1$. Indeed, we simulate cases for heterogeneous permeability fields with different coefficient of variation ($CV = 0.5, 1.0$). We also compare different longitudinal sections of the two-dimensional profile to a numerical solution of one-dimensional homogeneous problem (see Appendix C for more one-dimensional simulations). The parameters of the simulations are:

Computational domain:	$\Omega_{2D} = (-5, 20) \times (-5, 20)$	Final time of simulation:	$T = 10.0$
Left saturation value:	$S_L = 0.85$	Inflow flux:	$Q^{\text{in}} = 1.0$
Right saturation value:	$S_R = 0.10$	Reference pressure value:	$p_n^{\text{ref}} = 0.0$
Viscosity ratio:	$R_\mu = 2.0$	Capillary number:	$N_{Ca} = 1.0$
Density ratio:	$R_\rho = R_\mu$	Gravity number:	$N_{Gr} = 0.125, 0.25, 0.5$
Dynamic effect number:	$N_{Dy} = 0.25$	Stability parameter:	$\sigma_{\text{CFL}} = 0.5$

Figures 5.7 to 5.9 show the numerical solutions for different values of gravity number N_{Gr} , gravity direction ∇Z and coefficient of variation of permeability field $CV(K)$. Figures 5.7 and 5.8 show the solution for the direction of the gravity is $\nabla Z = \mathbf{e}_1$ and $\nabla Z = -\mathbf{e}_1$, respectively, with $CV_K = 0.5$. Figures 5.7 and 5.8 show the solution for the direction of the gravity is $\nabla Z = \mathbf{e}_1$ and $\nabla Z = -\mathbf{e}_1$, respectively, with $CV_K = 1.0$. From top to bottom, the gravity number N_{Gr} varies from 0.125 to 0.5. We find that the new procedure is accurate and robust for solving two-phase transport problems of pseudo-parabolic nature in two space dimensions with high-contrast geologic properties and gravity effects.

Finally, for the parameter range considered, along with distinct dimensionless gravity numbers, viscous fingers are found to undergo interaction with dynamic capillary pressure and gravity effects for typical flow path situations in porous media problems. The dominant feature for these flows is the saturation overshoot, which develops a delay mechanism when dynamic capillary pressure and gravity effects are in balance as seen from numerical simulations from Figures 5.7 to 5.9.

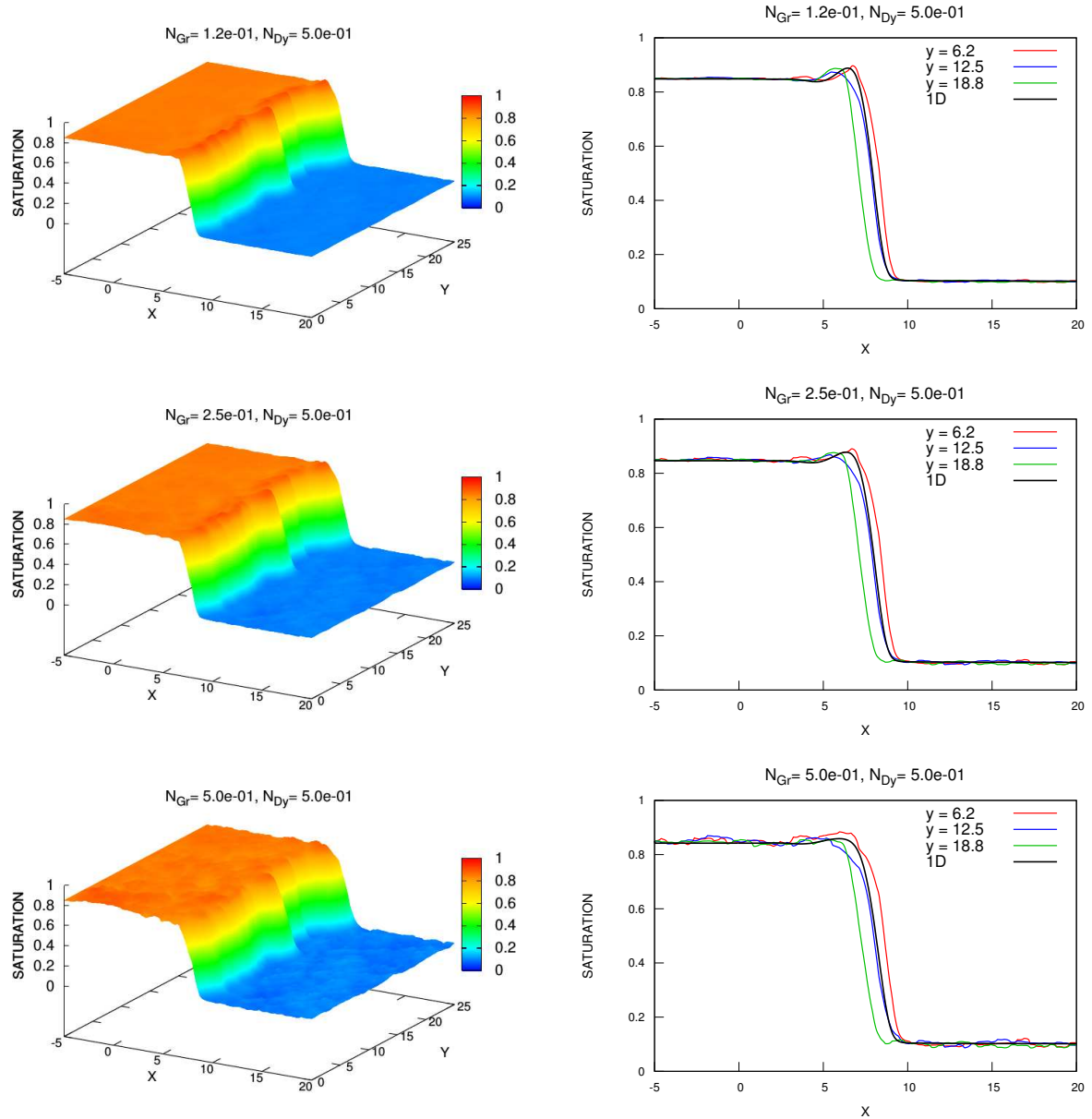


Figure 5.7: Numerical simulations for the flow in the gravity direction and heterogeneous permeability field ($CV_K = 0.5$). The left column presents saturation profile of the two-dimensional simulation. The right column presents longitudinal sections for $y = 6.25, 12.5, 18.75$ along with the reference solution of one-dimensional homogeneous problem (1D). The range of N_{Gr} varies from 0.125 (top) to 0.5 (bottom) and the gravity direction is $(1, 0)$. These simulations use a computational mesh of 512×512 elements.

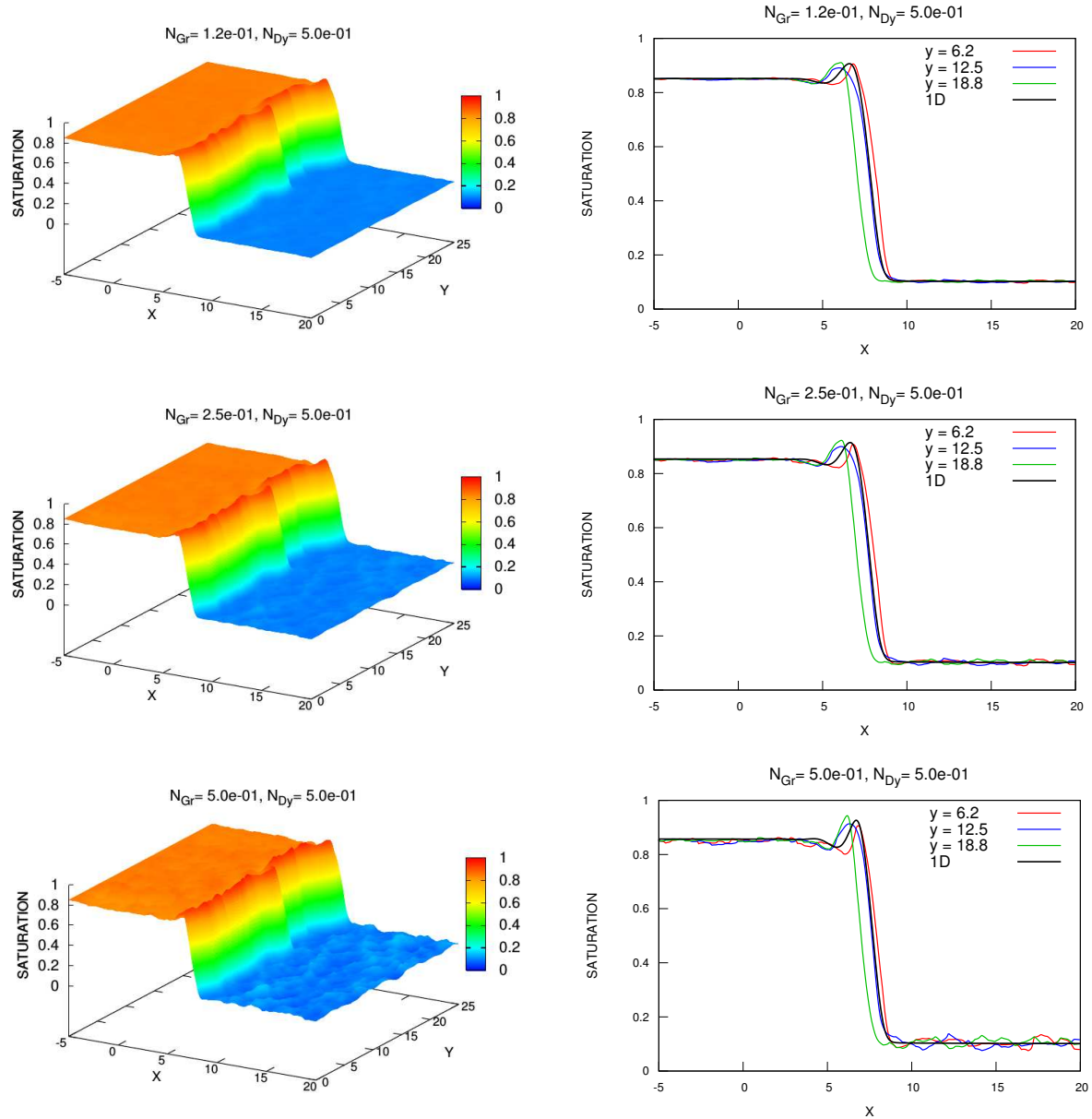


Figure 5.8: Numerical simulations for the flow against the gravity and heterogeneous permeability field ($CV_K = 0.5$). The gravity direction is $(-1, 0)$. The left column presents saturation profile of the two-dimensional simulation. The right column presents longitudinal sections for $y = 6.25, 12.5, 18.75$ along with the reference solution of one-dimensional homogeneous problem (1D). The range of N_{Gr} varies from 0.125 (top) to 0.5 (bottom) and the gravity direction is $(-1, 0)$. These simulations use a computational mesh of 512×512 elements

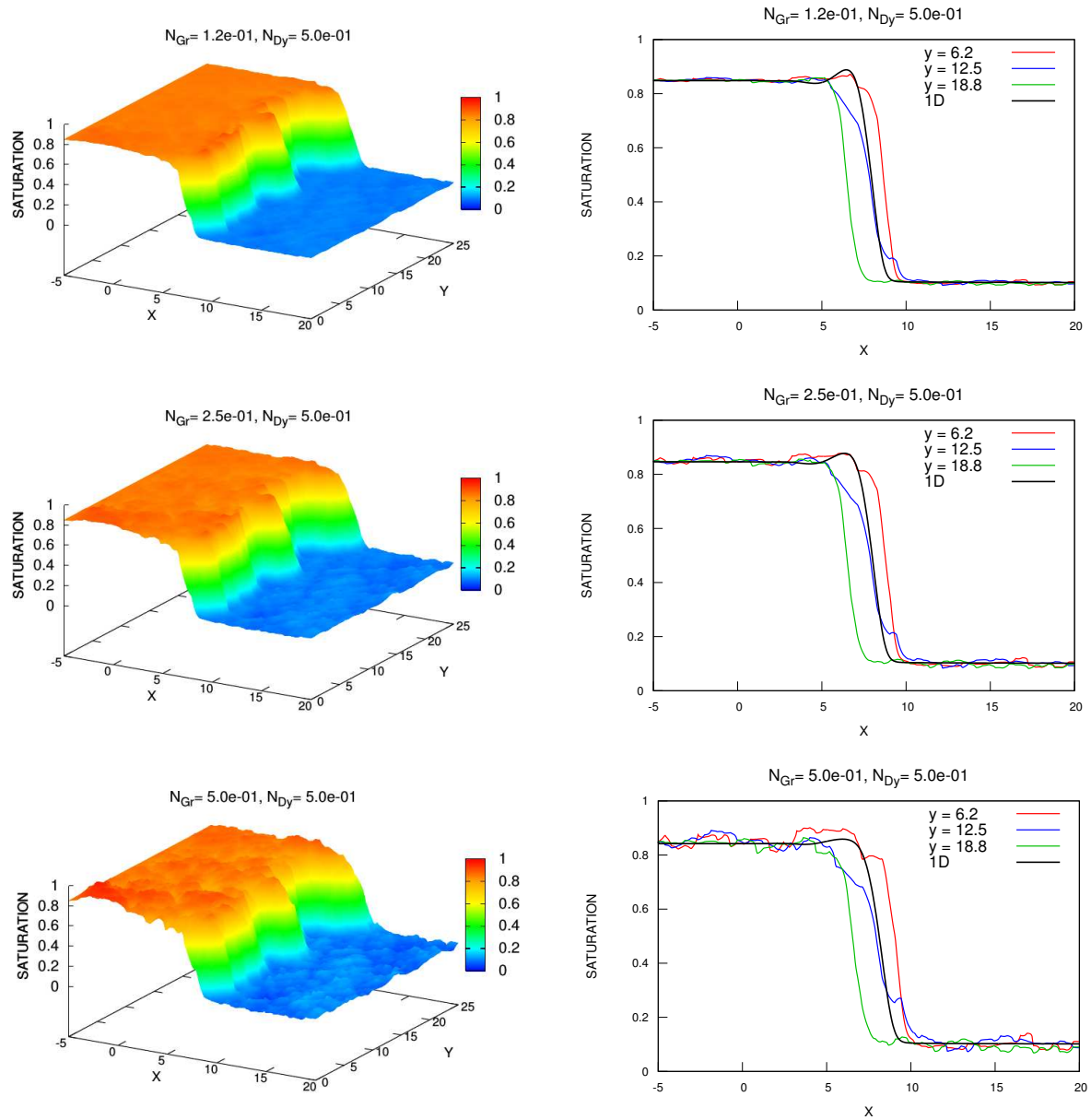


Figure 5.9: Numerical simulations for the flow in the gravity direction and heterogeneous permeability field ($CV_K = 1.0$). The left column presents saturation profile of the two-dimensional simulation. The right column presents longitudinal sections for $y = 6.25, 12.5, 18.75$ along with the reference solution of one-dimensional homogeneous problem (1D). The range of N_{Gr} varies from 0.125 (top) to 0.5 (bottom) and the gravity direction is $(1, 0)$. These simulations use a computational mesh of 512×512 elements.

5.4 Nonlinear model for capillary pressure

In the previous numerical experiments, we consider a linear model (5.4) for the static part $p_e(S_w)$ of dynamic capillary pressure p_c . Now, we investigate the solution behavior taking in account more realistic model for p_e . To study the nonlinear effects of static capillary pressure model, we use the following representative model [2]:

$$p_e(S_w) = \frac{(1 - S_w)}{\sqrt{S_w}}, \quad (5.9)$$

This model is more diffusive for smaller values of S_w , and less diffusive for S_w near to one. The parameters of this simulation were:

Computational domain:	$\Omega_{2D} = (-5, 12) \times (0, 20)$	Final time of simulation:	$T = 7.0$
Left saturation value:	$S_L = 0.85$	Inflow flux:	$Q^{\text{in}} = 1.0$
Right saturation value:	$S_R = 0.10$	Reference pressure value:	$p_n^{\text{ref}} = 0.0$
Viscosity ratio:	$R_\mu = 2.0$	Capillary number:	$N_{Ca} = 1.0$
Density ratio:	$R_\rho = 2.0$	Gravity number:	$N_{Gr} = 0.0$
Dynamic effect number:	$N_{Dy} = 0.25, 0.5, 1.0$	Stability parameter:	$\sigma_{\text{CFL}} = 0.25$

Figure 5.10 shows the numerical saturation profile for $N_{Dy} = 0.25, 0.5, 1.0$. We present one-dimensional homogeneous simulations (right) and two-dimensional experiments with heterogeneous porous media (left). We observe that the qualitative behavior of solution is preserved even for nonlinear model of $p_e(S_w)$. In addition, the solution can present nonmonotone profile for higher values of the dynamic number N_{Dy} .

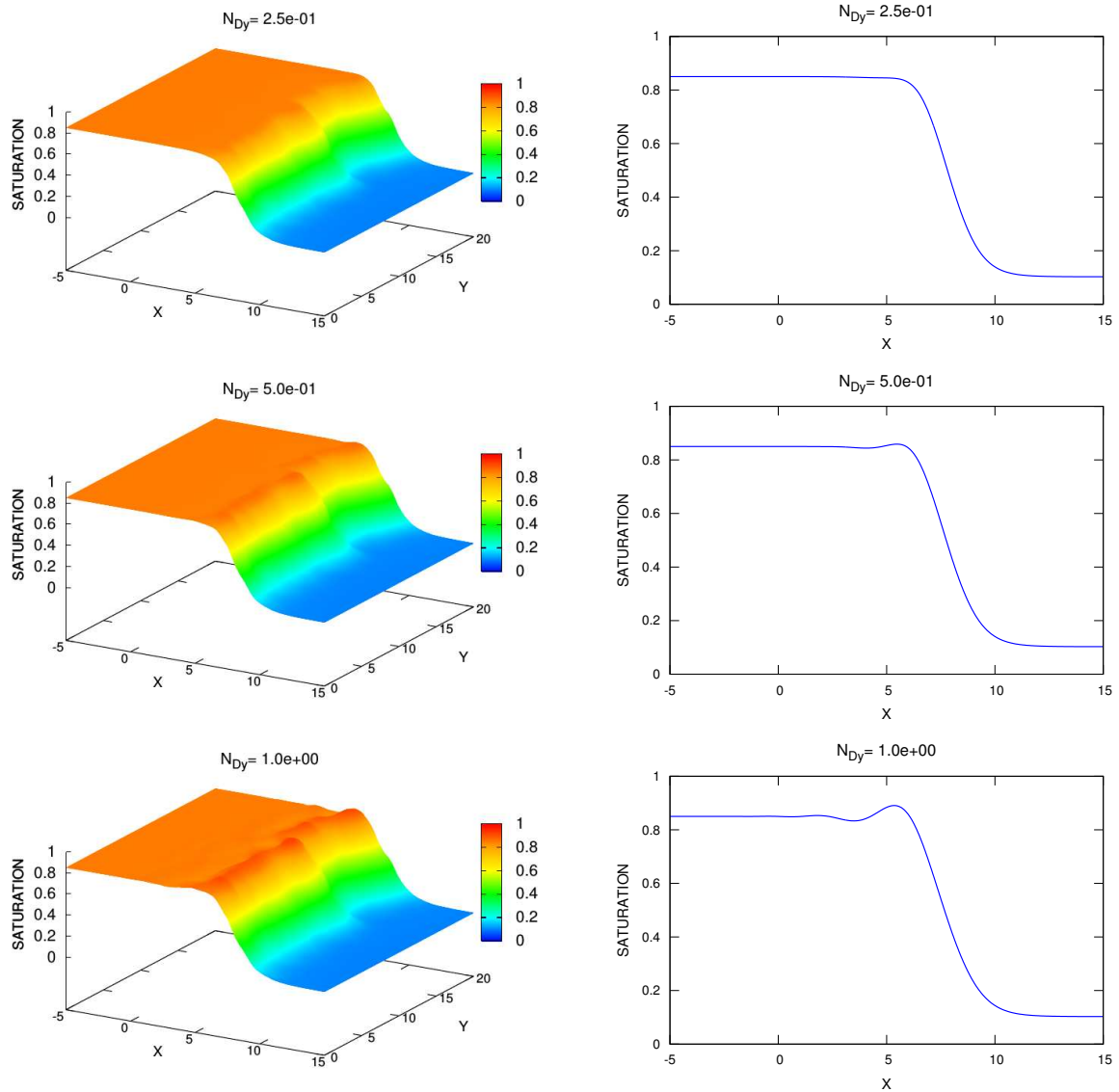


Figure 5.10: Numerical solution for nonlinear static capillary pressure. We present simulations for $N_{Dy} = 0.25, 0.5, 1.0$ (from top to bottom). The left column presents the two-dimensional experiments with heterogeneous permeability fields (512×512 elements). The right column presents the one-dimensional experiments in homogeneous porous media (512 elements).

Chapter 6

Concluding remarks

In this work, we were concerned with the construction of numerical methods to approximate a pseudo-parabolic equation describing two-phase flow in porous media. This equation, differently from the classical parabolic model, takes into account dynamic effects in the pressure difference between interfaces of the two phases. Our numerical approach is locally conservative by construction and combines mixed-hybrid finite element method with finite volume method.

6.1 Final Considerations

The governing system is composed by a saturation transport problem and a pressure-velocity system. We rewrote the transport problem in order to obtain a elliptic equation for capillary pressure along with a evolution equation for saturation. This very convenient formulation is a distinctive point of our work, because it allowed us to use the same numerical approach – mixed-hybrid finite element method – for two parts of the problem (the pressure-velocity and the transport problems). The appropriate choice of approximation spaces allows us to use numerical fluxes based on finite volume technique to deal with the hyperbolic term of the transport equation. The time discretization decouples the pressure-velocity system from the saturation transport problem resulting in two systems of nonlinear algebraic equations. We solved the discrete nonlinear systems through an iterative procedure.

We performed two-dimensional experiments with different flow conditions. Based on refinement study, we obtained good evidences of numerical convergence and accuracy of computed solution. We also studied numerically the gravity effects and the viscosity effects on the solution profile. We verified that for smaller viscosity ratio (wetting phase less viscous than non-wetting phase) the solution profile presents more finger-like patterns. In addition, we observed that when the flows occurs in gravity direction, the solution changes from nonmonotone to monotone by increasing gravity number.

6.2 Perspectives for future work

Finally, we point out some open subjects to explore in fields of theory, numerics and applications that can be issues for future works:

- We presented and implemented the numerical method for one and two-dimensional domains, but our framework can be extended to three spatial dimensions;
- The overall approach can be naturally parallelized by using, for instance, the ideas of the domain decomposition method for elliptic problems proposed in [29];
- Computational solution of many physical problems in large domains with high heterogeneous properties could be computationally intractable by standard fine-grid methods. The multiscale methods were developed to reduce the computational cost keeping needed accuracy of approximated solution. Many multiscale approaches are based on mixed finite element methods, e.g., [6, 40, 48]. Thus, our framework can be applied in the context of multiscale methods;
- Our approach does not handle degenerate values, however we can circumvent this by following the ideas of [3];
- New numerical analysis techniques can be exploited to access a stability condition based on rigorous convergence proof at least for the one-dimensional problem [7, 25];
- As mentioned in our literature review in Chapter 1, the pseudo-parabolic equations are related to other non-equilibrium models, which may extend the dynamic capillary pressure. A topic for future developments is to extend our framework in order to take into account other physical phenomena such as hysteresis [89, 105];
- The mixed finite element method combined with finite volume techniques have been successfully applied to study the three-phase in porous media with static capillary pressure models (see, e.g. [2, 3] and the references therein). Thus, we may use the same approach presented in this work to study numerically the three-phase problem with dynamic capillary pressure. It is worth to mention that, in the best of our knowledge, the three-phase flow in porous media with dynamic capillary pressure model after Hassanizadeh and Gray [51] is an open subject in theory, experiments and numerics.

References

- [1] L.K. Abidoye and D.B. Das. “Scale dependent dynamic capillary pressure effect for two-phase flow in porous media”. In: *Adv. Water Resour.* 74 (2014), pp. 212–230.
- [2] E. Abreu. “Numerical modelling of three-phase immiscible flow in heterogeneous porous media with gravitational effects”. In: *Math. Comput. Simul.* 97 (2014), pp. 234–259.
- [3] E. Abreu and D. Conceição. “Numerical modeling of degenerate equations in porous media flow”. In: *J. Sci. Comput.* 55 (2013), pp. 688–717.
- [4] E. Abreu, J. Douglas, F. Furtado, and F. Pereira. “Operator splitting based on physics for flow in porous media”. In: *Int. J. Comput. Sci.* 2 (2008), pp. 315–335.
- [5] E. Abreu and J. Vieira. “Computing numerical solutions of the pseudo-parabolic Buckley–Leverett equation with dynamic capillary pressure”. In: *Math. Comput. Simul.* 137 (2017), pp. 29–48.
- [6] T. Arbogast, G. Pencheva, M.F. Wheeler, and I. Yotov. “A multiscale mortar mixed finite element method”. In: *Multiscale Modeling & Simulation* 6.1 (2007), pp. 319–346.
- [7] D.N. Arnold, J. Douglas, and V. Thomée. “Superconvergence of a finite element approximation to the solution of a Sobolev equation in a single space variable”. In: *Math. Comput.* 36 (1981), pp. 53–63.
- [8] K. Aziz and A. Settari. *Petroleum reservoir simulation*. Vol. 476. Applied Science Publishers London, 1979.
- [9] G. Barenblatt, I.P. Zheltov, and I. Kochina. “Basic concepts in the theory of seepage of homogeneous liquids in fissured rocks [strata]”. In: *J. Appl. Math. Mech.* 24 (1960), pp. 1286–1303.
- [10] G.I. Barenblatt, T.W. Patzek, and D.B. Silin. “The mathematical model of nonequilibrium effects in water-oil displacement”. In: *SPE Journal* 8.4 (2003), pp. 409–416.
- [11] J. Bear and A.H.D. Cheng. *Modeling groundwater flow and contaminant transport*. Vol. 23. Springer, 2010.

- [12] A.Y. Beliaev and S.M. Hassanizadeh. “A theoretical model of hysteresis and dynamic effects in the capillary relation for two-phase flow in porous media”. In: *Transport in Porous media* 43.3 (2001), pp. 487–510.
- [13] T.B. Benjamin, J.L. Bona, and J.J. Mahony. “Model equations for long waves in nonlinear dispersive systems”. In: *Philosophical Transactions of the Royal Society of London A: Mathematical, Physical and Engineering Sciences* 272 (1972), pp. 47–78.
- [14] S. Bottero, S.M. Hassanizadeh, P.J. Kleingeld, and A. Bezuijen. “Experimental study of dynamic capillary pressure effect in two-phase flow in porous media”. In: *Proceedings of the XVI International Conference on Computational Methods in Water Resources (CMWR), Copenhagen, Denmark. 2006*, pp. 18–22.
- [15] R.H. Brooks and A.T. Corey. “Hydraulic properties of porous media”. In: *Hydrology Papers* 3 (1964). Ed. by Ft Colorado State University.
- [16] X. Cao and I.S. Pop. “Two-phase porous media flows with dynamic capillary effects and hysteresis: uniqueness of weak solutions”. In: *Computers & Mathematics with Applications* 69.7 (2015), pp. 688–695.
- [17] X. Cao and I.S. Pop. “Uniqueness of weak solutions for a pseudo-parabolic equation modeling two phase flow in porous media”. In: *Applied Mathematics Letters* 46 (2015), pp. 25–30.
- [18] X. Cao and I.S. Pop. “Degenerate two-phase porous media flow model with dynamic capillarity”. In: *Journal of Differential Equations* 260.3 (2016), pp. 2418–2456.
- [19] G. Chavent and J. Jaffre. *Mathematical Models and Finite Elements for Reservoir Simulation*. Elsevier, 1991.
- [20] G. Chavent and J.E. Roberts. “A unified physical presentation of mixed, mixed-hybrid finite elements and standard finite difference approximations for the determination of velocities in waterflow problems”. In: *Advances in Water Resources* 14.6 (1991), pp. 329–348.
- [21] P.J. Chen and M.E. Gurtin. “On a theory of heat conduction involving two temperatures”. In: *Z. Angew. Math. Phys.* 19 (1968), pp. 614–627.
- [22] G.M. Coclite, S. Mishra, N.H. Risebro, and F. Weber. “Analysis and numerical approximation of Brinkman regularization of two-phase flows in porous media”. In: *Computational Geosciences* 18.5 (2014), pp. 637–659.
- [23] C. Cuesta, C. van Duijn, and J. Hulshof. “Infiltration in porous media with dynamic capillary pressure: travelling waves”. In: *European Journal of Applied Mathematics* 11.4 (2000), pp. 381–397.

- [24] C. Cuesta and J. Hulshof. “A model problem for groundwater flow with dynamic capillary pressure: stability of travelling waves”. In: *Nonlinear Analysis: Theory, Methods & Applications* 52.4 (2003), pp. 1199–1218.
- [25] C. Cuesta and I.S. Pop. “Numerical schemes for a pseudo-parabolic burgers equation: discontinuous data and long-time behaviour”. In: *J. Comput. Appl. Math.* 224 (2009), pp. 269–283.
- [26] D.B. Das and M. Mirzaei. “Dynamic effects in capillary pressure relationships for two-phase flow in porous media: Experiments and numerical analyses”. In: *AIChE Journal* 58.12 (2012), pp. 3891–3903.
- [27] D.A. DiCarlo. “Experimental measurements of saturation overshoot on infiltration”. In: *Water Resources Research* 40.4 (2004).
- [28] J. Douglas Jr, F. Furtado, and F. Pereira. “On the numerical simulation of waterflooding of heterogeneous petroleum reservoirs”. In: *Comput. Geosci.* 1 (1997), pp. 155–190.
- [29] J. Douglas Jr, P.P. Leme, J. Roberts, and J. Wang. “A parallel iterative procedure applicable to the approximate solution of second order partial differential equations by mixed finite element methods”. In: *Numer. Math.* 65 (1993), pp. 95–108.
- [30] J. Douglas Jr, F. Pereira, and C. Zentsop. “Model development for the numerical simulation of CO₂ storage in naturally fractured saline aquifers”. In: *Computational Models for CO₂ Sequestration and Compressed Air Energy Storage*. Ed. by Al-Khoury R and J. Bundschuh. Taylor & Francis Group/CRC Press, 2014.
- [31] C. van Duijn, Y. Fan, L. Peletier, and I.S. Pop. “Travelling wave solutions for degenerate pseudo-parabolic equations modelling two-phase flow in porous media”. In: *Nonlinear Anal. Real World Appl.* 14 (2013), pp. 1361–1383.
- [32] C. van Duijn, L. Peletier, and I.S. Pop. “A new class of entropy solutions of the Buckley-Leverett equation”. In: *SIAM J. Math. Anal.* 39 (2007), pp. 507–536.
- [33] C. J van Duijn, X. Cao, and I.S. Pop. “Two-phase flow in porous media: dynamic capillarity and heterogeneous media”. In: *Transport in Porous Media* 114.2 (2016), pp. 283–308.
- [34] R.E. Ewing. “Time-stepping Galerkin methods for nonlinear Sobolev partial differential equations”. In: *SIAM Journal on Numerical Analysis* 15.6 (1978), pp. 1125–1150.
- [35] Y. Fan and I.S. Pop. “A class of pseudo-parabolic equations: existence, uniqueness of weak solutions, and error estimates for the Euler implicit discretization.” In: *Math. Methods Appl. Sci.* 34.18 (2011), pp. 2329–2339.

- [36] Y. Fan and I.S. Pop. “Equivalent formulations and numerical schemes for a class of pseudo-parabolic equations”. In: *J. Comput. Appl. Math.* 246 (2013), pp. 86–93.
- [37] W.H. Ford. “Galerkin approximations to non-linear pseudo-parabolic partial differential equations”. In: *Aequationes mathematicae* 14.3 (1976), pp. 271–291.
- [38] W.H. Ford and T.W. Ting. “Stability and convergence of difference approximations to pseudo-parabolic partial differential equations”. In: *mathematics of computation* 27.124 (1973), pp. 737–743.
- [39] W.H. Ford and T.W. Ting. “Uniform error estimates for difference approximations to nonlinear pseudo-parabolic partial differential equations”. In: *SIAM Journal on Numerical Analysis* 11.1 (1974), pp. 155–169.
- [40] A. Francisco, V. Ginting, F. Pereira, and J. Rigelo. “Design and implementation of a multiscale mixed method based on a nonoverlapping domain decomposition procedure”. In: *Math. Comput. Simul.* 99 (2014), pp. 125–138.
- [41] R. Fučík and J. Mikyška. “Numerical investigation of dynamic capillary pressure in two-phase flow in porous medium”. In: *Mathematica Bohemica* 136.4 (2011), pp. 395–403.
- [42] R. Fučík, J. Mikyška, T. Sakaki, M. Beneš, and T.H. Illangasekare. “Significance of Dynamic Effect in Capillarity during Drainage Experiments in Layered Porous Media”. In: *Vadose Zone Journal* 9.3 (2010), pp. 697–708.
- [43] S.E. Gasda, M.W. Farthing, C.E. Kees, and C.T. Miller. “Adaptive split-operator methods for modeling transport phenomena in porous medium systems”. In: *Advances Water Resour.* 34 (2011), pp. 1268–1282.
- [44] J. Glimm and D.H. Sharp. “A random field model for anomalous diffusion in heterogeneous porous media”. In: *Journal of Statistical Physics* 62.1 (1991), pp. 415–424.
- [45] Ö.F. Gözükızıl and Ş. Akçağıl. “Exact solutions of Benjamin-Bona-Mahony-Burgers-type nonlinear pseudo-parabolic equations”. In: *Boundary Value Problems* 2012.1 (2012), p. 144.
- [46] W.G. Gray and S.M. Hassanizadeh. “Paradoxes and realities in unsaturated flow theory”. In: *Water Resources Research* 27.8 (1991), pp. 1847–1854.
- [47] W.G. Gray and S.M. Hassanizadeh. “Unsaturated flow theory including interfacial phenomena”. In: *Water Resources Research* 27.8 (1991), pp. 1855–1863.
- [48] R.T. Guiraldello, R.F. Ausas, F.S. Sousa, F. Pereira, and G.C. Buscaglia. “The Multiscale Robin Coupled Method for flows in porous media”. In: *J. Comput. Phys.* 355 (2018), pp. 1–21.

- [49] S.M. Hassanizadeh, M. A Celia, and H.K. Dahle. “Dynamic effect in the capillary pressure–saturation relationship and its impacts on unsaturated flow”. In: *Vadose Zone Journal* 1.1 (2002), pp. 38–57.
- [50] S.M. Hassanizadeh and W.G. Gray. “Mechanics and thermodynamics of multiphase flow in porous media including interphase boundaries”. In: *Adv. Water Resour.* 13.4 (1990), pp. 169–186.
- [51] S.M. Hassanizadeh and W.G. Gray. “Thermodynamic basis of capillary pressure in porous media”. In: *Water Resour. Res.* 29 (1993), pp. 3389–3405.
- [52] S.M. Hassanizadeh and W.G. Gray. “Toward an improved description of the physics of two-phase flow”. In: *Advances in Water Resources* 16.1 (1993), pp. 53–67.
- [53] R. Helmig, A. Weiss, and B.I. Wohlmuth. “Dynamic capillary effects in heterogeneous porous media”. In: *Computational Geosciences* 11.3 (2007), pp. 261–274.
- [54] R. Hilfer, F. Doster, and P.A. Zegeling. “Nonmonotone saturation profiles for hydrostatic equilibrium in homogeneous porous media”. In: *Vadose Zone J.* 11.3 (2012).
- [55] R. Hilfer and R. Steinle. “Saturation overshoot and hysteresis for twophase flow in porous media”. In: *Eur. Phys. J. Spec. Top* 223.11 (2014), pp. 2323–2338.
- [56] H. Holden, K.H. Karlsen, K.A. Lie, and N.H. Risebro. *Splitting Methods for Partial Differential Equations with Rough Solutions: Analysis and MATLAB programs. Series of Lectures in Mathematics*. Zurich: European Mathematical Society, 2010.
- [57] T. Holstein. “Imprisonment of resonance radiation in gases”. In: *Phys. Rev.* 72 (1947), p. 1212.
- [58] T. Holstein. “Imprisonment of resonance radiation in gases. ii”. In: *Phys. Rev.* 83 (1951), p. 1159.
- [59] O. Iliev, G. Printsypar, and S. Rief. “A two-dimensional model of the pressing section of a paper machine including dynamic capillary effects”. In: *J. Eng. Math.* 83.1 (2013), pp. 81–107.
- [60] F.J.M. Kalaydjian. “Dynamic capillary pressure curve for water/oil displacement in porous media: Theory vs. experiment”. In: *SPE Annual Technical Conference and Exhibition*. Society of Petroleum Engineers. 1992.
- [61] C.Y. Kao, A. Kurganov, Z. Qu, and Y. Wang. “A fast explicit operator splitting method for modified Buckley–Leverett equations”. In: *Journal of Scientific Computing* 64.3 (2015), pp. 837–857.
- [62] G. Karch. “Asymptotic behaviour of solutions to some pseudoparabolic equations”. In: *Mathematical Methods in the Applied Sciences* 20.3 (1997), pp. 271–289.

- [63] K.H. Karlsen, K.A. Lie, J.R. Natvig, H.F. Nordhaug, and H.K. Dahle. “Operator splitting methods for systems of convection–diffusion equations: nonlinear error mechanisms and correction strategies”. In: *J. Comput. Phys.* 173.2 (2001), pp. 636–663.
- [64] K.H. Karlsen and N.H. Risebro. “Corrected operator splitting for nonlinear parabolic equations”. In: *SIAM J. Numer. Anal.* 37.3 (2000), pp. 980–1003.
- [65] S. Karpinski and I.S. Pop. “Analysis of an interior penalty discontinuous Galerkin scheme for two phase flow in porous media with dynamic capillary effects”. In: *Numer. Math.* 136.1 (2017), pp. 249–286.
- [66] S. Karpinski, I.S. Pop, and F.A. Radu. “Analysis of a linearization scheme for an interior penalty discontinuous Galerkin method for two-phase flow in porous media with dynamic capillarity effects”. In: *Int. J. Numer. Methods Eng.* (2017).
- [67] F. Kissling and K.H. Karlsen. “On the singular limit of a two-phase flow equation with heterogeneities and dynamic capillary pressure”. In: *ZAMM-Journal of Applied Mathematics and Mechanics/Zeitschrift für Angewandte Mathematik und Mechanik* 94.7-8 (2014), pp. 678–689.
- [68] M.O. Korpusov and A.G. Sveshnikov. “Blow-up of solutions of strongly nonlinear equations of pseudoparabolic type”. In: *Journal of Mathematical Sciences* 148.1 (2008), pp. 1–142.
- [69] E. Kreyszig. *Introductory functional analysis with applications*. Wiley New York, 1978.
- [70] R.J. LeVeque. *Finite difference methods for ordinary and partial differential equations: steady-state and time-dependent problems*. Vol. 98. Siam, 2007.
- [71] M. Liebmann. *A User Friendly Toolbox for Parallel PDE-Solvers*. 2006. URL: <http://paralleltoolbox.sourceforge.net/>.
- [72] G. Løvoll, M. Jankov, K.J. Måløy, R. Toussaint, J. Schmittbuhl, G. Schäfer, and Y. Méheust. “Influence of viscous fingering on dynamic saturation–pressure curves in porous media”. In: *Transport in porous media* 86.1 (2011), pp. 305–324.
- [73] S. Manthey. “Two-phase processes with dynamic effects in porous media–parameter estimation and simulation”. PhD thesis. Ph. D. thesis, Institut für Wasserbau. Universität Stuttgart, Germany, 2006.
- [74] S. Manthey, S.M. Hassanizadeh, R. Helmig, and R. Hilfer. “Dimensional analysis of two-phase flow including a rate-dependent capillary pressure–saturation relationship”. In: *Adv. Water Resour.* 31.9 (2008), pp. 1137–1150.

- [75] M.A. Mendes, M.A. Murad, and F. Pereira. “A new computational strategy for solving two-phase flow in strongly heterogeneous poroelastic media of evolving scales”. In: *International Journal for Numerical and Analytical Methods in Geomechanics* 36.15 (2012), pp. 1683–1716.
- [76] A. Mikelić. “A global existence result for the equations describing unsaturated flow in porous media with dynamic capillary pressure”. In: *Journal of Differential Equations* 248.6 (2010), pp. 1561–1577.
- [77] A. Mikelić and H. Bruining. “Analysis of model equations for stress-enhanced diffusion in coal layers. Part I: Existence of a weak solution”. In: *SIAM Journal on Mathematical Analysis* 40.4 (2008), pp. 1671–1691.
- [78] E.A. Milne. “The diffusion of imprisoned radiation through a gas”. In: *J. Lond. Math. Soc.* 1 (1926), pp. 40–51.
- [79] M. Mirzaei and D.B. Das. “Dynamic effects in capillary pressure–saturation relationships for two-phase flow in 3D porous media: Implications of micro-heterogeneities”. In: *Chemical engineering science* 62.7 (2007), pp. 1927–1947.
- [80] J.L. Nieber, R.Z. Dautov, A.G. Egorov, and A.Y. Sheshukov. “Dynamic capillary pressure mechanism for instability in gravity-driven flows; review and extension to very dry conditions”. In: *Transport in porous media* 58.1-2 (2005), pp. 147–172.
- [81] A. Novick-Cohen and R.L. Pego. “Stable patterns in a viscous diffusion equation”. In: *Trans. Am. Math. Soc.* 324 (1991), pp. 331–351.
- [82] O. Oung, S.M. Hassanizadeh, and A. Bezuijen. “Two-phase flow experiments in a geocentrifuge and the significance of dynamic capillary pressure effect”. In: *Journal of Porous Media* 8.3 (2005).
- [83] D.W. Peaceman. *Fundamentals of numerical reservoir simulation*. Elsevier, 2000.
- [84] M. Peszynska and S.Y. Yi. “Numerical methods for unsaturated flow with dynamic capillary pressure in heterogeneous porous media”. In: *Int. J. Numer. Anal. Model* 5 (2008), pp. 126–149.
- [85] M. Ptashnyk. “Nonlinear pseudoparabolic equations as singular limit of reaction–diffusion equations”. In: *Applicable Analysis* 85.10 (2006), pp. 1285–1299.
- [86] A. Quarteroni. “Fourier spectral methods for pseudoparabolic equations”. In: *SIAM journal on numerical analysis* 24.2 (1987), pp. 323–335.
- [87] P.A. Raviart and J.M. Thomas. “A mixed finite element method for 2-nd order elliptic problems”. In: *Mathematical Aspects of Finite Element Methods*. Springer, 1977, pp. 292–315.
- [88] L. Rubinstein. “On the problem of the process of propagation of heat in heterogeneous media”. In: *Izv. Akad. Nauk SSSR, Ser. Geogr* 1 (1948), pp. 12–45.

- [89] A. Rätz and B. Schweizer. “Hysteresis models and gravity fingering in porous media”. In: *ZAMM - J. Appl. Math. Mech. / Z. Angew. Math. Mech.* 94.7-8 (2014), pp. 645–654.
- [90] G.C. Sander, O.J. Glidewell, and J. Norbury. “Dynamic capillary pressure, hysteresis and gravity-driven fingering in porous media”. In: *Journal of Physics: Conference Series*. Vol. 138. 1. IOP Publishing. 2008, p. 012023.
- [91] B. Schweizer. “The Richards equation with hysteresis and degenerate capillary pressure”. In: *Journal of Differential Equations* 252.10 (2012), pp. 5594–5612.
- [92] M. Shearer, K.R. Spayd, and E.R. Swanson. “Traveling waves for conservation laws with cubic nonlinearity and BBM type dispersion”. In: *Journal of Differential Equations* 259.7 (2015), pp. 3216–3232.
- [93] R.E. Showalter. “Partial differential equations of Sobolev-Galpern type”. In: *Pacific Journal of Mathematics* 31.3 (1969), pp. 787–793.
- [94] R.E. Showalter. “A nonlinear parabolic-Sobolev equation”. In: *Journal of Mathematical Analysis and Applications* 50.1 (1975), pp. 183–190.
- [95] R.E. Showalter and T.W. Ting. “Pseudoparabolic partial differential equations”. In: *SIAM Journal on Mathematical Analysis* 1.1 (1970), pp. 1–26.
- [96] K. Spayd. “Generalizing the modified Buckley–Leverett equation with TCAT capillary pressure”. In: *European Journal of Applied Mathematics* 29.2 (2018), pp. 338–351.
- [97] K. Spayd and M. Shearer. “The Buckley–Leverett equation with dynamic capillary pressure”. In: *SIAM Journal on Applied Mathematics* 71.4 (2011), pp. 1088–1108.
- [98] F. Stauffer. “Time dependence of the relations between capillary pressure, water content and conductivity during drainage of porous media”. In: *IAHR symposium on scale effects in porous media, Thessaloniki, Greece*. Vol. 29. 1978, pp. 3–35.
- [99] M. Stecher and W. Rundell. “Maximum principles for pseudoparabolic partial differential equations”. In: *Journal of Mathematical Analysis and Applications* 57.1 (1977), pp. 110–118.
- [100] E. Tadmor. “Chapter 18 - Entropy Stable Schemes”. In: *Handbook of Numerical Methods for Hyperbolic Problems*. Ed. by Rémi Abgrall and Chi-Wang Shu. Vol. 17. Handbook of Numerical Analysis. Elsevier, 2016, pp. 467–493.
- [101] T.W. Ting. “Parabolic and pseudo-parabolic partial differential equations”. In: *Journal of the Mathematical Society of Japan* 21.3 (1969), pp. 440–453.
- [102] P.N. Vabishchevich and A.V. Grigor’ev. “Splitting schemes for pseudoparabolic equations”. In: *Differential Equations* 49.7 (2013), pp. 807–814.

- [103] D.A. Weitz, J.P. Stokes, R.C. Ball, and A.P. Kushnick. “Dynamic capillary pressure in porous media: Origin of the viscous-fingering length scale”. In: *Phys. Rev. Lett.* 59.26 (1987), p. 2967.
- [104] M. Yang. “Analysis of second order finite volume element methods for pseudo-parabolic equations in three spatial dimensions”. In: *Applied Mathematics and Computation* 196.1 (2008), pp. 94–104.
- [105] H. Zhang and P.A. Zegeling. “A numerical study of two-phase flow models with dynamic capillary pressure and hysteresis”. In: *Transp. Porous Media* 116.2 (2017), pp. 825–846.
- [106] F. Zürnacı. “Convergence Analysis and Numerical Solutions of the Fisher’s and Benjamin-Bono-Mahony Equations by Operator Splitting Method”. MA thesis. Izmir Institute of Technology, 2014.

Appendix A

Stability analysis for a simplified pseudo-parabolic model

The purpose of this appendix is to provide a preliminary stability analysis for the hybrid mixed finite element method employed in the solution of the pseudo-parabolic equation. We consider here a linear one-dimensional pseudo-parabolic model. We employ the Van-Neumann stability analysis to the fully discrete system to obtain a consistent stability condition. We also present a condition for the convergence of the (fixed point) iterative procedure used in this work.

A.1 One-dimensional simplified model

Consider the linear pseudo-parabolic system defined over the one-dimensional domain $\Omega = (x_a, x_b)$:

$$\frac{\partial s}{\partial t} + a \frac{\partial s}{\partial x} = -\varepsilon \frac{\partial^2 p}{\partial x^2}, \quad (\text{A.1a})$$

$$p = -\left(s + \tau \frac{\partial s}{\partial t}\right), \quad (\text{A.1b})$$

where $a > 0$, $\varepsilon > 0$ and $\tau > 0$. The initial and boundary conditions are given by,

$$s(x_a, t) = s_l, \quad s(x_b, t) = s_r, \quad t > 0, \quad (\text{A.2a})$$

$$s(x, 0) = s_0(x), \quad x \in \Omega, \quad (\text{A.2b})$$

We rewrite the system (A.1) as follows,

$$-\varepsilon \frac{\partial^2 p}{\partial x^2} + \frac{1}{\tau} p = a \frac{\partial s}{\partial x} - \frac{s}{\tau}, \quad (\text{A.3a})$$

$$\frac{\partial s}{\partial t} = -\frac{s + p}{\tau}. \quad (\text{A.3b})$$

The boundary conditions consistent with (A.2a),

$$p(x_a, t) = p_l = -s_l, \quad p(x_b, t) = p_r = -s_r. \quad (\text{A.4})$$

Remark A.1.1. It is worth to mention that pressure-velocity system linked to the one-dimensional two-phase flow in porous media has constant solution for the total velocity.

A.2 One-dimensional numerical scheme

The discretization of Eq. (A.3a) by mixed finite elements method and Eq.(A.3b) by backward Euler method leads to the numerical scheme:

$$-\varepsilon \left(\frac{p_{j-1}^{n+1} - 2p_j^{n+1} + p_{j+1}^{n+1}}{\Delta x^2} \right) + \frac{1}{\tau} p_j^{n+1} = a \left(\frac{s_j^n - s_{j-1}^n}{\Delta x} \right) - \frac{s_j^{n+1}}{\tau} \quad (\text{A.5a})$$

$$s_j^{n+1} = s_j^n - \Delta t \left(\frac{s_j^{n+1} + p_j^{n+1}}{\tau} \right). \quad (\text{A.5b})$$

We can rewrite Eq. (A.5b) as follows,

$$p_j^{n+1} = -s_j^{n+1} - \tau \left(\frac{s_j^{n+1} - s_j^n}{\Delta t} \right). \quad (\text{A.6})$$

By replacing (A.6) in (A.5a), we get:

$$\begin{aligned} & \varepsilon \left(\frac{s_{j-1}^{n+1} - 2s_j^{n+1} + s_{j+1}^{n+1}}{\Delta x^2} \right) + \frac{\varepsilon \tau}{\Delta t} \left(\frac{s_{j-1}^{n+1} - 2s_j^{n+1} + s_{j+1}^{n+1}}{\Delta x^2} \right) \\ & - \frac{\varepsilon \tau}{\Delta t} \left(\frac{s_{j-1}^n - 2s_j^n + s_{j+1}^n}{\Delta x^2} \right) - \left(\frac{s_j^{n+1} - s_j^n}{\Delta t} \right) = a \left(\frac{s_j^n - s_{j-1}^n}{\Delta x} \right). \end{aligned} \quad (\text{A.7})$$

After algebraic manipulations, we obtain

$$\begin{aligned} & - \left(\frac{\varepsilon \Delta t + \varepsilon \tau}{\Delta x^2} \right) s_{j-1}^{n+1} + \left(2 \frac{\varepsilon \Delta t + \varepsilon \tau}{\Delta x^2} + 1 \right) s_j^{n+1} - \left(\frac{\varepsilon \Delta t + \varepsilon \tau}{\Delta x^2} \right) s_{j+1}^{n+1} = \\ & - \left(\frac{\varepsilon \tau}{\Delta x^2} - \frac{a \Delta t}{\Delta x} \right) s_{j-1}^n + \left(2 \frac{\varepsilon \tau}{\Delta x^2} - \frac{a \Delta t}{\Delta x} + 1 \right) s_j^n - \left(\frac{\varepsilon \tau}{\Delta x^2} \right) s_{j+1}^n. \end{aligned} \quad (\text{A.8})$$

Consider,

$$c_1 = \frac{\varepsilon \Delta t}{\Delta x^2}, \quad c_2 = \frac{\varepsilon \tau}{\Delta x^2}, \quad c_3 = \frac{a \Delta t}{\Delta x}, \quad (\text{A.9})$$

thus we write the scheme as follows,

$$\begin{aligned} & - (c_1 + c_2) s_{j-1}^{n+1} + (2c_1 + 2c_2 + 1) s_j^{n+1} - (c_1 + c_2) s_{j+1}^{n+1} = \\ & - (c_2 - c_3) s_{j-1}^n + (2c_2 - c_3 + 1) s_j^n - (c_2) s_{j+1}^n. \end{aligned} \quad (\text{A.10})$$

A.3 Linear stability analysis

To analyze the stability of scheme (A.10), we use the Van-Neumann approach to stability analysis. The von Neumann stability analysis is based on Fourier analysis and hence is generally limited to constant coefficient linear PDEs [70]. For simplicity, in this section we apply this approach to the Cauchy problem (initial value problem).

Suppose we can express s_j^n as a linear combination of the grid functions $\exp(i j \xi \Delta x)$ for all ξ in the range $[-\pi/\Delta x, \pi/\Delta x]$. Consider the function $\hat{E}^n(\xi)$ corresponding to the direct analogue of the Fourier transform in the discrete case,

$$\hat{E}^n(\xi) = \frac{\Delta x}{\sqrt{2\pi}} \sum_{-\infty}^{\infty} s_j^n \exp(-i j \xi \Delta x). \quad (\text{A.11})$$

Multiplying Eq. (A.8) by $\exp(-i j \xi \Delta x)$ and summing over j , we obtain,

$$\begin{aligned} & - (c_1 + c_2) e^{-i\xi\Delta x} \hat{E}^{n+1} + (2c_1 + 2c_2 + 1) \hat{E}_j^{n+1} - (c_1 + c_2) e^{i\xi\Delta x} \hat{E}^{n+1} = \\ & - (c_2 - c_3) e^{-i\xi\Delta x} \hat{E}^n + (2c_2 - c_3 + 1) \hat{E}^n - (c_2) e^{i\xi\Delta x} \hat{E}^n; \end{aligned} \quad (\text{A.12a})$$

$$\begin{aligned} & \left[- (c_1 + c_2) e^{-i\xi\Delta x} + (2c_1 + 2c_2 + 1) - (c_1 + c_2) e^{i\xi\Delta x} \right] \hat{E}^{n+1} = \\ & \left[- (c_2 - c_3) e^{-i\xi\Delta x} + (2c_2 - c_3 + 1) - (c_2) e^{i\xi\Delta x} \right] \hat{E}^n; \end{aligned} \quad (\text{A.12b})$$

$$\begin{aligned} & \left[1 + (c_1 + c_2) \left(2 - \left(e^{-i\xi\Delta x} + e^{i\xi\Delta x} \right) \right) \right] \hat{E}^{n+1} = \\ & \left[1 + c_2 \left(2 - \left(e^{-i\xi\Delta x} + e^{i\xi\Delta x} \right) \right) - c_3 \left(1 - e^{-i\xi\Delta x} \right) \right] \hat{E}^n. \end{aligned} \quad (\text{A.12c})$$

Using the identities,

$$\cos(\xi\Delta x) = \frac{e^{-i\xi\Delta x} + e^{i\xi\Delta x}}{2}, \quad \sin^2\left(\frac{\xi\Delta x}{2}\right) = \frac{1 - \cos(\xi\Delta x)}{2}, \quad (\text{A.13})$$

we obtain,

$$\left[1 + 4(c_1 + c_2) \sin^2\left(\frac{\xi\Delta x}{2}\right) \right] \hat{E}^{n+1} = \left[1 + 4c_2 \sin^2\left(\frac{\xi\Delta x}{2}\right) - c_3 \left(1 - e^{-i\xi\Delta x} \right) \right] \hat{E}^n, \quad (\text{A.14a})$$

$$\hat{E}^{n+1} = \left[\frac{1 + 4c_2 \sin^2\left(\frac{\xi\Delta x}{2}\right) - c_3(1 - e^{-i\xi\Delta x})}{1 + 4(c_1 + c_2) \sin^2\left(\frac{\xi\Delta x}{2}\right)} \right] \hat{E}^n. \quad (\text{A.14b})$$

Thus, the amplification factor $G(\xi)$ is given by,

$$G(\xi) = \frac{1 + 4c_2 \sin^2\left(\frac{\xi\Delta x}{2}\right) - c_3(1 - e^{-i\xi\Delta x})}{1 + 4(c_1 + c_2) \sin^2\left(\frac{\xi\Delta x}{2}\right)}. \quad (\text{A.15})$$

For stability of the numerical scheme, the amplification factor must satisfy $|G| \leq 1$. We have,

$$|G|^2 = \frac{\left[1 + 4c_2 \sin^2\left(\frac{\xi\Delta x}{2}\right) - c_3(1 - \cos(\xi\Delta x))\right]^2 + [c_3 \sin(\xi\Delta x)]^2}{\left[1 + 4(c_1 + c_2) \sin^2\left(\frac{\xi\Delta x}{2}\right)\right]^2}, \quad (\text{A.16a})$$

$$|G|^2 = \frac{\left[1 + (4c_2 - 2c_3) \sin^2\left(\frac{\xi\Delta x}{2}\right)\right]^2 + [c_3 \sin(\xi\Delta x)]^2}{\left[1 + 4(c_1 + c_2) \sin^2\left(\frac{\xi\Delta x}{2}\right)\right]^2}, \quad (\text{A.16b})$$

$$|G|^2 = \left[\frac{1 + 4c_2 \sin^2\left(\frac{\xi\Delta x}{2}\right)}{1 + 4(c_1 + c_2) \sin^2\left(\frac{\xi\Delta x}{2}\right)} \right]^2 \left[\left(1 - \frac{2c_3 \sin^2\left(\frac{\xi\Delta x}{2}\right)}{1 + 4c_2 \sin^2\left(\frac{\xi\Delta x}{2}\right)}\right)^2 + \left(\frac{c_3 \sin(\xi\Delta x)}{1 + 4c_2 \sin^2\left(\frac{\xi\Delta x}{2}\right)}\right)^2 \right]. \quad (\text{A.16c})$$

We identify two factors, the first one linked to diffusion and the other to the advection term. For the first factor, we have,

$$\frac{1 + 4c_2 \sin^2\left(\frac{\xi\Delta x}{2}\right)}{1 + 4(c_1 + c_2) \sin^2\left(\frac{\xi\Delta x}{2}\right)} \leq 1, \quad \forall \xi \in \mathbb{R}. \quad (\text{A.17})$$

Thus we need to limit just the second factor. Using the identity,

$$\sin(\xi\Delta x) = 2 \sin\left(\frac{\xi\Delta x}{2}\right) \cos\left(\frac{\xi\Delta x}{2}\right), \quad (\text{A.18})$$

we obtain,

$$\begin{aligned}
& \left(1 - \frac{2c_3 \sin^2\left(\frac{\xi\Delta x}{2}\right)}{1 + 4c_2 \sin^2\left(\frac{\xi\Delta x}{2}\right)}\right)^2 + \left(\frac{c_3 \sin(\xi\Delta x)}{1 + 4c_2 \sin^2\left(\frac{\xi\Delta x}{2}\right)}\right)^2 = \\
& \left(1 - \frac{2c_3 \sin^2\left(\frac{\xi\Delta x}{2}\right)}{1 + 4c_2 \sin^2\left(\frac{\xi\Delta x}{2}\right)}\right)^2 + \left(\frac{2c_3 \sin\left(\frac{\xi\Delta x}{2}\right) \cos\left(\frac{\xi\Delta x}{2}\right)}{1 + 4c_2 \sin^2\left(\frac{\xi\Delta x}{2}\right)}\right)^2 = \\
& 1 - \frac{4c_3 \sin^2\left(\frac{\xi\Delta x}{2}\right)}{1 + 4c_2 \sin^2\left(\frac{\xi\Delta x}{2}\right)} + \frac{4c_3^2 \sin^2\left(\frac{\xi\Delta x}{2}\right) \sin^2\left(\frac{\xi\Delta x}{2}\right)}{\left[1 + 4c_2 \sin^2\left(\frac{\xi\Delta x}{2}\right)\right]^2} + \frac{4c_3^2 \sin^2\left(\frac{\xi\Delta x}{2}\right) \cos^2\left(\frac{\xi\Delta x}{2}\right)}{\left[1 + 4c_2 \sin^2\left(\frac{\xi\Delta x}{2}\right)\right]^2} = \\
& 1 - \frac{4c_3 \sin^2\left(\frac{\xi\Delta x}{2}\right)}{1 + 4c_2 \sin^2\left(\frac{\xi\Delta x}{2}\right)} + \frac{4c_3^2 \sin^2\left(\frac{\xi\Delta x}{2}\right)}{\left[1 + 4c_2 \sin^2\left(\frac{\xi\Delta x}{2}\right)\right]^2},
\end{aligned} \tag{A.19}$$

where we use the fundamental identity,

$$\sin^2\left(\frac{\xi\Delta x}{2}\right) + \cos^2\left(\frac{\xi\Delta x}{2}\right) = 1. \tag{A.20}$$

Consider the change of variables,

$$\eta = \sin^2\left(\frac{\xi\Delta x}{2}\right). \tag{A.21}$$

Thus, we define the function,

$$g(\eta) = 1 - \frac{4c_3\eta}{1 + 4c_2\eta} + \frac{4c_3^2\eta}{(1 + 4c_2\eta)^2}, \quad 0 \leq \eta \leq 1. \tag{A.22}$$

Now, we will study the maximum of the function $g(\eta)$. The first derivative of $g(\eta)$ is given by,

$$g'(\eta) = \frac{4c_3(c_3 - 1) + 16c_2c_3(1 - c_3)\eta}{(1 + 4c_2\eta)^3}. \tag{A.23}$$

The critical point of $g(\eta)$ is,

$$\eta^* = \frac{1}{4c_2}. \tag{A.24}$$

To classify this critical point, we study the sign of $g'(\eta)$. There are two cases,

$$c_3 < 1, \quad c_3 > 1. \tag{A.25}$$

Case $c_3 < 1$: Here we have,

$$\begin{aligned} g'(\eta) &< 0, & \eta < \eta^*, \\ g'(\eta) &> 0, & \eta > \eta^*. \end{aligned} \tag{A.26}$$

Thus the function $g(\eta)$ changes from decreasing to increasing and η^* is a local minimum. We have to evaluate $g(\eta)$ at the boundary of the interval,

$$g(0) = 1, \quad g(1) = 1 - \frac{4c_3}{1 + 4c_2} + \frac{4c_3^2}{(1 + 4c_2)^2}. \tag{A.27}$$

We have to impose,

$$1 - \frac{4c_3}{1 + 4c_2} + \frac{4c_3^2}{(1 + 4c_2)^2} < 1, \tag{A.28}$$

that is,

$$c_3 < 1 + 4c_2. \tag{A.29}$$

We have $c_3 < 1$ in this case.

Case $c_3 > 1$: Here we have,

$$\begin{aligned} g'(\eta) &> 0, & \eta < \eta^*, \\ g'(\eta) &< 0, & \eta > \eta^*. \end{aligned} \tag{A.30}$$

The function $g(\eta)$ changes from increasing to decreasing, thus η^* is a local maximum. If $0 \leq \eta^* \leq 1$, then we evaluate,

$$g(\eta^*) = 1 - \frac{c_3}{2c_2} + \frac{c_3^2}{4c_2}, \tag{A.31}$$

and we impose,

$$1 - \frac{c_3}{2c_2} + \frac{c_3^2}{4c_2} < 1, \tag{A.32}$$

that is,

$$0 < c_3 < 2. \tag{A.33}$$

If $\eta^* > 1$, we have to evaluate $g(1)$,

$$c_3 < 1 + 4c_2. \tag{A.34}$$

As the critical point is defined by,

$$\eta^* = \frac{1}{4c_2} = \frac{\Delta x^2}{4\varepsilon\tau}, \quad (\text{A.35})$$

we can always have $0 \leq \eta^* \leq 1$ with mesh refinement.

Therefore, a stability condition for the method is given by,

$$\frac{a\Delta t}{\Delta x} < 2. \quad (\text{A.36})$$

This condition resembles the CFL condition for explicit schemes for numerical solution of linear conservation laws. This reflects the fact that the hyperbolic flux is approximated by a explicit rule.

A.4 Convergence of iterative procedure

The numerical scheme defined by (A.5) is solved by a fixed-point iterative procedure. Let k be the iteration index, thus the iterative procedure is given by:

$$-\varepsilon \left(\frac{p_{j-1}^{n+1,k} - 2p_j^{n+1,k} + p_{j+1}^{n+1,k}}{\Delta x^2} \right) + \frac{1}{\tau} p_j^{n+1,k} = a \left(\frac{s_j^n - s_{j-1}^n}{\Delta x} \right) - \frac{s_j^{n+1,k}}{\tau} \quad (\text{A.37a})$$

$$s_j^{n+1,k+1} = s_j^n - \Delta t \left(\frac{s_j^{n+1,k} + p_j^{n+1,k}}{\tau} \right). \quad (\text{A.37b})$$

In this section, we proof the convergence of the iterative procedure by means of the Banach Fixed Point Theorem [69]. Thus, we write the scheme in an matrix form,

$$\mathbf{A} \mathbf{P}^{n+1,k} = \mathbf{B} \mathbf{S}^n - \frac{1}{\tau} \mathbf{S}^{n+1,k} + \mathbf{v}, \quad (\text{A.38a})$$

$$\mathbf{S}^{n+1,k+1} = \mathbf{S}^n - \frac{\Delta t}{\tau} (\mathbf{S}^{n+1,k} + \mathbf{P}^{n+1,k}), \quad (\text{A.38b})$$

where we define the vectors of unknowns,

$$\mathbf{S}^{n+1,k} = (s_j^{n+1,k}), \quad \mathbf{P}^{n+1,k} = (p_j^{n+1,k}). \quad (\text{A.39})$$

and the matrices

$$\mathbf{A} = (a_{i,j}) \quad a_{i,j} = \begin{cases} \frac{2\varepsilon}{\Delta x^2} + \frac{1}{\tau}, & j = i, \\ -\frac{\varepsilon}{\Delta x^2}, & j = i - 1, \\ -\frac{\varepsilon}{\Delta x^2}, & i = j + 1, \\ 0, & \text{otherwise.} \end{cases}$$

$$\mathbf{B} = (b_{i,j}) \quad b_{i,j} = \begin{cases} \frac{a}{\Delta x}, & j = i, \\ -\frac{a}{\Delta x}, & j = i - 1, \\ 0, & \text{otherwise.} \end{cases}$$

The vector \mathbf{v} is the boundary conditions vector.

We can write the solution of (A.38a) as a function of saturation,

$$\mathbf{P}^{n+1,k} = \mathbf{A}^{-1} \mathbf{B} \mathbf{S}^n - \frac{1}{\tau} \mathbf{A}^{-1} \mathbf{S}^{n+1,k} + \mathbf{A}^{-1} \mathbf{v} \quad (\text{A.41})$$

Thus, by replacing (A.41) in (A.38b) we have,

$$\mathbf{S}^{n+1,k+1} = \left(-\frac{\Delta t}{\tau} \mathbf{I} + \frac{\Delta t}{\tau^2} \mathbf{A}^{-1} \right) \mathbf{S}^{n+1,k} + \left(\mathbf{I} - \frac{\Delta t}{\tau} \mathbf{A}^{-1} \mathbf{B} \right) \mathbf{S}^n - \frac{\Delta t}{\tau} \mathbf{A}^{-1} \mathbf{v}, \quad (\text{A.42})$$

The matrix of the iterative procedure is given by,

$$\mathbf{M} = -\frac{\Delta t}{\tau} \mathbf{I} + \frac{\Delta t}{\tau^2} \mathbf{A}^{-1} \quad (\text{A.43})$$

For the convergence of the iterative procedure, we must have,

$$\rho(\mathbf{M}) = \max |\lambda_{\mathbf{M}}| \leq \alpha < 1. \quad (\text{A.44})$$

The matrix \mathbf{A} is a Toeplitz tridiagonal symmetric matrix and its eigenvalues are known,

$$\lambda_{\mathbf{A}}^r = \frac{2\varepsilon}{\Delta x^2} \left[1 + \cos \left(\frac{r\pi}{m+1} \right) \right] + \frac{1}{\tau}, \quad 1 \leq r \leq m. \quad (\text{A.45})$$

Thus we have

$$\min |\lambda_{\mathbf{A}}^r| > \frac{1}{\tau}, \quad \max |\lambda_{\mathbf{A}}^r| < \frac{4\varepsilon}{\Delta x^2} + \frac{1}{\tau} \quad (\text{A.46})$$

The eigenvalues of \mathbf{M} can be written as function of the eigenvalues of \mathbf{A} ,

$$\lambda_{\mathbf{M}}^r = -\frac{\Delta t}{\tau} + \frac{\Delta t}{\tau^2} (\lambda_{\mathbf{A}}^r)^{-1}, \quad (\text{A.47})$$

Thus,

$$|\lambda_{\mathbf{M}}^r| = \left| -\frac{\Delta t}{\tau} + \frac{\Delta t}{\tau^2} (\lambda_{\mathbf{A}}^r)^{-1} \right| < \frac{\Delta t}{\tau} + \frac{\Delta t}{\tau^2} (\min |\lambda_{\mathbf{A}}^r|)^{-1} < 2\frac{\Delta t}{\tau} \quad (\text{A.48})$$

Then we impose,

$$2\frac{\Delta t}{\tau} < 1, \quad (\text{A.49})$$

that is,

$$\Delta t < \frac{\tau}{2}. \quad (\text{A.50})$$

Condition (A.50) must be satisfied to ensure that the sequence defined by the iterative procedure (A.37) converges to the solution of (A.5). Therefore, besides the stability condition (A.36), we have to choose the time step Δt restricted by the dynamic effect coefficient τ .

Appendix B

Finite difference method for two-phase flow with dynamic capillary pressure

We present a finite difference scheme for two-dimensional pseudo-parabolic problems modeling the two-phase flow in porous media with dynamic capillary pressure. The purpose of using finite difference scheme in this work is corroborate the numerical results of our mixed finite element approach.

Here we use a uniform rectangular mesh and cell-centered finite differences. To construct this scheme, we use many ideas learned from the mixed finite element method. The mixed finite element framework has two advantages [20]: it yields a very natural and physical discretization of the boundary conditions; and it gives a consistent way of defining a gradient flux, as in the mixed formulation.

B.1 Finite difference scheme for the pseudo-parabolic transport equation

Consider the pseudo-parabolic transport equation written as follows,

$$\frac{\partial}{\partial t}(\phi S_w) + \nabla \cdot \mathbf{F}(\mathbf{v}, S_w) = \nabla \cdot \left[H(S_w) \nabla \left(p_e(S_w) + \tau \frac{\partial}{\partial t}(\phi S_w) \right) \right]. \quad (\text{B.1})$$

For convenience, here we assume that p_c is defined as $p_c = p_w - p_n$, thus $p_e(S_w)$ is a nondecreasing function. If we assume that the function $p_e(S_w)$ is differentiable, then we can write (B.1) as,

$$\frac{\partial}{\partial t}(\phi S_w) + \nabla \cdot \mathbf{F}(\mathbf{v}, S_w) = \nabla \cdot \left[H(S_w) p_e' \nabla S_w + \tau H(S_w) \nabla \frac{\partial}{\partial t}(\phi S_w) \right]. \quad (\text{B.2})$$

So we define the coefficients,

$$D(S_w) = H(S_w) p'_e(S_w) \quad C(S_w) = \tau H(S_w). \quad (\text{B.3})$$

We also identify the diffusive flux \mathbf{w} as given by,

$$\mathbf{w} = H(S_w) \nabla \left(p_e(S_w) + \tau \frac{\partial}{\partial t} (\phi S_w) \right) = D(S_w) \nabla S_w + C(S_w) \nabla \frac{\partial}{\partial t} (\phi S_w). \quad (\text{B.4})$$

Now, we will discuss a finite difference approach for the pseudo-parabolic equation (B.2).

Consider a uniform partition of Ω into rectangular subdomains Ω_i , for $i = 1, \dots, M$, with dimensions $\Delta x \times \Delta y$. The center of each subdomain Ω_i is denoted by (x_i, y_i) . Given a final time of simulation T , consider a uniform partition of the interval $[0, T]$ into N subintervals. The time step $\Delta t = T/N$ is usually defined by a stability condition. We denote the time instants as $t_n = n\Delta t$, for $n = 0, \dots, N$.

Let S_i^n be a finite difference approximation for $S_w(x_i, y_i, t_n)$. A discretization of (B.2) by the finite difference method is given by,

$$\phi_i \frac{S_i^{n+1} - S_i^n}{\Delta t} + \frac{F_{ir}^n - F_{il}^n}{\Delta x} + \frac{F_{iu}^n - F_{id}^n}{\Delta y} = \frac{W_{ir}^{n+1} - W_{il}^{n+1}}{\Delta x} + \frac{W_{iu}^{n+1} - W_{id}^{n+1}}{\Delta y}, \quad (\text{B.5})$$

where the approximation of the diffusive flux is given by a centered difference formula,

$$W_{ir}^{n+1} = D_{ir}^n \left(\frac{S_r^{n+1} - S_i^{n+1}}{\Delta x} \right) + \frac{C_{ir}^n}{\Delta t} \left(\frac{S_r^{n+1} - S_i^{n+1}}{\Delta x} - \frac{S_r^n - S_i^n}{\Delta x} \right), \quad (\text{B.6a})$$

$$W_{iu}^{n+1} = D_{iu}^n \left(\frac{S_u^{n+1} - S_i^{n+1}}{\Delta y} \right) + \frac{C_{iu}^n}{\Delta t} \left(\frac{S_u^{n+1} - S_i^{n+1}}{\Delta y} - \frac{S_u^n - S_i^n}{\Delta y} \right). \quad (\text{B.6b})$$

The coefficients are chosen as the arithmetic mean at interfaces,

$$D_{ir}^n = \frac{D_i^n + D_r^n}{2}, \quad D_{iu}^n = \frac{D_i^n + D_u^n}{2}, \quad (\text{B.7a})$$

$$C_{ir}^n = \frac{C_i^n + C_r^n}{2}, \quad C_{iu}^n = \frac{C_i^n + C_u^n}{2}. \quad (\text{B.7b})$$

where $D_i^n = D(S_i^n)$ and $C_i = C(S_i^n)$.

We chose to use the coefficients at time t_n . This choice leads to a algebraic

linear system over the unknowns S_i^{n+1} . The algebraic equations may be written as,

$$a_{i,d} S_d^{n+1} + a_{i,l} S_l^{n+1} + a_{i,i} S_i^{n+1} + a_{i,r} S_r^{n+1} + a_{i,u} S_u^{n+1} = b_i, \quad (\text{B.8})$$

where,

$$b_i = \phi_i S_i^n - \frac{\Delta t}{\Delta x} (F_{ir} - F_{il}) - \frac{\Delta t}{\Delta y} (F_{iu} - F_{id}) - \frac{C_{il} S_l^n - (C_{il} + C_{ir}) S_r^n + C_{ir} S_r^n}{\Delta x^2} - \frac{C_{id} S_d^n - (C_{id} + C_{iu}) S_i^n + C_u S_u^n}{\Delta y^2}, \quad (\text{B.9})$$

and the coefficients are given by,

$$a_{i,d} = -\frac{\Delta t D_{id} + C_{id}}{\Delta y^2}, \quad a_{i,u} = -\frac{\Delta t D_{iu} + C_{iu}}{\Delta y^2}, \quad (\text{B.10a})$$

$$a_{i,l} = -\frac{\Delta t D_{il} + C_{il}}{\Delta x^2}, \quad a_{i,r} = -\frac{\Delta t D_{ir} + C_{ir}}{\Delta x^2}, \quad (\text{B.10b})$$

$$a_{i,i} = -(a_{i,d} + a_{i,u} + a_{i,l} + a_{i,r}) + \phi_i \quad (\text{B.10c})$$

We still have to define how to impose the boundary conditions. Therefore, we will write the algebraic equations for the subdomains that intersects the boundary.

The zero flux condition is imposed at bottom (Γ_D) and the top (Γ_U) of the domain by taking,

$$F_{id} - V_{id} = 0, \quad \partial\Omega_i \cap \Gamma_D \neq \emptyset, \quad (\text{B.11a})$$

$$F_{iu} - V_{iu} = 0, \quad \partial\Omega_i \cap \Gamma_U \neq \emptyset. \quad (\text{B.11b})$$

On the other hand, to impose the Dirichlet conditions at left (Γ_L) and right (Γ_R) boundaries of the domain, we have to redefine the fluxes. We use the following approximation for the diffusive fluxes:

$$W_{il} = D_i \left(\frac{S_i^{n+1} - S_L}{\Delta x/2} \right) + \frac{C_i}{\Delta t} \left(\frac{S_i^{n+1} - S_L}{\Delta x/2} - \frac{S_i^n - S_L}{\Delta x/2} \right), \quad \partial\Omega_i \cap \Gamma_L \neq \emptyset, \quad (\text{B.12a})$$

$$W_{ir} = D_i \left(\frac{S_R - S_i^{n+1}}{\Delta x/2} \right) + \frac{C_i}{\Delta t} \left(\frac{S_R - S_i^{n+1}}{\Delta x/2} - \frac{S_R - S_i^n}{\Delta x/2} \right), \quad \partial\Omega_i \cap \Gamma_R \neq \emptyset. \quad (\text{B.12b})$$

The hyperbolic fluxes are given as follows,

$$F_{il} = f(S_L), \quad \partial\Omega_i \cap \Gamma_L \neq \emptyset, \quad (\text{B.13a})$$

$$F_{ir} = f(S_R), \quad \partial\Omega_i \cap \Gamma_R \neq \emptyset. \quad (\text{B.13b})$$

B.2 Finite difference scheme for the elliptic pressure-velocity problem

For reading convenience, let us rewrite the equations of pressure-velocity system,

$$\nabla \cdot \mathbf{v} = 0, \quad \mathbf{v} = -H_n \nabla p_n + \mathbf{v}_c + \mathbf{v}_G, \quad (\text{B.14})$$

where the coefficient $H_n(S_w)$ is given by,

$$H_n = N_{Ca} K(\mathbf{x}) [k_w(S_w) + R_\mu k_n(S_w)]. \quad (\text{B.15})$$

The terms \mathbf{v}_c and \mathbf{v}_G are correction velocities and they are given by,

$$\mathbf{v}_c = -L(S_w) \nabla S_w - M(S_w) \nabla \frac{\partial}{\partial t} (\phi S_w), \quad (\text{B.16a})$$

$$\mathbf{v}_G = M(S_w) \nabla Z. \quad (\text{B.16b})$$

and the coefficients $L(S_w)$, $M(S_w)$ and $N(S_w)$,

$$L(S_w) = N_{Ca} K(\mathbf{x}) k_w(S_w) p'_e(S_w), \quad (\text{B.17a})$$

$$M(S_w) = \tau N_{Ca} K(\mathbf{x}) k_w(S_w), \quad (\text{B.17b})$$

$$N(S_w) = N_{Gr} K(\mathbf{x}) [k_w(S_w) + R_\mu R_\rho^{-1} k_n(S_w)]. \quad (\text{B.17c})$$

Applying the divergent operator to Eq. (B.14), we obtain a second order elliptic equation for p_n ,

$$-\nabla \cdot (H_n \nabla p_n) = -\nabla \cdot \mathbf{v}_c - \nabla \cdot \mathbf{v}_G. \quad (\text{B.18})$$

Now, we will discuss a finite difference approach for the elliptic problem (B.14).

Let P_i^n be a finite difference approximation for $p_n(x_i, y_i, t_n)$. A discretization of (B.14) by the finite difference method is given by,

$$\frac{V_{ir}^n - V_{il}^n}{\Delta x} + \frac{V_{iu}^n - V_{id}^n}{\Delta y} = 0 \quad (\text{B.19})$$

where the approximation of the flux is given by a centered difference formula,

$$V_{ir}^n = H_{ir}^n \left(\frac{S_r^{n+1} - S_i^{n+1}}{\Delta x} \right) + V_{cir}^n + V_{Gir}^n, \quad (\text{B.20a})$$

$$V_{iu}^n = H_{iu}^n \left(\frac{S_u^{n+1} - S_i^{n+1}}{\Delta y} \right) + V_{ciu}^n + V_{Giu}^n. \quad (\text{B.20b})$$

The correction velocities are given by centered differences,

$$V_{cir}^n = -L_{ir}^n \left(\frac{S_r^n - S_i^n}{\Delta x} \right) - \frac{M_{ir}^n}{\Delta t} \left(\frac{S_r^{n+1} - S_i^{n+1}}{\Delta x} - \frac{S_r^n - S_i^n}{\Delta x} \right) \quad (\text{B.21a})$$

$$V_{ciu}^n = -L_{iu}^n \left(\frac{S_u^n - S_i^n}{\Delta y} \right) - \frac{M_{iu}^n}{\Delta t} \left(\frac{S_u^{n+1} - S_i^{n+1}}{\Delta y} - \frac{S_u^n - S_i^n}{\Delta y} \right) \quad (\text{B.21b})$$

$$V_{Gir}^n = N_{ir}^n \frac{\partial Z}{\partial x} \quad V_{Giu}^n = N_{iu}^n \frac{\partial Z}{\partial y} \quad (\text{B.22})$$

The coefficients are chosen as the arithmetic mean at interfaces,

$$H_{ij}^n = \frac{H_i^n + H_j^n}{2}, \quad L_{ij}^n = \frac{L_i^n + L_j^n}{2}, \quad M_{ij}^n = \frac{M_i^n + M_j^n}{2}, \quad N_{ij}^n = \frac{N_i^n + N_j^n}{2}, \quad (\text{B.23})$$

where $H_i^n = H(S_i^n)$, $L_i^n = L(S_i^n)$, $M_i^n = M(S_i^n)$ and $N_i = N(S_i^n)$.

This discretization leads to a algebraic linear system over the unknowns P_i^n . The algebraic equations may be written as,

$$c_{i,d} P_d^n + c_{i,l} P_l^n + c_{i,i} P_i^n + c_{i,r} P_r^n + c_{i,u} P_u^n = b_{ni}, \quad (\text{B.24})$$

where,

$$b_{ni} = - \left(\frac{V_{cir}^n - V_{cil}^n}{\Delta x} + \frac{V_{ciu}^n - V_{cid}^n}{\Delta y} \right) - \left(\frac{V_{Gir}^n - V_{Gil}^n}{\Delta x} + \frac{V_{Giu}^n - V_{Gid}^n}{\Delta y} \right). \quad (\text{B.25})$$

and the coefficients are given by,

$$c_{i,d} = -\frac{H_{id}^n}{\Delta y^2}, \quad c_{i,u} = -\frac{H_{iu}^n}{\Delta y^2}, \quad c_{i,l} = -\frac{H_{il}^n}{\Delta x^2}, \quad c_{i,r} = -\frac{H_{ir}^n}{\Delta x^2}, \quad (\text{B.26a})$$

$$c_{i,i} = -(c_{i,d} + c_{i,u} + c_{i,l} + c_{i,r}) \quad (\text{B.26b})$$

The boundary conditions may be imposed in the same way as the transport problem.

B.3 Numerical experiments

In this section, we present numerical experiments in order to verify the viability of the finite difference method for pseudo-parabolic equations. The numerical accuracy and convergence study for the proposed computational procedure is based on a simple mesh refinement study. We present the same numerical tests reported in 5.1. For convenience of reading, we present again the simulation parameters,

Computational domain:	$\Omega_{2D} = (-5, 20) \times (0, 25)$	Final time of simulation:	$T = 5.0$
Left saturation value:	$S_L = 0.85$	Inflow flux:	$Q^{\text{in}} = 1.0$
Right saturation value:	$S_R = 0.10$	Right pressure value:	$p_n^{\text{ref}} = 0.0$
Viscosity ratio:	$R_\mu = 1.0$	Capillary number:	$N_{Ca} = 1.0$
Density ratio:	$R_\rho = 1.0$	Gravity number:	$N_{Gr} = 0.0$
Dynamic effect number:	$N_{Dy} = 0.5$	Stability parameter:	$\sigma_{\text{CFL}} = 0.5$

Figure B.1 shows the solution profile (right column) and refinement study (left column) for homogeneous (top) and heterogeneous (bottom) permeability fields. We used meshes from 64×64 to 512×512 cells and the reference solution was obtained on 1024×1024 cell mesh. We observe the numerical convergence from numerical experiments reported in Figure B.1 and Table B.1 and Table B.2, which shows a good resolution first-order convergence rate behavior (see right column in Figure B.1). As in the mixed-hybrid element approach, no spurious numerical artifacts are observed on the numerical solution by finite difference.

Table B.1: Refinement study with homogeneous permeability field for the finite difference scheme.

Mesh	h	$\ E\ _1$	$\ E\ _2$	$\ E\ _\infty$	Run time (s)
64×64	3.13×10^{-1}	2.40×10^0	3.92×10^{-1}	1.86×10^{-1}	1.41×10^0
128×128	1.56×10^{-1}	8.64×10^{-1}	1.70×10^{-1}	1.05×10^{-1}	1.13×10^1
256×256	7.81×10^{-2}	3.34×10^{-1}	7.06×10^{-2}	4.28×10^{-2}	9.64×10^1
512×512	3.91×10^{-2}	1.47×10^{-1}	2.86×10^{-2}	1.32×10^{-2}	8.05×10^2

Table B.2: Refinement study with heterogeneous permeability field for the finite difference scheme.

Mesh	h	$\ E\ _1$	$\ E\ _2$	$\ E\ _\infty$	Run time (s)
64×64	3.13×10^{-1}	1.78×10^0	2.454×10^{-1}	1.81×10^{-1}	3.17×10^0
128×128	1.56×10^{-1}	7.60×10^{-1}	1.06×10^{-1}	7.55×10^{-2}	2.70×10^1
256×256	7.81×10^{-2}	3.30×10^{-1}	$4.93e \times 10^{-2}$	3.44×10^{-2}	2.29×10^2
512×512	3.91×10^{-2}	1.55×10^{-1}	2.19×10^{-2}	1.14×10^{-2}	1.96×10^3

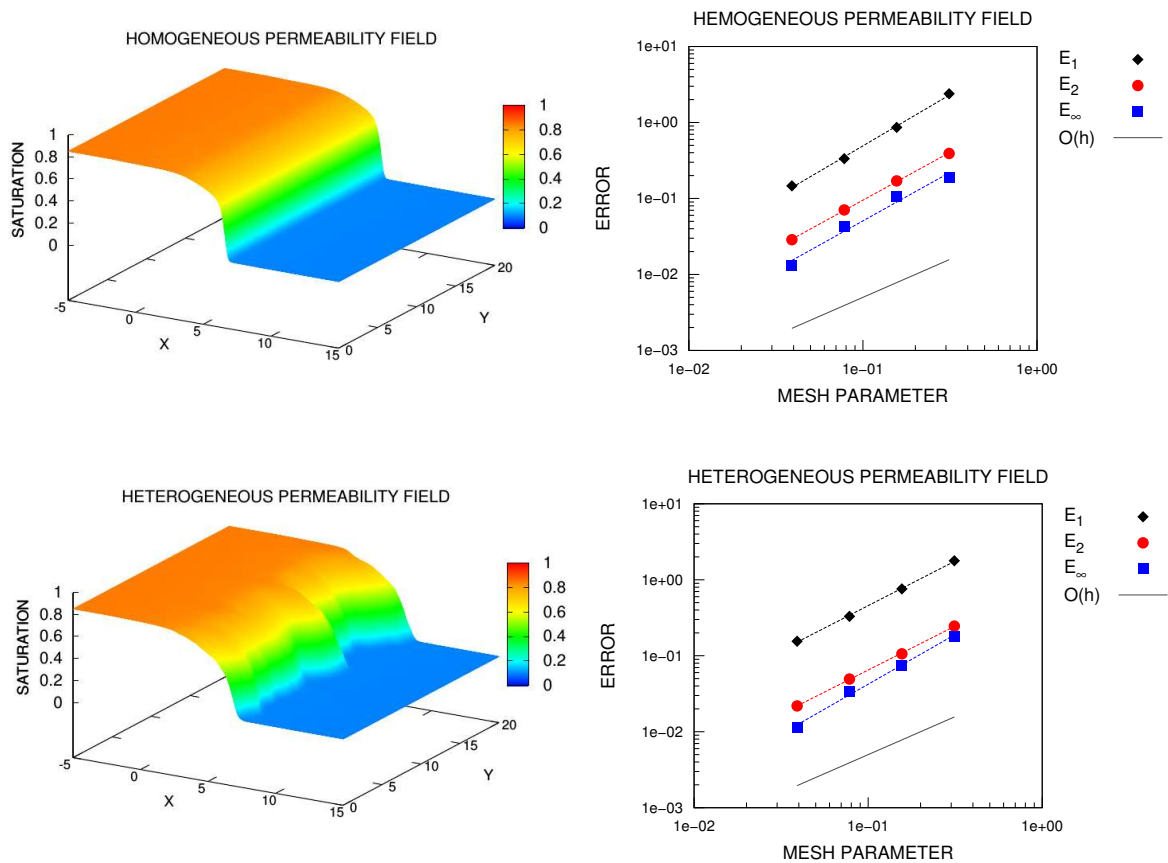


Figure B.1: Numerical solutions for saturation and refinement study for the finite difference scheme. Simulations are presented for homogeneous (top) and heterogeneous permeability fields (bottom). The left columns present the saturation profile for 1024×1024 cell mesh. The right column presents the numerical error with respect the reference numerical solution (1024×1024 elements). Dots denote the numerical error on different norms, while dashed lines are the linear adjusted curve.

Appendix C

Further one-dimensional simulations

In this appendix, we present additional numerical experiments in one-dimension. The propose is complement the discussion about the solution behavior of the pseudo-parabolic model. Here, we consider two situations: no gravity effects and nondecreasing initial data; non-increasing data with gravity effects.

Consider the two-phase flow problem with dynamic capillary pressure in one-dimensional domain $\Omega = (a, b)$, given as follows,

$$\frac{\partial}{\partial t}(\phi S_w) + \frac{\partial}{\partial x}F(S_w) = -\frac{\partial}{\partial x} \left[H_c(S_w) \frac{\partial}{\partial x} \left(p_e(S_w) - \tau \frac{\partial}{\partial t}(\phi S_w) \right) \right], \quad (\text{C.1})$$

where $\tau = N_{Dy}$, the capillary induced diffusion function H_c and the convective flux $F(S_w)$ as given by,

$$H(S_w) = N_{Ca} K(x) k_w(S_w) f_n(S_w), \quad (\text{C.2a})$$

$$F(S_w) = f_w S_w + N_{Gr} K(x) k_w(S_w) f_n(S_w) (1 - R_\rho^{-1}) \frac{\partial Z}{\partial x}. \quad (\text{C.2b})$$

We remark that it is not mandatory to solve the pressure-velocity problem for one-dimensional problems.

We consider here the initial values given by Riemann data as follows,

$$S_w(x, 0) = \begin{cases} S_L, & x \leq 0, \\ S_R, & x > 0, \end{cases} \quad (\text{C.3})$$

along with consistent boundary conditions,

$$S(a, t) = S_L, \quad S(b, t) = S_R, \quad t > 0. \quad (\text{C.4})$$

To perform the numerical simulations, we use a one-dimensional version of the method presented in Cap. 4. The mixed-hybrid finite element method for the transport equation along with the semi-implicit time discretization and the fixed-point iterative procedure result in algebraic linear systems with a tridiagonal symmetric positive defined matrix. To solve the linear systems we employ the Thomas algorithm. For further

informations in respect to the one-dimensional numerical scheme see [5].

For all simulations in this section, we have used the stability parameter $\sigma_{\text{CFL}} = 0.5$ to define the time step. The tolerance for the iterative procedure was taken as $\epsilon_{\text{TOL}} = 10^{-11}$. We used the linear model for static capillary pressure $p_e(S_w) = -S_w$. We took homogeneous permeability and porosity fields with the values $K(x) \equiv 1$ and $\phi(x) \equiv 1$.

C.1 Numerical experiments for nondecreasing initial data

In this section, we study numerically the solution behavior of pseudo-parabolic equation along with nondecreasing initial Riemann data. In [97], the authors analyze the solution profile of simplified pseudo-parabolic model for some nondecreasing initial data. We present a mesh refinement study for linear and nonlinear high order terms. In general, the profile structure is very similar to the solution of the parabolic model. This is illustrated by the numerical study of variation of dynamic effect parameter τ .

Linear diffusion case

Here we consider the relative permeability functions as follows,

$$k_w(S_w) = S_w^2, \quad k_n(S_w) = (1 - S_w)^2. \quad (\text{C.5})$$

However, we consider a constant diffusion coefficient $H_c(S_w) \equiv 1$. The nondimensional groups are given by,

$$N_{Ca} = 0.5, \quad N_{Dy} = 5.0, \quad R_\mu = 2.0, \quad R_\rho = 2.0. \quad (\text{C.6})$$

The computational domain is the interval $\Omega = (-60, 210)$ and the final time of simulation is $T = 150$. We consider two case for the initial data: $S_L = 0.0$ and $S_R = 0.9$; $S_L = 0.0$ and $S_R = 0.55$. Figure C.1 presents the mesh refinement study. In first case, we can say that the structure is composed by a rarefaction and a shock. In the other case, we have a pure rarefaction wave.

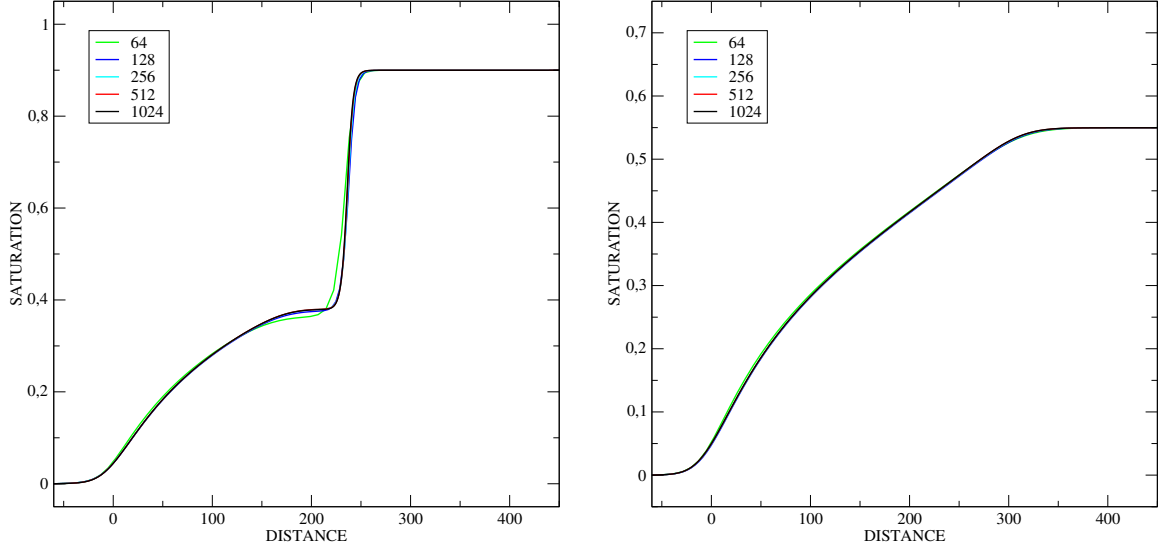


Figure C.1: Mesh refinement study for non-increasing initial data and linear high order terms. Left: initial data $S_L = 0.0$ and $S_R = 0.9$; Right: initial data $S_L = 0.0$ and $S_R = 0.55$. Computational meshes: 64, 128, 256, 512 e 1024 elements.

Non-linear diffusion case

For this case we consider the relative permeability functions as follows,

$$k_w(S_w) = S_w^{1.5}, \quad k_n(S_w) = (1 - S_w)^{1.5}. \quad (\text{C.7})$$

Here we use the nonlinear model for the diffusion coefficient $H_c(S_w)$ as given by (C.2). The nondimensional groups are given by,

$$N_{Ca} = 0.5, \quad N_{Dy} = 5.0, \quad R_\mu = 2.0, \quad R_\rho = 2.0. \quad (\text{C.8})$$

The computational domain is $\Omega = (-5, 15)$ and the final time of simulation is $T = 10$. We consider two initial data: $S_L = 0.85$ e $S_R = 0.1$; $S_L = 0.9$ e $S_R = 0.1$. For these examples, the solution does not attain degenerated values. Figure C.2 presents the refinement study for the case with nonlinear high order terms. For both initial data, we can say that the solution profile consists on a rarefaction and a shock wave.

Numerical study of the dynamic effect coefficient variation

Figures C.3 and C.4 show the numerical solutions for three values of the dynamic effect coefficient $N_{Dy} = \tau$. Hence, we can observe numerically the influence of this parameter on the solution structure. Figure C.3 presents the linear diffusion case for $\tau = 0.05, 5.0, 15.0$. Figure C.4 presents the nonlinear diffusion case for $\tau = 0.005, 0.5, 1.5$.

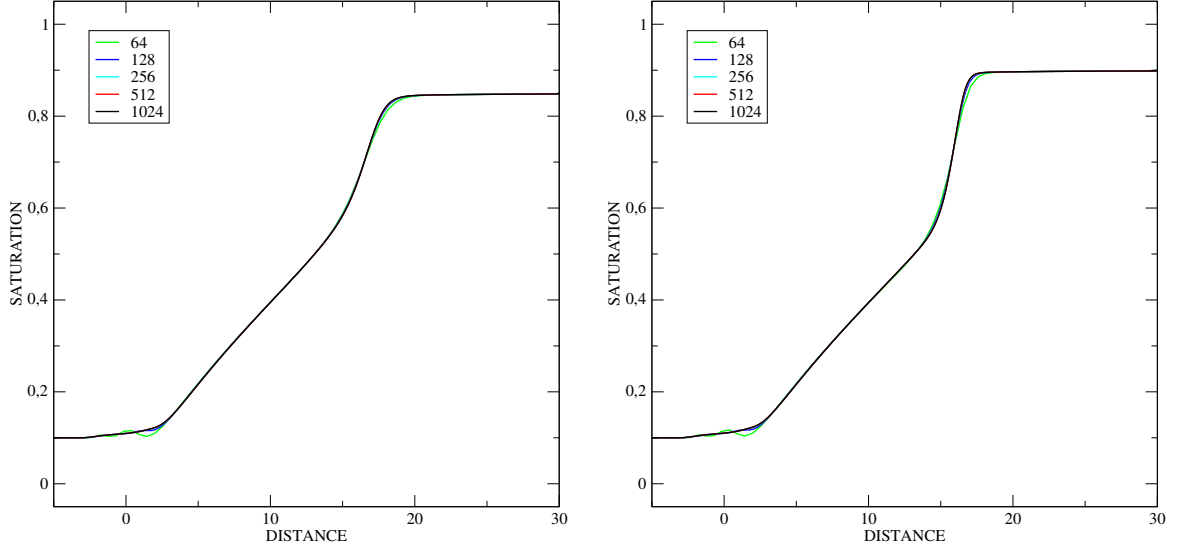


Figure C.2: Mesh refinement study for non-increasing initial data and nonlinear high order terms. Left: initial data $S_L = 0.1$ and $S_R = 0.85$; Right: initial data $S_L = 0.1$ and $S_R = 0.9$. Computational meshes: 64, 128, 256, 512 e 1024 elements.

For small values of τ the solutions are too similar to the parabolic model, presenting monotone profiles. On the other hand, for larger values of τ the solution may exhibit damped oscillations.

C.2 Numerical study of gravity effects on solution profile

In this section, we present some numerical experiments with different values of gravity number N_{Gr} to study its effects on the solution structure. In general, we observe that the gravity effects may change the behavior of solution from monotone to non-monotone. Traveling wave solutions for pseudo-parabolic problems in porous media with gravity effects are analyzed and numerically approximated in [61].

We consider the following relative permeability models,

$$k_w(S_w) = S_w^{1.5}, \quad k_n(S_w) = (1 - S_w)^{1.5}, \quad (\text{C.9})$$

and the values of nondimensional numbers,

$$N_{Ca} = 0.5, \quad R_\mu = 2.0, \quad R_\rho = 2.0. \quad (\text{C.10})$$

For the simulations, we use two values of dynamic effect number: $N_{Dy} = 5 \times 10^{-1}$ as

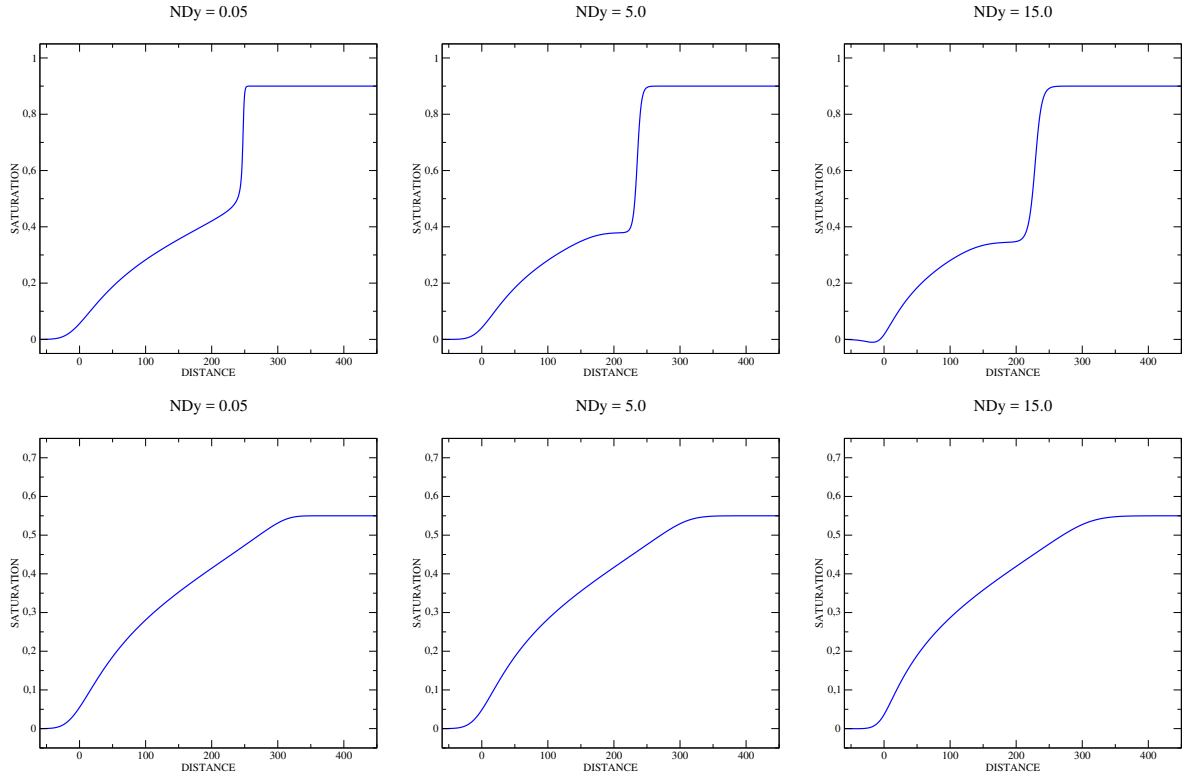


Figure C.3: Numerical solutions for the linear diffusion case with different values of the dynamic effect coefficient τ . Top: initial data $S_L = 0.0$ and $S_R = 0.9$; Bottom: initial data $S_L = 0.0$ and $S_R = 0.55$. Dynamic effect coefficient: $\tau = 0.05$ (left); $\tau = 5$ (center); $\tau = 15$ (right). Computational mesh: 1024 elements.

reported in [31, 36]; and $N_{Dy} = 5 \times 10^{-3}$ for which the solution is very similar to the two-phase flow parabolic model. The computational domain is the interval $\Omega_{1D} = (-5, 20)$ and the final time of simulation is defined as $T = 10$. For the initial and boundary conditions, we consider $S_L = 0.85$ and $S_R = 0.1$. The solution profiles do not attain degenerated values.

Figures C.5 and C.6 present the numeric solutions for different values of dynamic effect number N_{Dy} and gravity number N_{Gr} . In Figure C.5 the gravity acts in the direction of the flow (from left to right), while in Figure C.6 the gravity acts in opposite direction. From left to right, the dynamic effect number varies from $N_{Dy} = 5 \times 10^{-3}$ to $N_{Dy} = 5 \times 10^{-1}$. The values of the gravity number N_{Gr} varies from 0 (no gravity effects) to 3. As expected, in general, when gravity acts in flow direction the flow speed increases with N_{Gr} ; the opposite occur when the flow goes against gravity, i.e., the velocity decreases for larger values of N_{Gr} . However, unlike the parabolic model, the profile may change from non-monotone to monotone with increasing gravity number N_{Gr} .

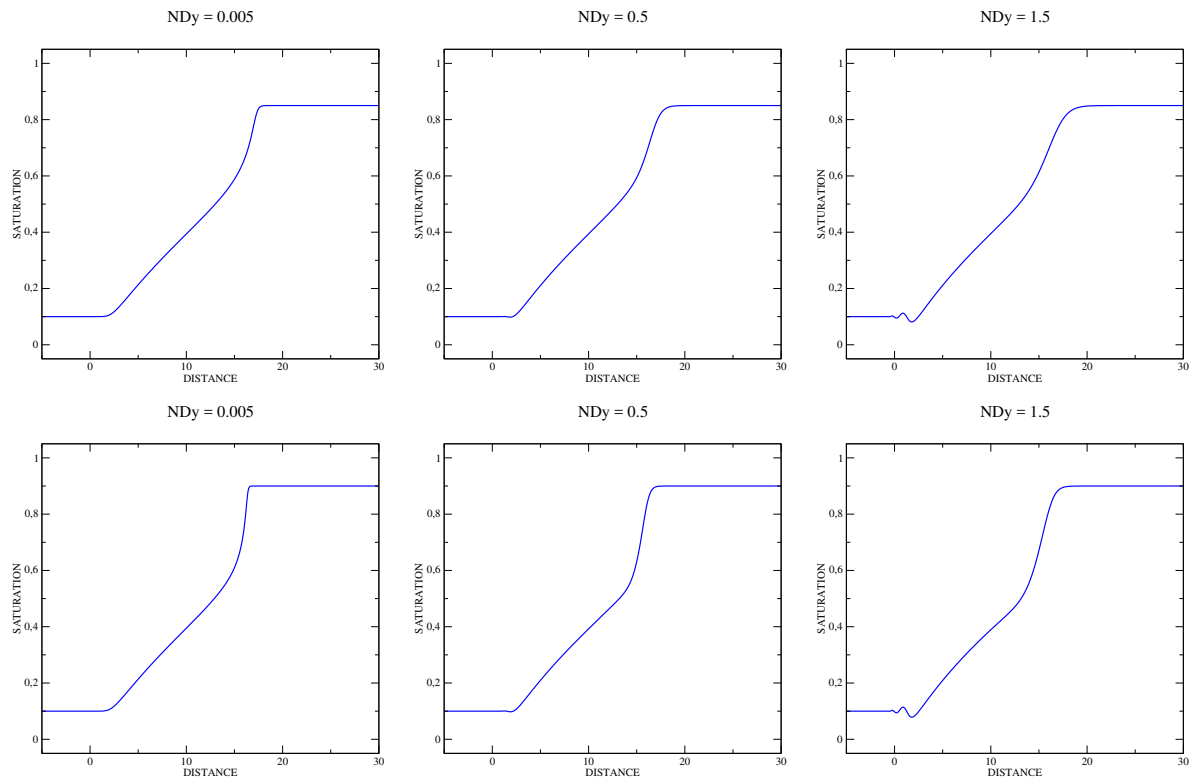


Figure C.4: Numerical solutions for the nonlinear diffusion case with different values of the dynamic effect coefficient τ . Top: initial data $S_L = 0.1$ and $S_R = 0.85$; Bottom: initial data $S_L = 0.1$ and $S_R = 0.9$. Dynamic effect coefficient: $\tau = 0.005$ (left); $\tau = 0.5$ (center); $\tau = 1.5$ (right). Computational mesh: 1024 elements.

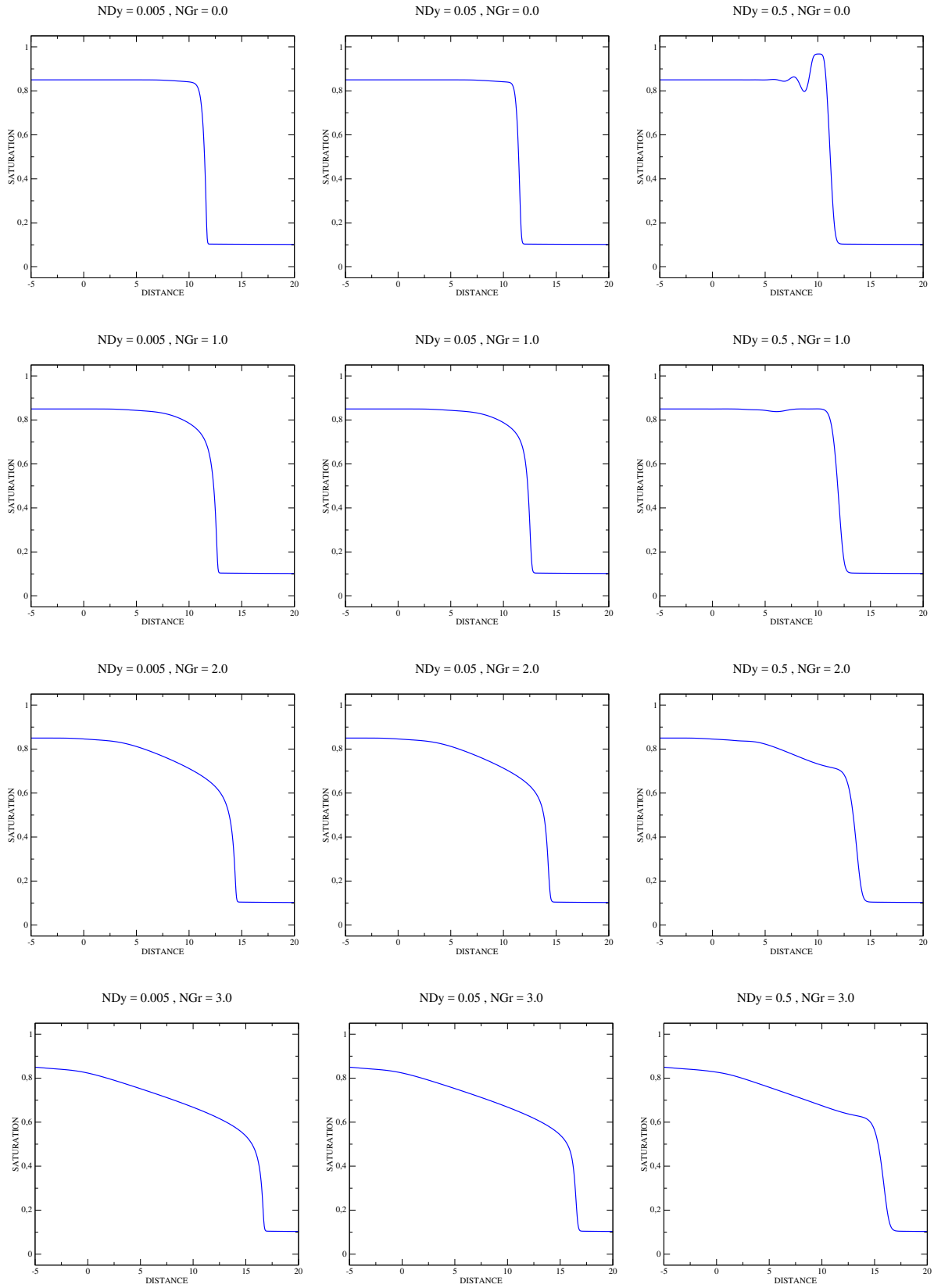


Figure C.5: Numerical solutions when the gravity acts in flow direction with different values of dynamic effect number N_{Dy} and gravity number N_{Gr} . Dynamic effect number: $N_{Dy} = 5 \times 10^{-3}$ (left), $N_{Dy} = 5 \times 10^{-2}$ (center) and $N_{Dy} = 5 \times 10^{-1}$ (right). The gravity number increases from $N_{Gr} = 0.0$ (top) to $N_{Gr} = 3.0$ (bottom). Computational mesh: 512 elements.

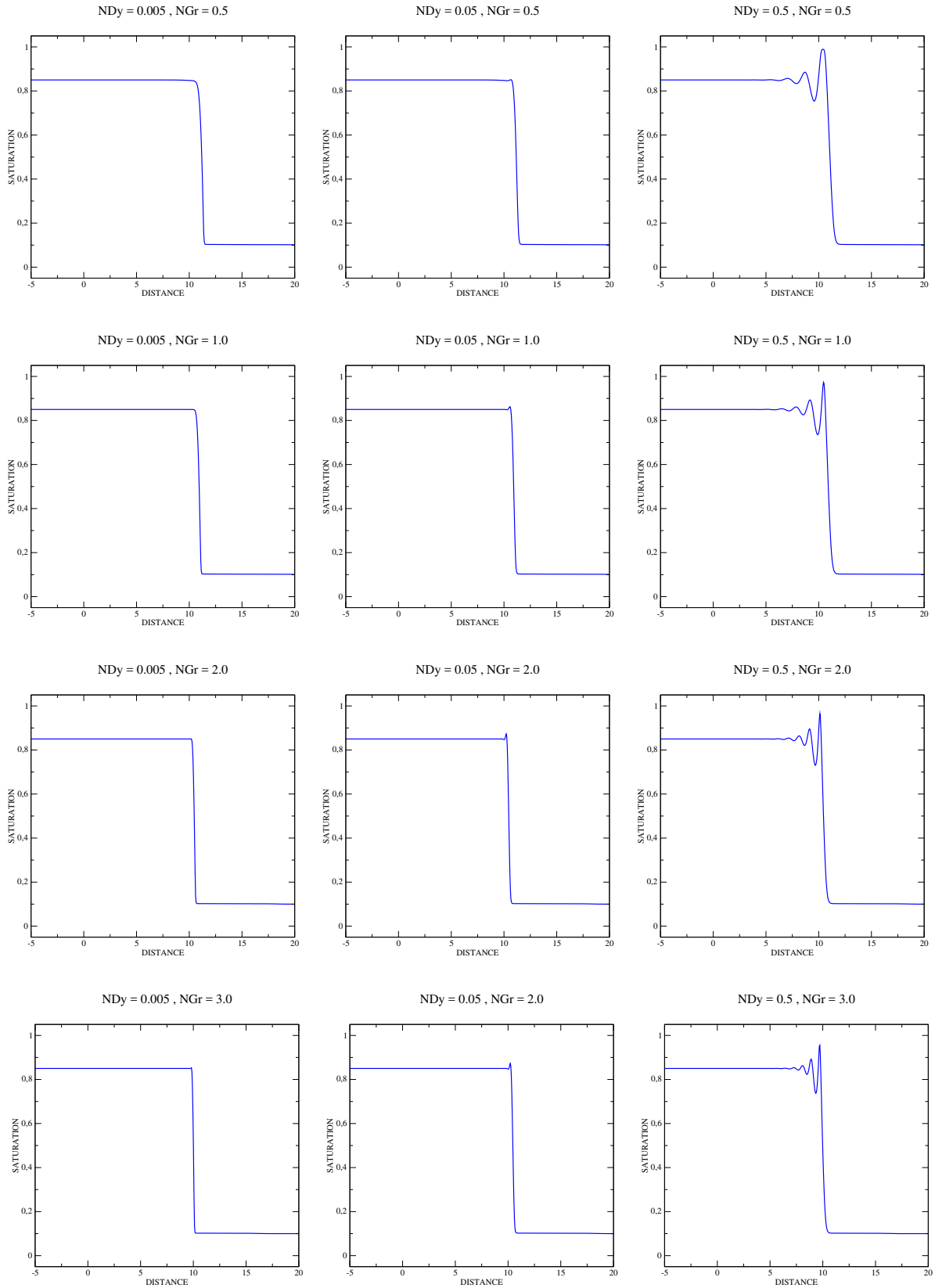


Figure C.6: Numerical solutions when the gravity acts in the direction opposite to the flow with different values of dynamic effect number N_{Dy} and gravity number N_{Gr} . Dynamic effect number: $N_{Dy} = 5 \times 10^{-3}$ (left), $N_{Dy} = 5 \times 10^{-2}$ (center) and $N_{Dy} = 5 \times 10^{-1}$ (right). The gravity number increases from $N_{Gr} = 0.5$ (top) to $N_{Gr} = 3.0$ (bottom). Computational mesh: 512 elements.